UNIVERSITÀ
DEGLI STUDI
DI PADOVA

UNIVERSITÀ DEGLI STUDI DI PADOVA

Sede Amministrativa: Università degli Studi di Padova

Dipartimento di Ingegneria Industriale - DII

SCUOLA DI DOTTORATO DI RICERCA IN INGEGNERIA INDUSTRIALE
INDIRIZZO INGEGNERIA DE MATERIALI
CICLO XXX

ENHANCEMENT OF Ti6Al4V MACHINABILITY THROUGH THE USE OF INNOVATIVE COOLING/LUBRICATING TECHNOLOGIES

Direttore della Scuola: Ch.mo Prof. Paolo Colombo
Coordinatore: Ch.mo Prof. Enrico Bernardo
Supervisore: Ch.mo Prof. Stefania Bruschi

Dottorando: Stefano Sartori

Abstract

The machining operations of Difficult-to-cut materials such as Titanium and its alloys, has an important role in the development of new techniques with the aim to improve both the process productivity and the final product quality.

The performances of the cutting fluids have recently been under investigation to drive machining operations towards cleaner and more sustainable targets. Several efforts are being made to test new formulations of coolants and to implement cooling/lubricating strategies alternative to standard flooding. As reported in literature the low-temperature cooling seems to be an efficient solution to enhance the process sustainability, among its several advantages, no contaminants are left on the chips and workpiece, hence reducing the chip disposal costs and limiting skin and breath diseases for the machine tool operators. Furthermore, in case of surgical prosthesis, it can help reducing the cleaning steps before the final sterilization. However its industrial application is still limited due to the cryogenic coolant extremely low temperatures that could determine a loss of geometrical accuracy of the machined components as a consequence of the thermal contraction induced mechanical components of the CNC machine tool.

Another interesting solution that minimizes the consumption of cutting fluid consumption without determine the above mentioned problems typical of the pure cooling techniques, consists in the use of Minimum Quantitative Lubrication (MQL) technologies. Nevertheless the low lubricating capacity of the cutting fluid does not allow to efficiently inhibit the tool activated wear mechanisms responsible to cutting edge degradation.

In this PhD thesis, several cooling, lubricating and hybrid technologies have been developed and implemented to improve the machinability of Ti6Al4V alloys, as promising alternatives to standard cooling methods applied in semi-finishing turning operations.

To reduce the main critical issues of the cryogenic cooling strategies different solutions have been proposed:

(i) For the first time an innovative cooling approach based on the use of gaseous Nitrogen (N2) cooled by LN2 in a range of temperature between 0° and -150°C.

(ii) Tool holder re-designed in order to make competitive the use of cryogenic coolant (LN2) reducing the thermal distortions.

As concerning the strategies to improve the minimal lubricating technologies both the Solid Lubricant assisted technologies and the hybrid ones (Minimum Quantitative Cooling Lubrication) were investigated. Two SL-assisted strategies were considered, namely an MQL vegetable oil enriched with PTFE particles and an aqueous solution added with graphite at different percentages, while for the MQCL technology the MQL system was implemented together with Liquid Nitrogen (LN2) and Carbon Dioxide (CO2) distribution systems designing the position of the nozzles to optimize the lubrication and cooling effects.

The Ti6Al4V machinability has been firstly investigated through an experimental approach, evaluating both the tool wear mechanisms and the surface integrity, using the dry cutting and the wet strategies as a reference.

Lastly the effects onto the machinability of Ti6Al4V alloy of different microstructure variants produced though both conventional and Additive Manufacturing technologies and different insert coatings were evaluated.

Index

Chapter 1

Introduction

1.1 Industrial and scientific background

The demand of titanium alloys in different sectors has increased in recent years thanks to their outstanding properties, such as high strength-to-weight ratio, ability to retain high strength at elevated temperatures, resistance to chemical degradation, excellent biocompatibility and wear resistance. These advanced alloys are especially used in manufacturing components for aerospace, chemical and biomedical devices. On the other hand, they are classified as Difficult-To-Cut (DTC) alloy due to their poor machinability attributable to its high thermal reactivity, low thermal conductivity, high hardness and low Young's modulus. These characteristics cause high temperature increases during the cutting process that negatively affect the tool life and result in a poor quality of the machined surface.

Effective methods for lengthening the tool life consist of applying suitable cutting fluids to the cutting zone as well as using proper cutting tools with engineered coatings whose choice must be function of the cutting parameters. The former solution represents the current state-of-the-art, with the most common cutting fluids either water- or oil-based enriched with additives (anti-wear, friction modifier, corrosion inhibitor, antioxidants, biocides, emulsifiers, etc.). However, the extensive use of large quantities of these cutting fluids raises important environmental issues in terms of their recovery and disposal, in addition to the needed time-consuming cleaning steps in order to guarantee the required cleaning specifications of the machined product surfaces, especially in the case of the biomedical components. Due to the stricter and stricter regulations, imposed by the international agreements, the concept of sustainability manufacturing has become of great interest within the international community. Therefore, the manufacturing companies are nowadays exploring new solutions to reduce or completely eliminate the conventional cutting fluids in favour of more efficient, less polluting and cheaper technologies. The simplest solution consists in machining without cutting fluids, namely carrying out dry cutting, but this means accepting a lower machinability of the workpiece alloy.

An interesting solution recently developed is represented by the use of low-temperature fluids, as the Liquid Nitrogen (LN2), Carbon Dioxide and air cooled that can be identified as one of the best candidates since it is safe, clean, non-toxic and non-inflammable. The studies to identify the best experimental configurations highlighted that the most effective approach consisted in simultaneously applying the LN2 to the tool rake and flank faces. Several advantages have been found in machining heat-resistant and DTC alloys, such as titanium or nickel alloys, especially in roughing turning in which the low temperatures of the cutting fluid showed to be able to limit the main wear mechanisms responsible of the rapid failure of the tool insert, and to improve both the machined surface integrity in terms of residual stresses and surface defects and the tribo-corrosion behaviour during the machined part service life. Furthermore, a costs analysis carried out considering the economic, environmental (energy consumption, waste management,..) and social (operational safety, personal health,..) aspects highlighted how the cryogenic machining reduced the overall production costs in comparison with the conventional strategy up to 30%. Despite the several advantages highlighted hitherto, the industrial application of this technology is still limited due the cryogenic coolant

extremely low temperatures. These low temperatures levels could damage the mechanical parts of the CNC machine tool and cause thermal distortions of the machined components with loss of dimensional accuracy.

Another strategy, nowadays increasingly used also in industrial applications, is the Minimum Quantity Lubrication (MQL)-assisted machining, which, as a consequence of the very low flow rate of the used cutting oil (of the order of 0.2 l/h), is classified as near-dry machining. Several research works have demonstrated its benefits in improving the cutting performances in terms of both tool wear resistance and surface integrity with respect to dry cutting as well as in avoiding not only the costs associated with the cutting fluid disposal but also the costs related to the machine tool cleaning. Nevertheless, when machining difficult-to-cut alloys, such as titanium, cobalt or nickel alloys, where high dimensional accuracy and machined surface quality are mandatory, the conventional flood strategies still represent the best solution since.

To improve the cooling effect of the MQL techniques two strategies have been recently proposed in literature: one uses low-temperature fluids, to provide a hybrid technology in which the tool flank face is lubricated and the rake one cooled simultaneously (techniques named as Minimum Quantity Cooling Lubrication (MQCL); while the other aims at improving the oil heat transfer characteristics thanks to specific additives. The latter solution, named Solid Lubricant (SL)-assisted MQL strategy, is nowadays receiving wider attention since it allows a drastic improvement of the fluid performances by controlling both the heat generation and the friction between the tool and workpiece without significant increase of the process costs, and, at the same time, it also avoids those issues related to the use of cryogenic temperatures as happens when using the aforementioned hybrid techniques. The second method to improve the DTC alloys machinability consists of adopting surface engineered tools. The scientific literature suggests that the tool inserts should exhibit characteristics of hot hardness (to maintain sharp and stable the geometry of the cutting edge at elevated temperatures), thermal shock resistance (not to be affected by the cyclic heating and cooling), low chemical affinity (to limit the Build-Up-Layer formation), oxidation resistance (to resist at the accelerate wear rate at elevated temperatures) and toughness (to withstand high cutting forces and mechanical socks). The most common inserts used in titanium alloys machining are made of cemented carbide (WC), though at high cutting speeds the WC is subjected to a rapid deterioration due to its chemical reactivity that actives the adhesion

and diffusion wear mechanisms. A common way to improve the surface characteristics of the cutting inserts is based on the use of coatings deposited by means of Chemical Vapour Deposition (CVD) and Physical Vapour Deposition (PVD) techniques, able to reduce both the friction coefficient, thanks to their self-lubricant properties, and the wear mechanisms since they present chemical inertness and high mechanical properties. TiN, TiCN, TiC, TiAlN, Al_2O_3, TiB_2 are common materials used in single, multiple and nano-layers to enhance the DTC alloys machining performances: their influence on the tool life and surface integrity of the machined components have been extensively investigated, highlighting how the best solution does not exist, but it changes as a function of the machining operation (milling, turning,..), cutting parameters set (feed rate, cutting speed and depth of cut), and cooling strategy (dry, wet, MQL etc.).

The aim of the present work is to investigate the machinability of Ti6Al4V alloys in turning operation though experimental approach, proposing innovative cooling and lubricating technologies devoted to fulfil the reduction of post-machining cleaning step making the process more sustainable. In order to achieve this main purpose, the following main goals can be distinguished:

- Design and implement an innovative clean cooling, lubricating and hybrid methods applicable for the turning operation of Ti6Al4V components.
- Quantify the machinability of wrought Ti6Al4V in semi-finish turning under the different tested cooling, lubricating and hybrid strategies evaluating both the tool wear and surface integrity.
- Analysis of the influences of different TI6Al4V microstructures onto the alloy machinability under dry cutting and cryogenic cooling.
- Analysis of the effect of cryogenic cooling technologies based on the use of Liquid Nitrogen (LN2) and cooled gaseous nitrogen (N2) at -100°C onto the tool wear when using uncoated and coated cemented carbide inserts in semi-finishing turning of the Ti6Al4V titanium alloy.
- Re-design of tool holder in order to minimize the thermal distortion and to stabilize the temperature field during the cryogenic machining.
- Develop of reliable thermo-mechanical numerical model of the tool holder behaviour during the cryogenic machining process that will be further applied to improve the tool holder redesign.

1.2 Overview of dissertation

The work is organised in eight chapters:

The second chapter reports the literature reviews of the main topics afforded in this thesis. An overview on the latest scientific methodologies to investigate and to improve the machinability of Difficult-to-cut alloys trough experimental approach is presented, reporting the main findings and results regarding the Ti6Al4V alloys. A particular emphasis is given to the alternative cooling and lubricating strategies.

The third chapter defines the experimental approaches, the methodologies and the instrumentations used to investigate the machinability of Ti6Al4V in terms of tool wear and surface integrity.

The fourth chapter consist of the main experimental finding achieved by the turning tests to characterize the material machinability under different cooling, lubricating and hybrid technologies. The tool wear is quantified by means of SEM analysis and optical profiler. The surface integrity is defined though the measurement of surface quality (roughness, topography and defects) and the evaluating of the material microstructure and surface properties alteration (altered layer, residual stresses, nano-hardness and Young's modulus). The chapter evidences the main effects carried by the application of different innovative cooling (LN2, LCO2, cooled N2 at different temperatures), lubricating (MQL, SL-assisted MQL, SL-assisted MQC) and hybrid (MQCL) techniques.

The fifth chapter reports the experimental investigations conducted in order to verify the effectiveness of the cryogenic cooling strategy in comparison with the dry cutting in semi-finishing turning different Ti6Al4V microstructural variants produced by two Additive Manufacturing (AM) techniques, namely Direct Metal Laser Sintering (DMLS) and Electron Beam Melting (EBM). The obtained results prove a correlation between the mechanical and thermal properties of the investigated alloys and the tool wear mechanisms in both dry cutting and cryogenic cooling conditions.

The sixth chapter presents the effect of cryogenic cooling technologies based on the use of Liquid Nitrogen (LN2) and cooled gaseous nitrogen (N2) at -100°C onto the tool wear when using uncoated and coated cemented carbide inserts in semi-finishing turning of the Ti6Al4V titanium alloy. Four commercially available insert grades commonly used in machining heat-resistant alloys were tested using the cutting parameters recommended

by the tool manufacturer. The investigation combined scanning electron microscopy and optical profiler analyses to efficiently define and quantify the mainly tool wear mechanisms.

The seventh chapter introduces a preliminary tool holder re-design in order to minimize the thermal contraction responsible to the loss of geometrical accuracy of the machined samples, and to protect the mechanical components of the CNC lathe from the cryogenic temperature that could damage them. Moreover in this section description of the thermo-mechanical numeric model of the newly redesigned apparatus that will be further applied to improve the tool holder redesign was reported.

Finally in the eighth chapter the main findings and conclusions are summarized.

Chapter 2

Literature review

2.1 Introduction

In this chapter a literature review of the latest work regarding the ambitious challenge to machine difficult-to-cut materials is presented. The analysis starts with some considerations of the Ti6Al4V alloy object of investigation describing its proprieties, the differences obtainable between the different producing technologies and the reasons that have led to its wide use especially in technical field such as the biomedical and aerospace ones. To follow a detailed description of the recent approaches in evaluating the machinability of metal alloys in terms both of tool wear and surface integrity explaining some interesting case studies. Last, but not the least the current researches on innovative coating and strategies based on the use of not conventional coolant or lubricant cutting fluids able to resolve the machining problems are discussed giving emphasis of titanium alloys.

2.2 Ti6Al4V alloy

Titanium exists in two allotropic forms, at low temperature it has a closed packed hexagonal crystal structure (chp) which is commonly known as α, whereas above 883°C it has a body centred cubic structure (bcc) called β. The α to β transformation temperature of pure titanium increases or decreases based on the alloying elements, in detail Al, O, N etc. tend to stabile the α phase increasing the beta transus temperature, while elements such as V, Mo, Nb, Fe, Cr etc. are beta stabilizers since their addition depress the beta transus temperature. The transition temperature plays a key role in evolution of microstructure and is of a great technological importance in determining heat treatment and processing schedule in order to obtain the required mechanical and physical properties.

The normally accepted classification of titanium alloys is based on the α and β phases percentage content: the α alloy contains only α phase, in the α+β ones instead the β content is about 10-30% while with higher percentages they are known as metastable β alloys. The most widespread alloy is Ti6Al4V, which belongs to the α+β group and accounts for more than 70% of the titanium alloy production in USA and UE, its chemical composition in according to the ASTM F136-82 standard [1] is reported in Table 2.1.

Table 2.1 Nominal chemical composition for Ti6Al4V (%weight)

Chemical composition (wt %)								
Designation	Ti	Al	V	C	Fe	O	N	H
Ti grade 5	Bal.	6.0	4.0	< 0.25	< 0.2	< 0.2	-	-
Ti grade 23 (ELI)	Bal.	5.5-6.5	3.5-4.5	0.08	0.25	0.13	0.05	0.012

In order to understand the peculiar microstructure that characterizes the Ti6Al4V alloy is fundamental to clarify the effects of cooling rate from β phase on the material microstructure at room temperature. Depending on the required mechanical properties, the following heat treatments can be applied: partial annealing (600 – 650 °C / 1h), full annealing (700 – 850 °C / furnace cooling to 600 °C / air cooling), or solutioning (880 – 950 °C / water quenching) and ageing (400 – 600 °C).

One important characteristic of the alloy is a range of α+β→β phase transformation temperature that determines conditions of thermomechanical processing intended for development of suitable microstructure (Figure 2.1). Start and finish temperatures of

α+β→β phase transformation, vary depending on the contents of β stabilizing elements (Table 2.2).

Table 2.2. Start and finish temperature of the α+β → β phase transformation for the Ti6Al4V alloy (Vc=0.08°C s-1) [2].

Phase transformation	
Temperature (°C)	**Ti6Al4V**
$T^{ns}_{\alpha+\beta\rightarrow\beta}$ $T^{f}_{\beta\rightarrow\alpha+\beta}$	890
$T^{ps}_{\alpha+\beta\rightarrow\beta}$	930
$T^{f}_{\alpha+\beta\rightarrow\beta}$	985
$T^{s}_{\beta\rightarrow\alpha+\beta}$	950
$T^{f}_{\beta\rightarrow\alpha+\beta}$	870
ns - nucleation start	s - start
ps - precipitation start	f - finish

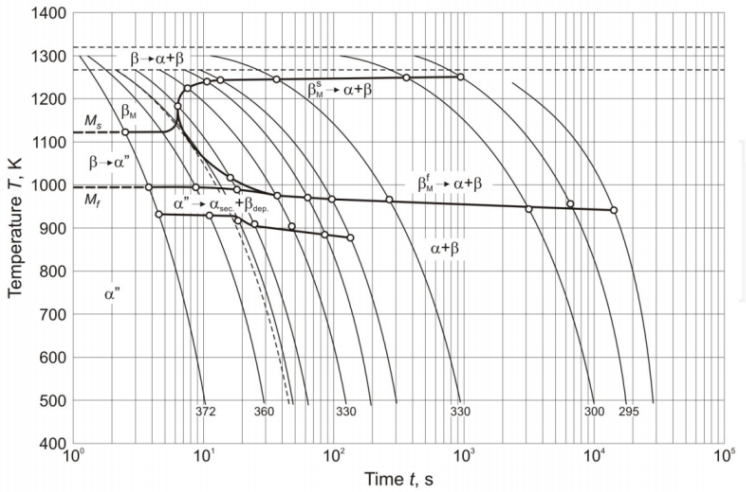

Figure 2.1 CCT diagram for Ti6Al4V alloy [2].

Cooling of Ti-6Al-4V alloys from above β transus temperature at the rate higher than 18°C s-1 leads to development of martensitic microstructure consisting of α'(α") phases For the intermediate cooling rates, down to 3.5°C s-1, martensitic transformation is accompanied by diffusional transformation β→α + β and the volume fraction of martensitic phases decreases to the benefit of stable α and β phases. Cooling rates below 2°C s-1 lead to a diffusion controlled nucleation and growth of stable α and β phases in the shape of colonies of parallel α-phase lamellae in primary β-phase grains [2]. Increases in cooling rate leads to refinement of the microstructure both α colony size and α-lamellae thickness are reduced. Additionally new colonies tend to nucleate not only on β-phase boundaries but also on boundaries of other colonies, growing perpendicularly to the

existing lamellae. This leads to formation of characteristic microstructure called “basket weave” or Widmanstätten microstructure (Figure 2.2.a) [3][4].

When these alloys are mechanically processed below the β-transus temperature and annealing in the α+β region the obtainable microstructure consists of mixture of α and β equiaxed grains (Figure 2.2.b), moreover changing the heat treatment temperature and cooling rate is possible obtain bimodal (duplex) microstructures containing equiaxed primary α in a lamellar α+β matrix (Figure 2.2.c), the details of phase transformation and processing-microstructure-property relationships are reviewed in several paper and book [5][6][7].

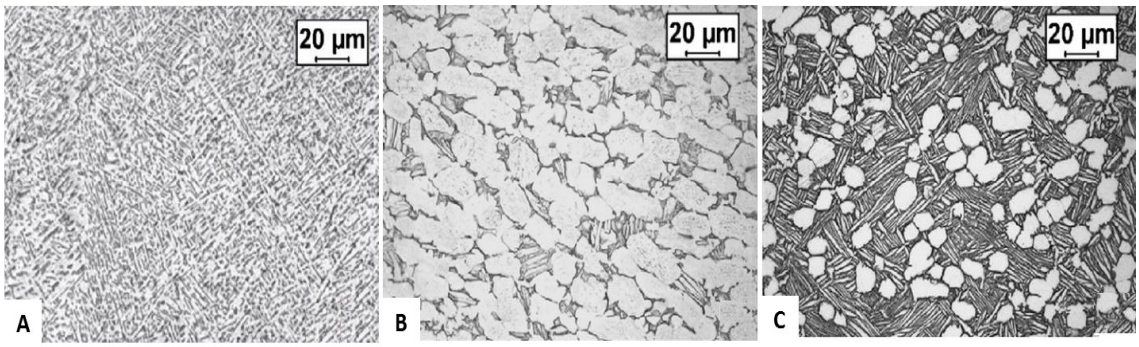

Figure 2.2. Ti6Al4V microstructures: (A) Widmanstätten, (B) equiaxed and (C) bimodal [8].

The Ti6Al4V manufacturing process include casting, wrought, powdered metallurgy and in the recent years also the Additive Manufacturing (AM) technologies. AM technologies for metals can be broadly classified into two categories: (i) Powder Bed Fusion (PBF). (ii) Directed Energy Deposition (DED). The first is based on the principles of laying down a layer of metal powder on the build platform and scanning the bed of powder with a heat source to completely reach the deposited power melt, the Directed Energy Deposition instead use the directly material injection in to the melt-pool. In both cases the commercially available AM technologies are based on two types of heat sources, namely laser and electron beam, for the purpose of melting the feedstock (powder or wire). Laser based systems operate under inert atmosphere in contrast to the vacuum environment of the electron beam systems [9]. Among the power bed AM technologies available in the market Electron Beam Melting (EBM) and Direct Melting Laser Sintering (DMLS) are those most employed, studied and diffused.

The microstructure obtainable using the rapid prototyping strategies is quite different from that typical of hot worked ones, since the large undercooling and no mechanical deformations is over imposed on the workpiece and promotes the formation of an

acicular/lamellar α phase, which is less ductile than the globular (equiaxed) microstructure formed during the hot working. Significant differences can be appreciated also between the most common AM technologies, the DMLS promotes the formation of a martensitic microstructure constituted by α' phase with lattice parameters very similar to the hcp pattern, since the martensite is not suitable for structural and mechanical components a post-building heat treatments are necessary to transform it into a biphasic α+β microstructure [10], in which the new α lamellae nucleate along the martensitic grain boundaries maintaining the previous orientations [11][12]. The EBM as-built microstructure instead is composed from fine acicular α phase with 8% of β phase at the grain boundaries [13][14].

The effect of these various microstructures is well demonstrated in their mechanical behaviours (see Table 2.3), namely the equixed grain is usually preferable for strength, ductility and fatigue crack initiation while the lamellar microstructure is better for fracture toughness, fatigue, crack propagation and oxidation resistance.

Table 2.3. Comparison between the mechanical properties of the wrought, EBM, DMLS and heat treated DMLS Ti6Al4V alloys.

Material	**E (GPa)**	**UTS (MPa)**	**YS (MPa)**	**Elongation (%)**	**HRC**
Wrought	118	872	790	16	31
EBM [a]	120	965	910	13.1	35
DMLS[b]	110	1095	990	8.1	44
Heat treated DMLS[b]	117	915	835	10.6	34

[a] Facchini et al. [13]

[b] Facchini et al. [12]

Nowadays the Ti6Al4V alloy is used extensively in technical fields such as aerospace, automotive, petrochemical and military thank to its high strength-to-weight ratio, fracture toughness, fatigue strength, high corrosion resistance and ability to operate at higher temperature. These alloys show higher strength than aluminium alloys and less density than steel, making it suitable for structural components. Moreover the Ti6Al4V alloy is the most used as biomaterial because presents a well-documented biocompatibility (appropriate tissue response and biological safety) and bio-functionality (mechanical properties close to the tissue to replaced) [15], [16]. Despite its increased usage and production, the titanium alloys are yet expensive when compared to many other metals

because presents several problems associated to its extraction, melting, production and machining [17].

2.3 Metallic alloys machinability

The term machinability refers to the ease with which a metal can be cut (machined) permitting the removal of the material with a satisfactory finish at low cost [18]. Despite this simple definition the machinability concept depends on a large number of factors such as tool life, surface quality, final product dimensional accuracy, force and power consumption, productivity, machining costs and chip control, each of which are differently influenced by the mechanical and thermal properties of the machined workpiece material (hardness, tensile stress, Young's modulus, thermal conductivity, etc.), tool material (substrate and coating) and geometries (tool shape, characteristics angles, etc.), cooling/lubricating capacity of the adopted cutting fluid, type of machining operations (turning, milling, grinding, etc.) and processing conditions (cutting parameters and nature of cutting).

Due to this, since is impossible to combine these factors in a univocal machinability definition, it is often assessed case by case basis, and the tests and the main considered parameters are tailored to the needs of a specific manufacturing process. For example in a roughing operation the main considered parameters are the tool wear and the productivity while in finishing machining the product surface quality is commonly used.

However in literature several different methods to qualitative measure the machinability are available, the most used consists to define a machinability index I_i which formulae is shown in the Formula.2.1

$$I_i = \left({}^{P_i}/_{P_r}\right) X\ 100 \tag{2.1}$$

Where P_i is the parameter value accepted for machinability evaluation of the i-th material while P_r is the parameter value of the material used as standard. The tool wear since directly influences both the productivity and the surface integrity is the most accepted parameter to define the index machinability, the general abovementioned definition becomes:

$$I_i = \left({}^{V_{60}}/_{V_{60R}}\right) X\ 100 \tag{2.2}$$

Where V_{60} is the cutting speed for the target material that ensure 60 minutes of tool wear, while V_{60R} is the cutting speed of reference material for the same 60 minutes of tool life. The standard material is AISI 1112 steel resulfurized which is given a rating of 100. For a

tool life of 60 minutes this steel should be machined at a cutting speed of 30 m/min (100 ft/min).

If I_i is greater than 100 the machinability of the target material is better that this of the reference material, and vice versa. For example C-20 steel has a machinability rating of 65, this means that when it I machined at a cutting speed of 20 m/min (65 ft/min), tool life will be 60. Machinability ratings for various materials are reported in Table 2.4.

Table 2.4. Machinability index of common materials [19].

Material	Machinability index
C-20 steel	65
C-45 steel	60
Stainless steel	25
Copper	70
Brass	180
Aluminium alloys	300-1500
Magnesium alloys	600-2000

Other criteria based on the cutting force and surface roughness are used namely when the rigidity of machine tool is critical and is necessary to supress chatter and vibratory related issues and when the surface finish is critically required for the product functionality.

Note that all these methods can be misleading because the index changes as function both of the used machining process and by the process parameters and conditions.

In this work two main targets are considered as the most important: the improvements of production rates and the improvement of the final surface integrity of the machined products, according to that the machinability evaluation was simplified at the sole tool wear and surface integrity analysis. In the following paths, the material machinability can be classified into two categories, in the first the study of the tool wear mechanism and tool life is conducted highlighting the effects of different tool coating and different cooling/lubricating strategies, in the second one instead the surface integrity analysis is discussed reporting the main experimental methods and results.

At least an overview of the state of the art of the experimental approaches conducted to improve the titanium alloys machinability is presented.

2.3.1 Tool wear

The tool wear is a crucial phenomenon that has to be taken into account when investigating the material machinability; regardless it is a metallic alloy, composite or plastic. During the machining operation the cutting edge alteration can be determine

higher needed cutting forces, increase of temperature fields, loss of dimensional accuracy of the machined components, the onset of chatter phenomenon, difficulty to evacuate the chip from the cutting area, etc.. All these aspects contribute to reduce the product surface quality and the tool life thus improving the process costs. The knowledge of the predominant wear mechanisms involved during a cutting operations allows to plan an efficiently strategies able to minimizing the tool degradation.

The tool insert is subjected to different wear mechanisms because the interactions between the tool and workpiece material changes depending on the different tool areas (see Figure 2.3). In literature different classifications have been proposed, the simplest one considering the temperature as the most critical parameter. In the tool areas interested by higher temperature values, the main wear mechanisms are diffusion and adhesion, while in those zones characterized by lower temperatures the predominant mechanism becomes the abrasive one, mainly mechanically-induced [20]. Another consolidated classifications subdivides the tool wear mechanisms into five categories, namely adhesion, diffusion, tribo-corrosion (or cratering) abrasion and fatigue, considering the tool failure caused by their combination [21]. In addition to the above sources of tool failure, the following also pertain: microchipping, gross fracture, thermal fatigue and plastic deformation. Generally speaking, the predominant wear mechanism depends on several factors, among which the workpiece material, the tool insert geometry and material, the cutting parameters and the cooling strategies [22].

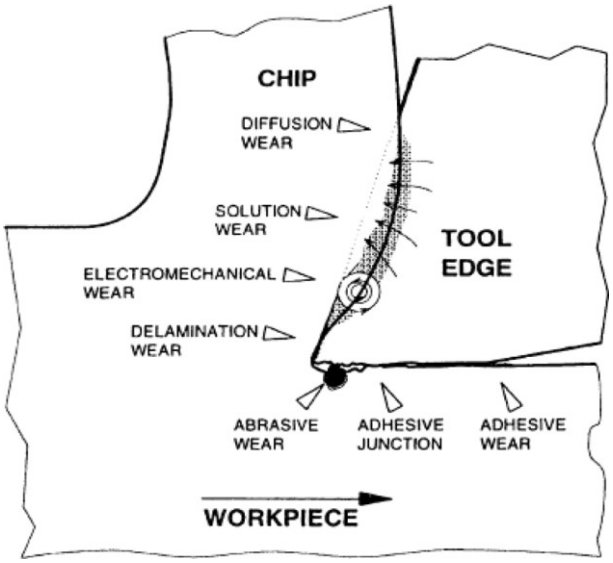

Figure 2.3. Wear mechanisms on the different tool areas in titanium machining using WC inserts adapted from [23].

The adhesive wear is the result of the atomic interaction deriving during the frictional contact between tool and workpiece material, the temperatures and pressures generated during the cutting process determine the formation of weld micro-junctions. When the two contact surfaces undergo relative motions the rupture of welding take place localizing the tearing inside the softer material. The transferred fragment is plastically deformed during continued action of sliding so that it frequently has a plate-like morphology.

During the machining process the workpiece material adheres on the rake and flank tool faces in two different and almost simultaneous, forms. The first one is the most known and involves the formation of a Build-Up-Edge (BUE) by adhesion of workpiece material to the cutting edge. In the second mechanism instead the tool rake is interested, in which the transferred material giving rise to so-called Built-Up-Layer (BUL) [24][25].

Specialised literature devoted to the study of the BUE and BUL formation mechanisms and their influences in the machining process reported that the BUE formation is commonly associated to the mechanical adhesion forces in the interface tool-chip [26][27], on the contrary thermal and mechanical workpiece proprieties have a relevant influence on to the BUL development [28].

In the first stage of machining process a BUL is formed onto the tool rake face, the adhered layer so-formed has lower hardness than the tool, thereby the temperatures diminish promoting the BUE formation on the cutting tool edge [29]. Also the chemical reactivity of the machined material play an important role in the adhered layer development, for an example during the dry cutting of titanium alloys the formation of titanium oxides in the Multi-Built-Up-Layer (MBUL) favoured by the high generated temperatures determines an alteration of the chemical and mechanical properties giving rise to a BUE adhesion, this characteristic phenomenon is detected through iridescence visible on the tool [30]. The Figure 2.4 shows a schematic illustration on this behaviour.

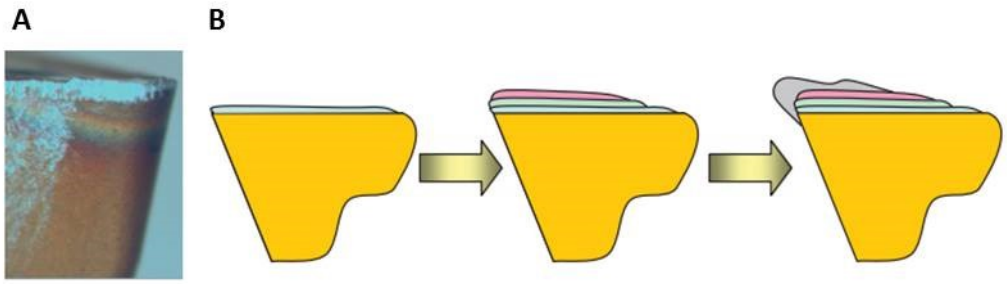

Figure 2.4. (A) MBUL (iridescent) and BUE developed on a tool after machining a Ti alloy. (B) Schematised MBUL and BUE formation mechanism in the dry machining of Ti alloys (adapted from [31])

The presence of adhered layer onto the tool surface protects the tool substrate from the abrasive wear, but in addition to alter the cutting edge geometry it makes possible the diffusion mechanism responsible to the chemical pauperization of the tool matrix elements determining its embrittlement [32][33].

Being a thermally activated mechanism the diffusive wear necessities of high temperatures, for these reason this mechanism is particularly relevant when machining difficult-to-cut or heat resistant alloys such as nickel, cobalt or titanium based alloys. Moreover a chemical affinity between the tool elements and the workpiece material must exist, the most well documented case is represented by coupling of carbide insert (composed by WC and Co) and titanium alloys [34][35] or CBN insert and steel [36].

In metal cutting the abrasion wear is caused by hard particles in the workpiece material or trapped in the cutting zone which indent the tool surface and generate wear debris through the applied relative motion. It can be classified as three or two body abrasion depending on the presence of free wear particles. The material could be removed by micro-cutting, pull out of grain or micro-fracture, generally the tool surface highlights abrasive marks parallel to the cutting or chip sliding direction. The literature review revealed that the abrasion is a dominant wear mechanism that appears in combination with adhesion [37][38].

The combination of abrasion, adhesion and diffusion is responsible to the formation of the cratering phenomenon onto the rake tool face. The tool matrix embrittlement due to the loss of binder elements that migrate toward the chip material as a consequence of the diffusive process has a deleterious impact on to the tool mechanical properties. In machining the loss of the tool mechanical strength determines an increase of the abrasive action due to the chip flowing, this process leading to the extraction of the tool grains and resulting in the crater wear formation [39]. At the same time, the friction at the chip-tool rake face interface contributes to increase the tool temperature, and, therefore, the diffusion phenomenon [40]. The crater wear, since causes a rapid tool rake degradation that could lead to the catastrophic failure of the cutting edge is considered in many machining operation as the critical wear mechanism to control and limit adopting particular strategies and precautions, for example limiting the cutting speed or using appropriate lubricants or coolant.

Fatigue wear is commonly observed when machining hard material; it is caused by a cycling loading during friction that determines progressive and localized structure

damages. Fatigue crack start at the material surface and spread to the subsurface regions, the cracks may connect to each other resulting in separation or delamination of the material. Cyclic thermal stress is another reason for fatigue wear.

The cutting edge chipping or breakage is another commonly wear mechanism resulting of an overload of mechanical tensile stresses, these stresses can be due to a numerous different reasons, such as chip hammering, vibration, excessive tool wear and cutting parameters (depth of cut or feed rete) too high. The chipping phenomenon may be caused in addition to a too high mechanical load also to the BUE instability during the cutting process that periodically breaks taking off small lumps of the tool material. Lastly the plastic deformation, that takes places when the thermal softening of the tool material as a consequence of the high generated temperatures is occurred.

The machining performance may be controlled by limit the tool wear, however this solution needs the knowledge of the physical and chemical mechanisms that involve the wear processes. The Figure 2.5 plot a reference graph, using a δ average parameter for comparing the influence of the different tool wear mechanisms as a function of the value of the generated cutting temperature.

At relative low temperature the adhesion and abrasion present the same probability, at high values instead the diffusion, that present a linear behaviour as a function of the temperature, is the most important.

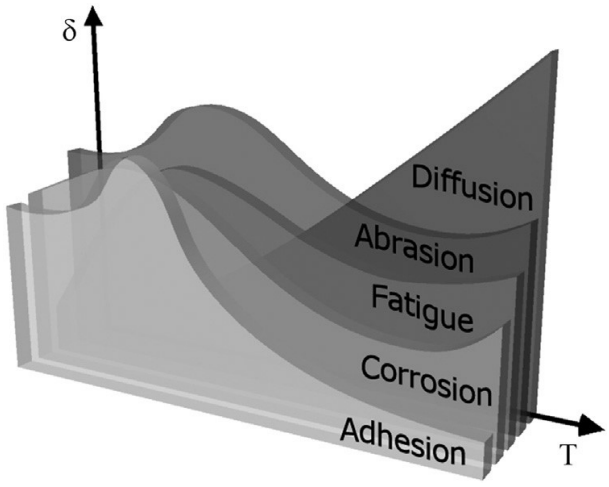

Figure 2.5. Average relevance of tool wear mechanisms as a function of cutting temperature (an extended graph of the original ones included in [41][42]).

The leading wear mode may also change each time when the cutting conditions are adjusted to produce the targeted product shape. This dynamic nature of the wear process is described in wear-maps that chart the tool's wear as a function of two or more cutting parameters. A typical wear-map, developed by Quinto et al. [43], is presented in Figure

2.6 depicting the effects of cutting speed (y-axis) and feed rate (x-axis) on the tool's wear. Increasing the cutting speed will eventually cause crater-wear failure of the tool; while similarly, an excessive feed rate would cause fracture and breakage of the tool. A combination of both high cutting speeds and high feed rates will lead to a sequence of cratering, plastic deformation, breakage, and related mechanisms that define the upper limit of the depicted "safe zone": the area in the wear map in which the tool can be used safely in a controllable and predictable manner.

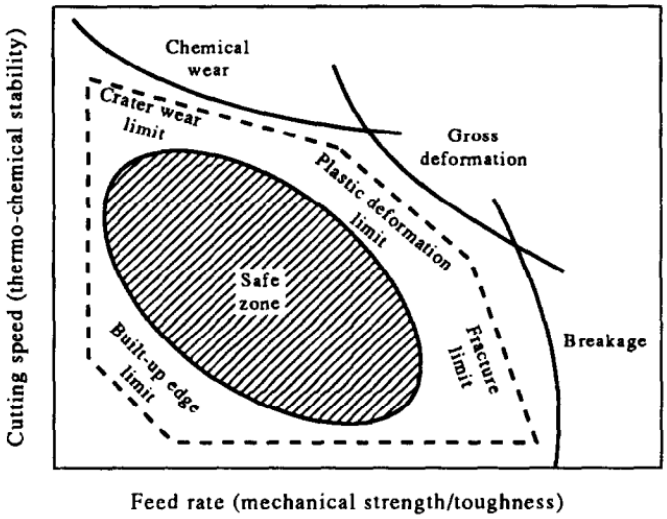

Figure 2.6. Failure mode diagram for a tool material in machining a given workpiece material that maps the mechanisms of wear as functions of metal-cutting variables [43].

Increasing the tool life when used inside the "safe zone" and/or expanding the "safe zone" area for reliable machining at increasingly higher cutting speed, feed rate, or depth of cut are synonymous with increasing productivity and optimizing the manufacturing process. Introduction of new tools that are capable of enlarge the safe zone or enhanced level of cutting performance is the primary object of the tool development.

However often the workpiece material characteristics and the productivity requirements do not allows to choice the cutting parameters that guarantee to remain inside the safe zone. A compromise thus must be accepted making necessary the tool wear mechanisms analysis in order to adopt the better machining set-up.

The separate analysis of each one of them in order to know both their relevance and importance in the wear process is recommended but often not possible since these mechanisms can be change during the machining time and often the tool failure is caused by their combination. For these reasons this complex and expensive analysis procedure is

not use in the industrial fields where the tool wear quantification represents the most important parameter that define the process productivity.

The adopted solution consist to evaluate the total tool geometric degradation fixing limit values over that the tool must be considered worn and therefore substituted in order to guarantee an acceptable product surface quality. The general standard that regulates the tool wear measurements in machining process is normed by the ISO 3685 [44]. According to this standard, the two main geometrical variables measured to quantify the tool wear are: the flank wear width and the depth of the crater wear onto the tool rake face.

The Figure 2.7 shows the three wear zones generated on the primary cutting edge flank, below the tool tip VB_C, along the straight portion of the cutting edge VB_B and on to the zone the firstly approaches the material, the so called notch wear VB_N.

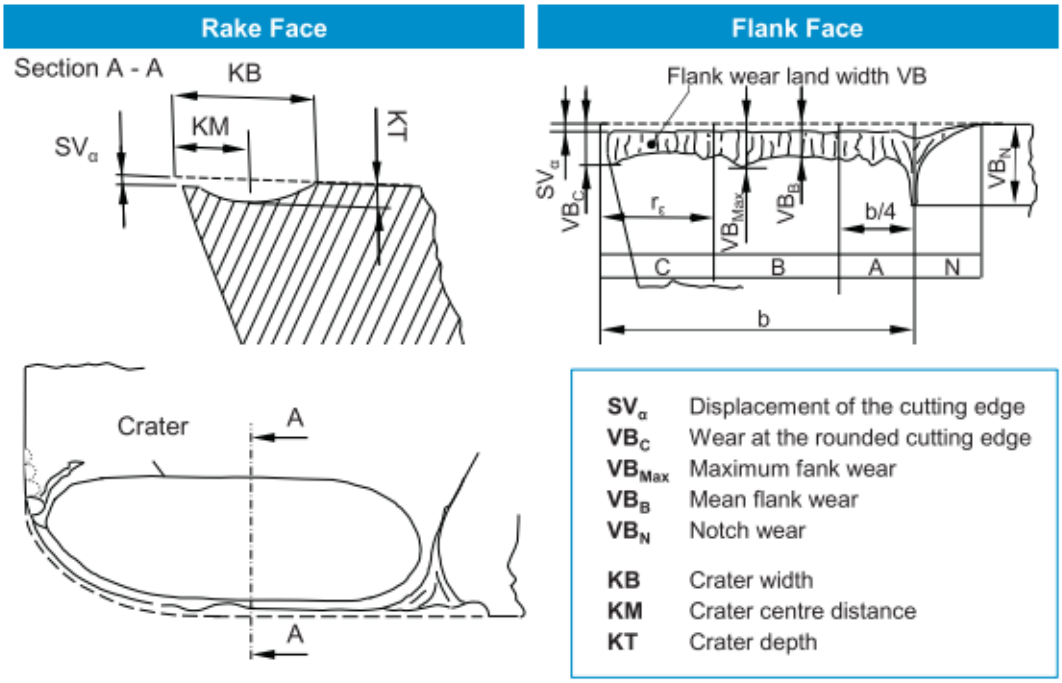

Figure 2.7. Wear phenomena and measured variables at the cutting tool [45] in according to the standard ISO 3685:1993 [44]

The tool's reject criterion that practically states when the tool wear reaches its maximum and become unstable defines the following conditions:

- The maximum value of the flank wear VB is equal to 0.6 mm if the flank wear is not regularly worn in zone B.
- The average width of the flank wear land VB is equal to 0.3 mm if the flank wear is regularly worn in the zone B.

- The depth of crater K_T given by the formula (2.3) where f is the feed rate expressed in (mm/rev) is equal to one of the value listed in Table 2.5.

$$\mathbf{K_T = 0,6 + 0,3f} \quad (2.3)$$

Table 2.5. Threshold values for feed rate and corresponding KT values according to ISO 3685 [44].

Feed rate f, (mm/rev)	0.25	0.4	0.63
Crater depth KT, (mm)	0.14	0.18	0.25

- The crater front distance reduces to a value of Kf = 0,02 mm according to the Figure 2.16.
- The crater breaks through at the minor cutting edge, causing a poor finish of the machined surface.
- Catastrophic failure.

These threshold conditions are often followed nonetheless there are exceptions, in particular in finishing operations a tool wear limit rejecting criterion was chosen by fixing a threshold value for the VB_c parameter equal to 100 μm, which is a conservative condition usually employed for aerospace and automotive components.

The measurements of the flank wear width can be easily conducted using a stereo microscope, however the main instrument used in many of the most advanced tool wear analysis already published is the Scanning Electron Microscope (SEM) that also allows the individuation of the main tool degradations modes, the adoption of Back Scattered Electron Detector (BSED) and X-Ray spectroscopy detector (EDS) are powerful tool to evidence and quantify different chemical elements present in the adhered cutting tool surfaces.

The quantification of the crater depth and position instead is more difficult to measure, in the recent years many microscopy techniques commonly used to characterized the surface topography such as atomic force microscope (AFM), stylus profiler, reflected light interference microscope (RLIM) and the confocal laser scanning microscopy (CLSM) have been used. The first two are tactile instruments while the others are no-contact instruments.

The abovementioned strategies represent a post-machining analysis, to control the tool wear during the cutting process the current adopted strategy consists to measure on-line some characteristics variables that are directly influenced by the tool degradation. An a

increase of cutting forces, temperatures, chattering, power consumption and acoustic emission reveal an excessive tool wear, making thus necessary the tool change.

Nowadays, the cutting forces measurement represents the easiest and the most important analysis to efficiently control the machining process. Several instruments can be adopted to achieve it, nevertheless the piezoelectric dynamometers are the most used devices thanks their rapid dynamic response and their high sensitivity. The correlation between the cutting forces and the tool wear evolution has been well documented: Sun et al. [46] highlighted that during the turning of Ti6Al4V alloy the increase of the cutting forces in all three directions (axial F_X, radial F_Y and tangential F_Z) were caused by the combined effect of the change in the chip flow angle and direction and by the dramatic increases in friction between the tool flank faces and newly produced chamfer surface due to rapid nose radius alteration associated both to the build-up edge formation and flank wear. Also Thamizhmanii et al.[47] reported that exist a clear relationship between the flank wear and the cutting forces turning hard martensitic stainless steel by CBN and PCBN tools, reporting that the highest values were found for the tools that present the highest flank wear area. Moreover the cutting forces analysis is commonly used also to compare different cooling/lubricating strategies, coatings and cutting parameters, since provide important information concerning the material machinability.

Noordin et al. [48] studied the effects of depth of cut, cutting speed and feed rate on cutting forces while machining with coated carbide tools. They observed feed as the most significant factor which influenced the tangential forces during turning of AISI 1045 steel. Sahoo et al. [49] investigated flank wear, cutting forces, chip morphology in hard turning of AISI 4340 steel using uncoated and multilayer TiN and ZrCN coated carbide inserts. Experimental results showed that multilayer TiN/TiCN/Al2O3/TiN coated carbide inserts performed better than the uncoated and TiN/TiCN/ Al2O3/ZrCN coated carbide inserts. Armendia et al. [50] compared the machinability of the of newly developed Ti54M titanium alloy and the standard wrought Ti6Al4V alloy, demonstrating that the different microstructures could be the reason for the lower cutting forces measured during the Ti54M alloy machining being the mechanical properties are very similar.

Bermingham et al. [51] demonstrated that the main cutting force is influenced by the cooling strategies, nozzles position and adopted cutting parameters. The simultaneously cooling of the flank and rake face with the liquid nitrogen determined a decrease of the

main cutting forces regardless the adopted cutting set parameters, while its increase was observed when the cryogenic coolant is applied to the sole rake faces (see Figure 2.8). The cutting temperature is the second most important variable to acquire on line when dealing with machining operations, its increase is associated at the increase of the friction between the workpiece material and the cutting tool due to the cutting edge alteration.

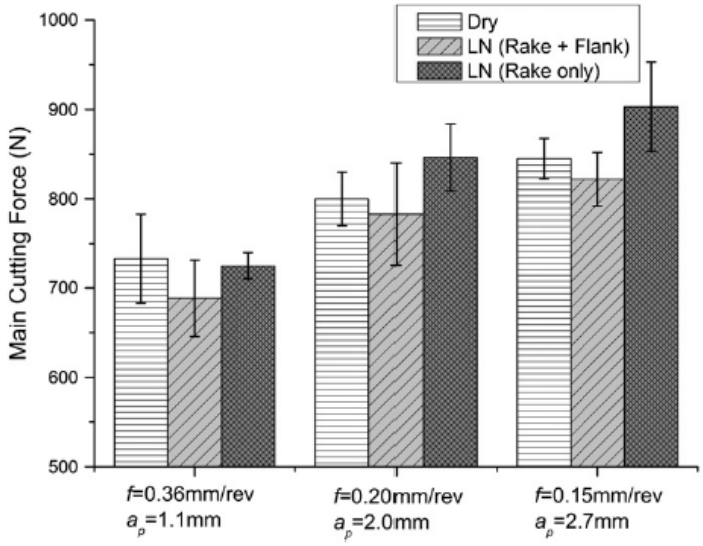

Figure 2.8. Main cutting force for each cutting and coolant conditions [51].

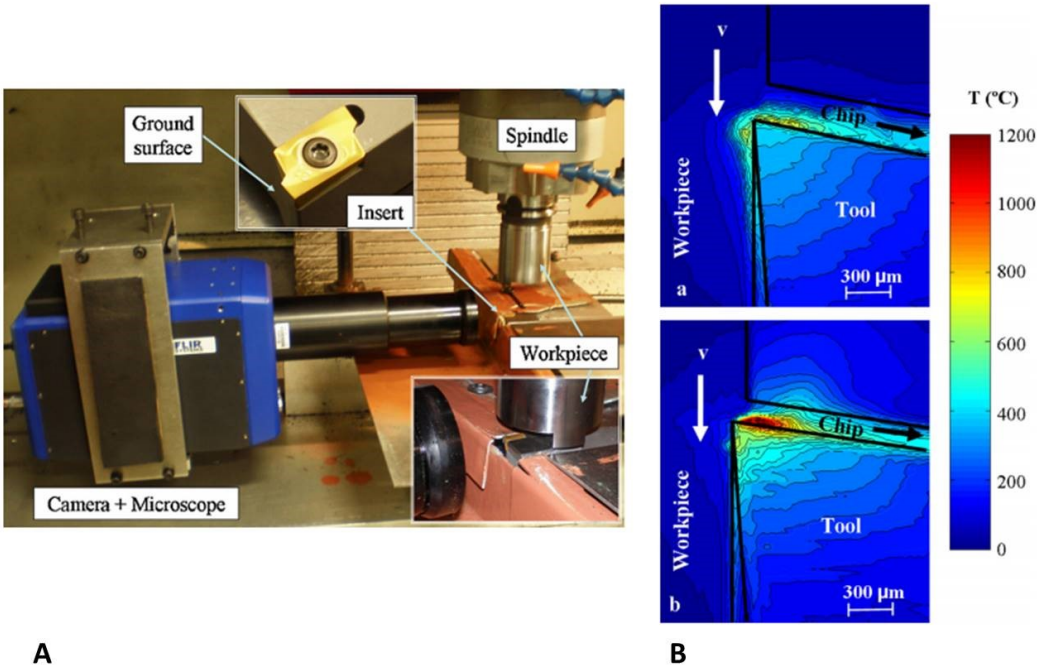

Figure 2.9. (A) Experimental set-up for measuring the cutting temperature by means of infra-red camera. (B) acquired thermal field in milling AISI 4140 (in the upper figure) and in Ti6Al4V alloy (in the lower figure) [52]

On the basis of the considered machining process several methods to measure the cutting temperature were developed. In milling operations is more suitable the adoption of an

infrared camera positioned frontally of the cutting zone (see Figure 2.9), while in the other process as turning the best solutions consist to embedding a thermocouple inside the insert as close as possible to the tool tip, or stick it onto the tool rake face (Figure 2.10).
Both of these solutions are affected by uncertainty that limits their use, because the chip covers the cutting zone and the affect tool involved by the overheating is very small of the order of the cubic millimetres.

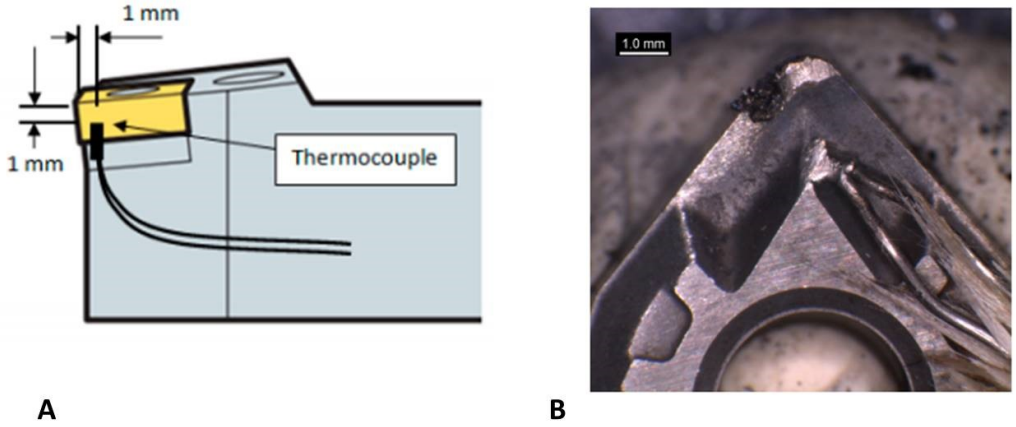

Figure 2.10. Temperature measurement trough thermocouple: (A) inside the insert [53], (B) stick onto the tool rake [51]

In the recent also the acoustic emission AE signals can be used as indicator for monitoring the cutting operations. In the metal cutting the major sources of AE emission are:

- Plastic deformation of workpiece material in the shear zone.
- Plastic deformation and sliding friction between chip and tool rake face.
- Sliding friction between workpiece and tool flank face.
- Collision, entangling and breakage of chip.

The main advantages of AE are that the signal frequency range is much higher than the ambient noise and vibration which could be not associated to the cutting process, and is possible to correlate its signal characteristics (amplitude and frequency) with the wear mechanisms as reported by the Figure 2.11 and the Table 2.6.
Marinescu et al.[59] studied the effectiveness of acoustic emission signals in the detection of failure in double-coated carbide tools in milling operations of Inconel 718, demonstrating that it has a greater sensitivity to wear than the cutting forces signals. While Maia et al. [60] correlated it to the tool wear and wear mechanisms using a Power Spectrum Density PSD and auto-covariance method, when turning AISI 4340 steel,

finding that this strategies is effective for the detection of wear mechanisms as the frequencies excited by each mechanism can be accurately determined.

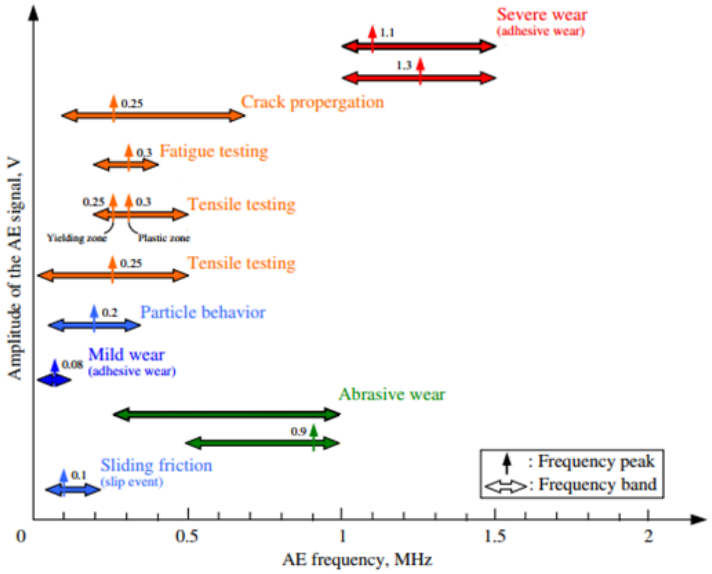

Figure 2.11. Correlation map of AE frequency spectra for phenomenon involving deformation and fracture [54]

Table 2.6. AE signal frequencies of principal wear mechanisms.

Phenomenon	**AE frequency range (kHz)**
Mild adhesive wear [55]	0-120
Severe adhesive wear [55]	1000-1500
Adhesion and dragging [56]	25-110
Abrasive wear [57]	200-1000
Crack propagation [58]	350-550
Plastic deformation [58]	50-150

Lastly also the CNC power consumption [61]and vibration amplitude [62][63] being directly associated to the cutting process can be used. The first one is easier to evaluate because the modern CNC lathes measured it instantaneously and automatically while for the second is necessary to install a vibrometer or accelerometer onto the tool holder, moreover an accurate data elaboration is required both to eliminate possible disturbances associated to other cause and to obtain a clear results.

2.3.2 Surface integrity

The quality and performance of a product is directly related to the surface integrity achieved by the final machining operations, the physical and mechanical properties

alterations may have drastic effects on the operating life of the final product. The correct choice of cutting fluids, cutting parameters, tool coating and geometry represents the parameters on which to intervene to ensure the better surface quality. Unfortunately often the best combinations of the above mentioned parameters do not guarantee the needed productivity especially during the DTC machining.

The main parameters that must be considered in the surface analysis are the microstructure alterations (phase transformations, residual stresses, grains deformations and orientations) and the surface finish (roughness, topography and defects); since both affect the mechanical, chemical and physical surface properties.

The surface roughness is considered to be the primary indicator of the quality of the surface finish, the formation of BUE, initiation of chip plastic side flow and the tool wear are the major factor that affecting its value [64]. However, also the cutting parameters, cooling techniques, cutting tool geometries and the tool and workpiece materials have important influences.

The roughness value, being linked to the tool edge geometry provides information about the tool wear, e.g. as demonstrated in Figure 2.12 its rapid increase indicates an excessive tool degradation making necessary the insert substitution.

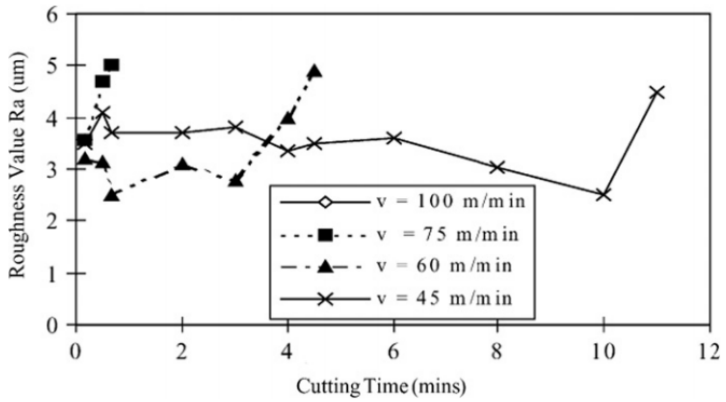

Figure 2.12. Surface roughness values when turning Ti6Al4V using different cutting speed values [65]

Che-Haron et al. [65] noticed that when the tool is fresh, the surface roughness values are found to be higher than with slightly used tools, and the tool wear close to its half-life resulted in slightly decreased surface roughness values than its fresher times. This effect can be considered as the ‘warming up’ of the tool material, because when the tool is first used, there can be micron-level sharp edges or peaks at its surface that can be trimmed out to create a smoother, or at least a better fit contact surface with the workpiece. When approaching its half-life, the tool is more fit to the workpiece that the surface roughness

values decrease. However, after the half-life, the tool starts wearing even more, and this causes anomalies in the tool-workpiece contact surface, which increases the surface roughness values significantly.

Feed rate was declared to be the most dominant parameter to affect the surface roughness, in details its increase often determines a lower surface quality [66]. The cutting speed instead determines different results, e.g. Umbrello et al. [67] found that its increase reduces the roughness value since determines a BUE reduction. On the contrary, Thakur et al. [68] reported an increase in surface roughness with cutting speed, as a consequence of higher tool wear.

Since the residual stresses directly influences the fatigue life they have been considered as one of the most important parameters, the manufacturing process induce residual stresses through plastic deformation and/or thermal gradients created at the tool-workpiece interface. Numerous studies have been conducted to determine its correlation with the process conditions, highlighting that the feed rate, tool rake angle have a strong effect while the depth of cut does not significantly affect their values [69] [70]. Outeiro et al.[71] found that if coated tools were used, the surface residual stresses became less tensile, while the peak compressive residual stresses increased in the compressive direction, as well as occurring at a deeper level (see Figure 2.13).

Also the cooling adopted strategies have an important effect, the reduction of the temperature in the cutting zone limit the thermal contribute, promoting the plastic deformation one. Pusavec et al. [72] demonstrated that in turning of Nickel alloys more compressive tensile stress were obtained using the liquid nitrogen respect to the wet and dry cutting. However a lesser amount of researchers investigated the effect of the cryogenic coolant during the Ti6Al4V semi-finishing turning operations.

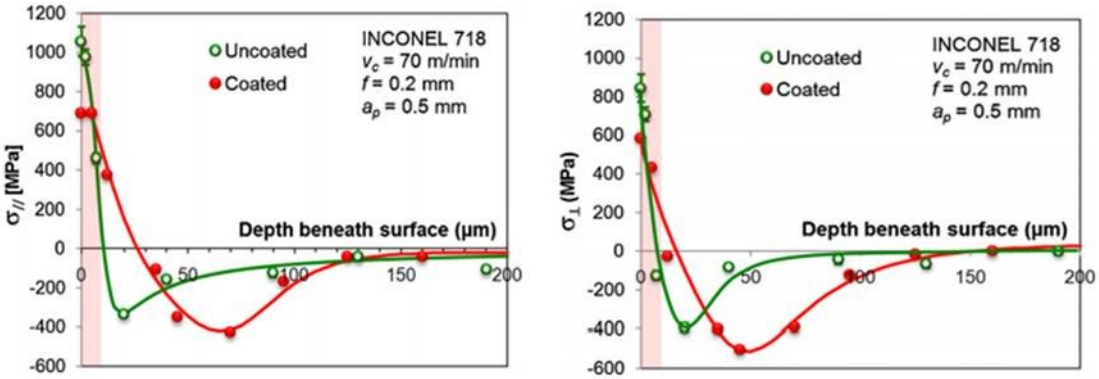

Figure 2.13. Residual stress profile of Inconel 718 samples machined using uncoated and coated inserts.

The altered layer induced by the machining operations can be subdivided in three distinct regions [73] as shows in Figure 2.14: the P1 zone corresponds to the bulk material; clearly, the machining process does not visually affect this part of the material. The P2 zone is affected by the cutting process; the grains rotate in the cutting direction as a consequence of the intense plastic deformation induced by the cutting process. Lastly the P3 zone is just below the free surface of the work piece. The transition between P2 and P3 zone can be recognized by a drastic modification in terms of shape and direction of the grains. The intense plastic deformation induced by the cutting process leads to a thinning and elongation of the grains with an alignment of the grains parallel to the surface. Rotella [74] reported the effects of cryogenic cooling strategies onto the surface hardness founding that it generally increase as a results of grain refinements when a drastic cooling is applied.

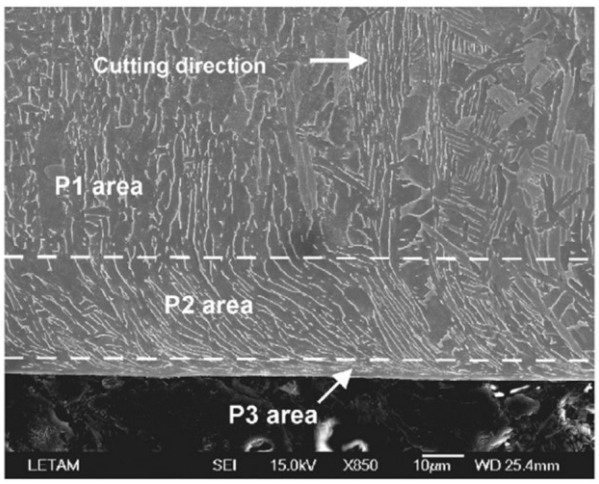

Figure 2.14. Microstructure of the sub-surface layer [73].

A faster and easier experimental investigation that can be carried out to determine the machining effects on the materials microstructure is achieved by measuring the micro-hardness trend along a normal direction with respect to the machined surface.

This analysis gives important information on possible metallurgical alterations that occur during the cutting process, such as aging, work-hardening and grain refinements. Ezugwu et al.'s[75] study reveals that increasing feed rate and depth of cut in their work increased the micro-hardness of the material at both surface and sub-surface locations.

The hardness measurements from machined samples conducted by Sun et al.[76] demonstrated that cryogenic machining induces higher hardness on the machined surface of Ti- 6Al-7Nb alloy, in comparison with dry and flood-cooled machining. The increase was estimable around the 33.6% compared to the dry machining and about 14.7% respect

to the flood cooled one. The authors affirmed that due to the rapid cooling effect with liquid nitrogen, the heat generated in the cutting zone is taken away within a very short time, and the strain hardening effect plays a more dominant role in cryogenic machining as it counters the thermal softening effect with a greater influence in dry and flood-cooled machining. The hardness increase in the machined surface layer is very beneficial to improve the wear resistance of Ti-6Al-7Nb alloys.

The extent of the surface damage that occurs during machining and how it develops are important information since the in-service performances of the machined components are strongly influenced by the state of the surface layers [77]. In literature, a strong emphasis has been paid to characterize surface damages generating during rough milling and turning of wrought titanium and nickel alloys, but very few works are available about finishing turning of DTC alloys. Many variables are involved, such as the ductility of the workpiece material, its microstructure, the tool mechanical properties, and the thermo-mechanical conditions arising during the process; furthermore, the tool wear and cutting parameters significantly affect the machined surface damage [78].

In general, material side flow, double feed marks, long grooves, micro-particles adhered on the machined surface (BUE and chips fragments), tearing surface, cavities and cracks are the typical defects arising by the DTC alloys machining.

The material side flow can be ascribed to the plastic deformation of the surface material induced by the tool motion, enhanced by an increased plasticity provoked by the higher temperatures reached when the most severe cutting parameters were adopted. According to Zhou et al. [79], the grooves are generated by small fragments of the BUE that are randomly detached by the rubbing action, hence, when they pass below the tool flank face, they leave grooves on the softer underlying material.

Ginting et al. [80] in his work described accurately the formation mechanisms of tearing surface. The mechanism is proposed and illustrated in Figure 2.15A, he ascribed this defect to the three bodies contact generated into the tool workpiece interface because of the presence of small parts removed from the cutting tool that are peeled off forming the tool wear, and portions of the Build-Up Edge which is deposited on the machined surface. Since both of these particles are harder than the workpiece material, they cause scratches and tears on the machined surface due to the relative motion between the tool and the workpiece.

Another common surface defects especially in dry machining are the adhered material onto the machined surface. The high temperatures and pressure generated during the cutting process facilitate the welding of BUE and/or chips fragments on to the surface.

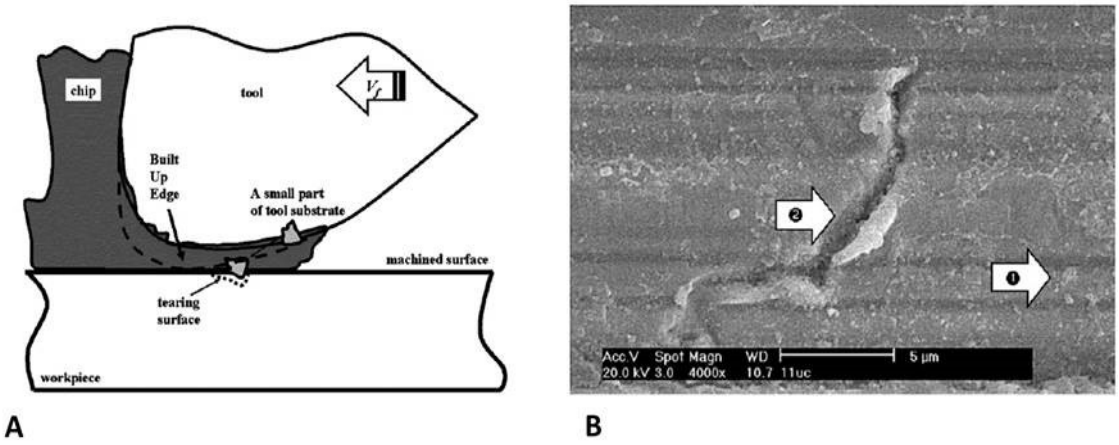

Figure 2.15. (A) The proposed mechanism of tearing surface, (B) tearing surface defect [80].

Many workpiece materials include carbide particles in their structure. As the tool wears, and the workpiece is machined, these carbide particles are sometimes removed from the machined surface or the tool and get stuck on the workpiece surface [79]. This phenomenon is called carbide cracking, and it causes a sudden increase in the shear stress during cutting that leads to surface cavities. This process causes residual cavities and cracks to be formed inside the machined surface, causing even further problems. As a result, carbide cracking can be a serious problem in terms of micro-scale surface integrity. Especially when the depth of cut and feed values are very small, the carbide particle sizes become too close to a concerning level that carbide cracking might gain significant importance in the surface of the end product.

Several studies concluded that the defect dimensions generally are associated to the generated temperature, especially for the Heat resistant and DTC alloys that are characterized by a poor thermal conductivity compared to other metal alloys. The thermal flux that is dissipated through the workpiece encounters more resistance, and higher temperatures are concentrated on its surface. If no coolant is applied, higher temperatures are reached at the workpiece–tool interface making the material softer, thus leading to more surface defects in comparison to wet turning carried out at the same cutting parameters.

2.4 Methods to improve the alloys machinability

Effective methods for lengthening the tool life consist of applying suitable metalworking fluids (MWFs) to the cutting zone as well as using proper cutting tools with engineered coatings whose choice must be function of the cutting parameters. In the following paragraphs a literature review of the state of art both of the innovative cooling, lubricating and hybrid technologies and the effects of different coatings are presented.

2.4.1 Cooling and Lubricating techniques

Traditional methods to increase the metal alloys machinability include the use of proper metalworking cutting fluids. The main requirements as stated by Anton et al. [81] are:

- dissipation of heat produced during the cutting process (coolant function);
- cooling of the machine, workpiece, fixture and tool;
- reduction of friction (lubricant function);
- favouring the chip break and chip transport (assistance in chip flow);
- reduction of the built-edge formation;
- corrosion protection for machine and workpiece;

According to DIN 51385 standard [82] the MWFs can be classified in two main families following their composition as oil-based or water based. Specific properties are achieved by adding specific chemical additives. The Figure 2.16 shows the MWFs classification and includes some typical classes of additives.

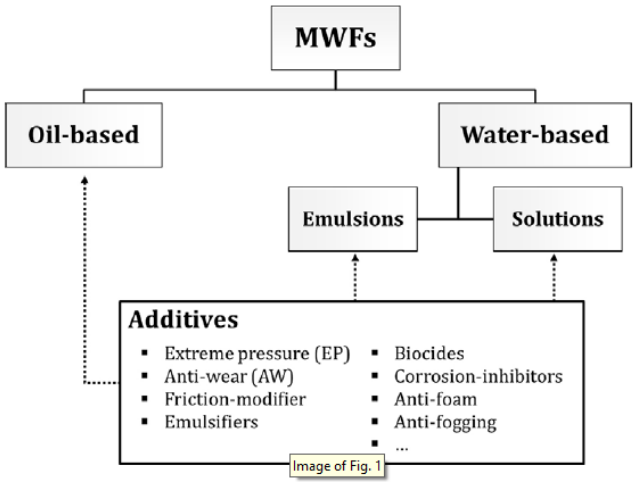

Figure 2.16. Classification of the MWFs types according to DIN 51385 [82]

The functionality and stability of MWFs are ensure by a number of additives such as anti-wear, friction modifier, corrosion inhibitors, biocides, emulsifier, etc., the most common ones are summarized and described in Table 2.7.

Table 2.7. Compilation of additives used in MWFs [83].

Additive type	**Mode of action, function**
Anti-aging-additive, oxidation inhibitor	Prevention of oxidation of base oil at high temperatures and stabilization
Anti-wear additive, AW	Reduces abrasive wear of rubbing surfaces by physic absorption
Biocides	Prevention of excessive microbial growth
Detergent, dispersant	Prevents build-up of varnishes on surfaces, and agglomeration of particles to form solid deposits, promotes their suspension
Emulsifier	Emulsion formation and stabilization
Extreme pressure additive, EP	Protection against wear by formation of adsorption or reaction layers, prevent micro-fusing of metallic surfaces
Foam inhibitor	Destabilize foam in oil
Friction modifier, FM	Lowers friction and wear, improve adhesion of lubricating film
Metal-deactivators	Adsorptive film formation
Passive extreme-pressure-additive, PEP	Kind of solid lubricant, surface separation by film formation
Corrosion inhibitor	Limits rust and corrosion of ferrous and non-ferrous metals (prevention of oxidation)
Viscosity index improver, VI	Increases viscosity index of the lubricant

However, the extensive use of large quantities of these additives and cutting fluids raises several environmental and human safety issues, as reported by Aggarwal et al. [84]:the conventional cutting fluids presents the following limitation :

- Environmental pollution due to chemical dissociation/break-up of cutting fluid at high temperature;
- Biological (dermatological) problems to operators like skin and breathing problems coming in physical contact with cutting fluid;
- water pollution and soil contamination during disposal;
- requirement of extra floor space and additional system for pumping, storage, refining, recycling, cooling, etc.;

- cost of disposal of cutting fluids is becoming higher as environmental regulations are becoming tougher;

Due to this problems, to the stricter and stricter regulations imposed by the international agreements) and to its elevated costs (metal-working fluids cost ranges from 7 to 17% of the total machining cost [85]), the concept of sustainability manufacturing has become of great interest within the international community; therefore, the manufacturing companies are nowadays exploring new solutions to reduce or completely eliminate the conventional cutting fluids in favour of more efficient, less polluting and cheaper technologies.
In the recent year several work proposed different solutions able to achieve these goal, in details two strategies have been widely studied and in some cases also used in industrial machining process, namely the Minimum Quantitative Lubrication (MQL), and a low temperature cooling-assisted machining, as described in the following paragraphs.

2.4.1.1 Low temperature cooling-assisted machining

In order to reduce the cutting temperature the scientific literature proposes several approaches based on the use both of alternative and environmental friendly low-temperature coolants such as Liquid Nitrogen (LN2), Carbon Dioxide (CO2) and compressed cooled air. Some potential benefits of low-temperature assisted machining are [86]:

- sustainable machining (a cleaner, safety, environmental friendly method);
- increased material removal rate (MRR) with no increase in tool wear and with reduced cutting tool change over cost, resulting in higher productivity;
- increased tool life due to lower abrasion and chemical wear;
- improved machined part surface integrity with the absence of mechanical and chemical degradation of the machined surface;

The low-temperature cooling method is mainly classified in four categories, namely workpiece pre-cooling, indirect cooling, jet cooling and cutting tool treatment.
The first method consists to cool the workpiece before the machining in order to have its properties changed from ductile to brittle making thus easier the chip breaking [87]. However those studies conclude that this approach is not efficient for three reasons: 1) metals tend to increase in hardness and strength at cryogenic temperature; 2) exposing the workpiece at low temperature may increase the abrasion to the cutting tool; 3) precooling the workpiece will increase the cutting forces. In addition, for dimensional accuracy and

distortion reduction, it is best to maintain the workpiece at constant room temperature to avoid thermal expansion/shrinkage effects [88]. As for the indirect cooling strategy only the cutting insert is cooled by an internal fluid circulation system, in this way the workpiece properties do not undergo significant changes providing the better performance machining. However, the effects of this approach is highly dependent on thermal conductivity of the cutting tool material, the distance from the LN2 source to the highest temperature point at the cutting edge and insert thickness. It can be more effective if a larger area of the tool insert is in contact with LN2 [88].

In jet cooling the low-temperature cutting fluid is applied in the cutting zone, particularly tool-chip interface by using nozzles (rake and flank tool faces) as shown in Figure 2.17. This method presents distinct advantages, the cooling power is not wasted on any unnecessary areas, without modify the workpiece properties thus resulting in a prolonged cutting tool life and better product quality [69]. In addition the low-temperature fluid cannot circulate inside the machine tool like the conventional ones risking to damage it, as it is released into a normal atmospheric pressure and absorbs heat during the cutting process, it quickly evaporates.

Lastly the cryogenic treatment in which the cutting tool is cooled down and maintained at the cryogenic temperature for a long time and then heated back to the room temperature to improve wear resistance and dimensional stability [90]. However, the effects of cryogenic treatment on cutting performance are not stable for all cutting conditions and machining applications [91].

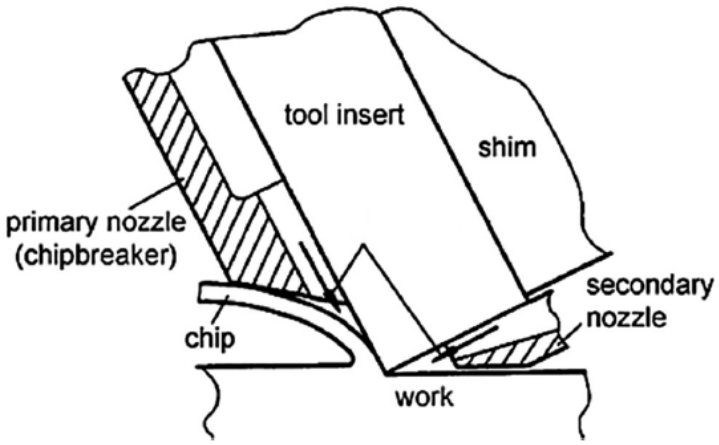

Figure 2.17. Schematic illustration of jet cooling approach [88].

Typically one of the following cryogenic fluids is adopted: liquid nitrogen, liquefied oxygen frozen carbon dioxide and air cryogenically cooled. Nevertheless in most cases,

under the term cryogenic machining LN2 and LCO2 are proposed as cryogenic fluids, although both are stored as a liquid several differences are present. Liquid nitrogen boils at -195.8°C at atmospheric pressure; carbon dioxide instead is a refrigerated liquefied gas. At room temperature it can be held liquid by a minimum pressure of 57 bar, when it fuses with the ambient air, the instantaneous pressure drop causes a phase transformation forming a mixture of solid (dry ice) and gaseous state, at the ratio approximately of 45% and 55%, respectively, at the temperature of -78.5 °C.

Both the above mentioned solutions represent innovative environmental friendly strategies since spontaneously evaporating leave the machined product surface clean eliminating the post-process cleaning step needed instead in conventional lubrication to eliminate the pollutant residues. However the use of CO2 presents some criticalities, it is one of the greenhouse gas responsible to the climate change, what is more, CO2 has slightly irritating odour, is colourless and heavier than the air. Both LN2 and CO2 can cause serious problems to workers safety unless proper air exchange is assured, their excessive concentration in the working environmental may determine inert gas asphyxiation associated to the reduction of oxygen concentrations. Comparing both gases from the operator's safety point of view, there are regulations that OSHA's [92] carbon dioxide exposure limit in the breathing atmosphere is 0.5%, while the increase of N2 level in the air should not cross the 2%. Additionally, as an opposite of carbon dioxide, which is 1,5 times as heavy as air, nitrogen is lighter than air an is not concentrated at low levels (working environment).

Lastly also the cooling capacity of the LN2 defined on the basis of its boiling point, latent heat of vaporization, sensible heat to heat up the gas estimable around 428 kJ/Kg is higher than the liquid CO2 (347 kJ/Kg), making it the preferred coolant to implemented the machining of DTC alloys.

Most of the studies presented in literature studied the influence of the LN2 onto the tool wear, in particular examined the flank wear since it is frequently used to define the tool life criterion. Several materials were tested, although currently the most studied are stainless steels, the heat resistant alloys and the difficult-to- cut alloys such as titanium, tantalum, cobalt or nickel due to their low machinability.

Bicek et al. [93] reported that the cryogenic machining of normalized bearing steel AISI 52100 prolonged tool life for 370%, while turning hardened bearing steel the improvement is increased for approximately 15%. Sun et al. [94] used in their machining

experiments the innovative Ti5553 titanium alloy, finding that the thrust forces generated from cryogenic cutting were reduced up to 30 % compared with that of flood-cooled and MQL machining. Also the nose wear of the insert was improved in cryogenic machining due to reduced material adhesion.

However in the last years the Ti6Al4V alloy has received particular interest, especially in heavy rough operations due its low machinability and its wide use in aerospace, chemical automotive, etc. fields. The advantages in term of tool life increment were well documented by several works presents in literature, both Venuopal et al. [95] and Khan et al. [96] highlighted as the growth of the tool wear, at moderate cutting speeds was effectively hindered, while at higher values the benefits were decreased possibly to improper penetration of cutting fluids in the chip-tool interface. Bermingham et al. [97] reported that both liquid nitrogen and high pressure emulsion are effective coolants and extended tool life significantly over dry cutting. Though the high pressure emulsion determined slightly better advantages than those obtainable by means of LN2 cooling being it less sensitive to the coolant nozzle position.

A similar results in terms of tool wear were detected also using carbon dioxide snow as cutting fluids [98], [99] making it a potential alternative. Cakir et al. [100] affirmed that the CO2 gases produce the better surface finish of the machined product, the lower friction coefficient and cutting forces respect the use of other gases as cutting fluids. Jerold et al. [101] compared the LCO2 and LN2 in turning of AISI 1045 steel, its work highlighted that the LN2 use reduced the cutting temperature about 34% and 17% when compared to wet and CO2 machining conditions respectively, while the lowest cutting forces were measured under CO2 conditions, where the percentage reduction overtakes about 38% and 12% respect to the wet and LN2 cases. Also the better surface finishing and chip control were reported applying the CO2.

To overcome the problems of the machine operator safety associated to the oxygen lack resulting by the use of inert gas, the use of cryogenic cooled air cooling represents an interesting solution. Publication by Sun et al. [102]showed that the cryogenically cooled air method is safe, easy to apply and also capable of generating high air flow rates with very low temperature. The cryogenic compressed air was generated by passing the compressed air through a coiled copper tube which was immersed inside a LN2 Dewar, as shown schematically in Figure 2.18. The presence of moisture in the compressed air will

crystallise and block the copper tube, for this reason it is essential that an air dryer is incorporated in the air supply line.

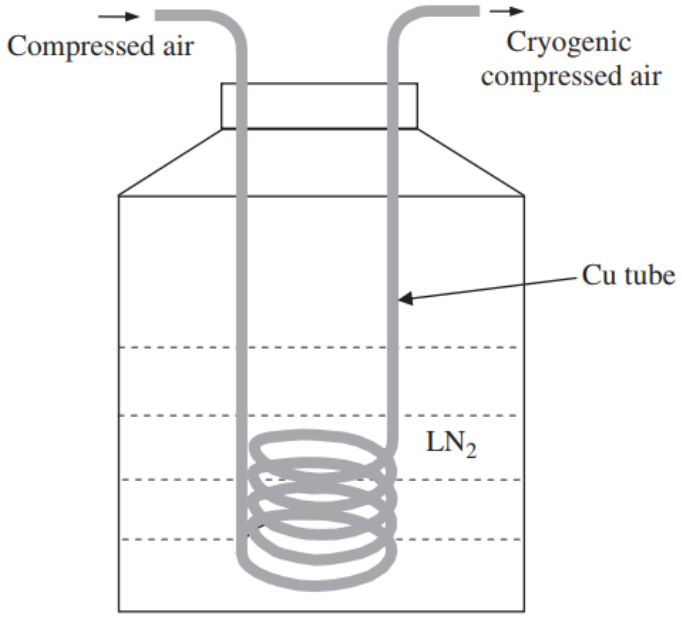

Figure 2.18. Schematic illustration of cryogenic cooling compressed air strategy [103].

The turning experiments conducted on to the Ti6Al4V alloy confirmed that this solution produces tool life improvements and cutting forces reduction as observed using the other cooling strategies. In details under dry machining at a cutting speed of 150 m/min the tool failure mode is the flank wear while at 220 m/min the tool fails as a result of plastic deformation at the tool nose radius. In both cases the application of cryogenic compressed air reduces this mechanism, the low temperature inhibits the adhesive mechanisms and the material thermal softening responsible both of the higher friction coefficient and thus tool degradation.

2.4.1.2 Minimum Quantity Lubrication (MQL) machining

Minimal quantity lubrication is a recent technique introduced in machining (in particular, in drilling) to obtain safe, environmental and economic benefits in metal cutting. In details it was developed to merge the advantages of both dry and wet cutting, allows to reduce the cutting fluid consumption nevertheless ensuring the lubricating effects. Figure 2.19 shows the schematic view of MQL delivery system, which consists in spraying a small quantities of cutting fluids in the form of aerosol using pressurised air into the cutting zone at very high velocity (100m/s).

Two different mixing methods can be used: mixing inside nozzle and mixing outside nozzle. Using the mixing inside nozzle equipment, pressurized air and lubricant are mixed into the nozzle by a mixing device, as shown in Fig. 2.20a. Lubricant performs the lubrication action, while the pressurized air that reaches the cutting surface performs cooling action. This method has several advantages. Mist and dangerous vapors are reduced and the mixture setting is very easy to control. In the mixing outside nozzle method as shown in Fig. 2.20b the mixture is obtained in a mixing device positioned in a specific tank. In this method, lubrication between workpiece and tool can also be achieved [105].

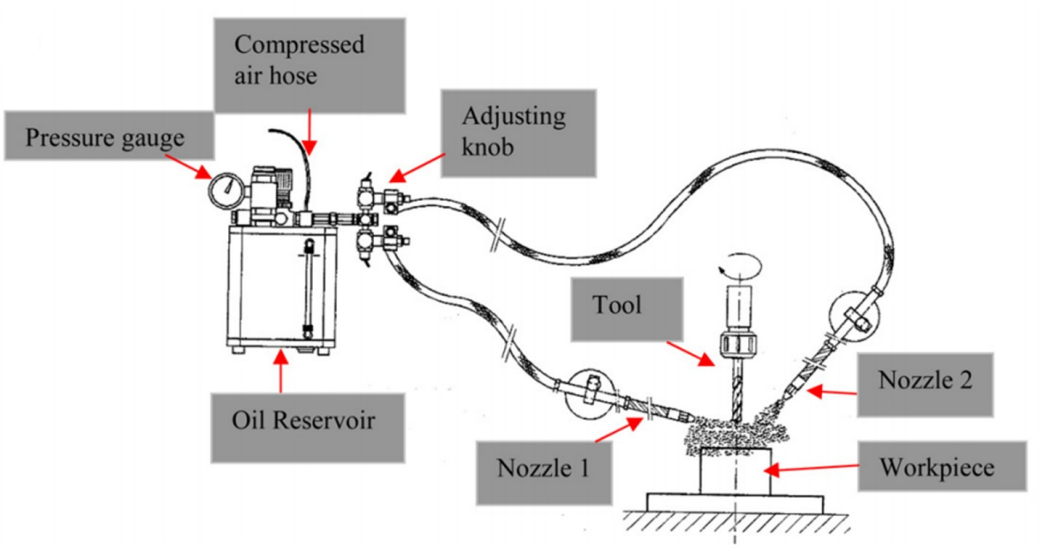

Figure 2.19. Schematic view of MQL delivery system [104].

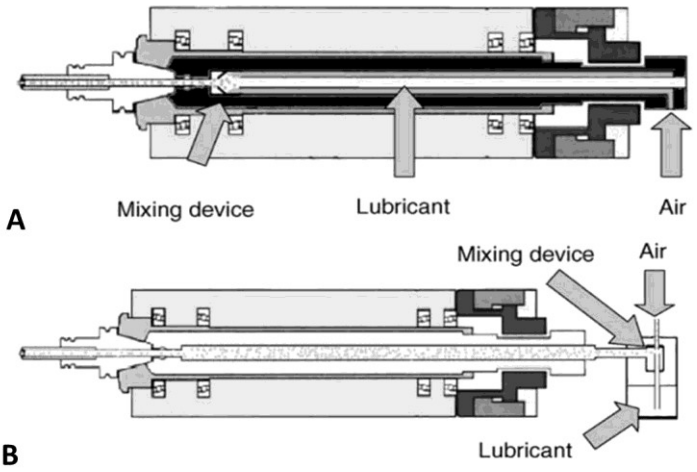

Figure 2.20. Mixing methods. (A) inside and (B) outside the nozzles [105]

The supply and disposal costs are reduced because the flow rate is between 50 ml/h and 250 ml/h, which is several order of magnitude lower than the traditional lubrication that has a flow rate of tens of litres per hour [106][107].

MQL fluids are divided into two main groups: synthetic esters and fatty alcohol. Synthetic ester (vegetable oil) is more commonly used because it presents a good lubricating proprieties, high flash and boiling points. However, the fatty alcohols achieve better heat removal and when vaporized, producing little in terms of waste compared to synthetic ester. Synthetic ester usually used in operations where lubrication is a key requirement for cutting fluids, while the fatty alcohols are used in applications that require cutting liquid for heat removal [108]

Table 2.8. Characteristics of MQL fluids [109]

Synthetic ester	Faddy alcohol
• good biodegradability; • low level of hazard to water; • toxicologically harmless ; • high flash and boiling point with low viscosity; • very good lubrication properties; • good corrosion resistance; • inferior cooling properties; • vaporizes with residuals;	• good biodegradability; • low level of hazard to water; • toxicologically harmless; • low flash and boiling point, comparatively high viscosity; • poor lubrication properties; • better heat removal due to evaporation heat; • little residuals;

Sreejith et al. [110] investigated the effects during machining of 6061 aluminium alloys testing different cutting speeds values (up to 400 m/min) under different conditions, namely dry, MQL and flooded coolant/lubricant using diamond-coated carbide inserts, finding that the MQL strategy produces results in terms of tool wear, surface roughness and cutting forces comparable with that of wet condition.

Dhar et al. [111] evaluated the effect of minimum quantity lubrication on tool wear and surface finish in turning of AISI 4340 steel alloys. As shown in Figure 2.21A the rate of average principal flank wear is decreased using MQL technique. The cause behind reduction in VB observed may reasonably be attributed to reduction in the flank temperature, which helped in reducing abrasion wear by retaining tool hardness and also adhesion and diffusion types of wear which are highly sensitive to temperature. While, it appears from Figure 2.21B that surface roughness grows quite fast under dry machining due to more intensive temperature and stresses at the tool-tips, MQL appeared to be effective in reducing surface roughness. However, it is evident that MQL improves surface finish depending upon the work–tool materials and mainly through controlling the

deterioration of the auxiliary cutting edge by abrasion, chipping and built-up edge formation. As reported by Attanasio et al. [106] also the nozzle position influences the tool wear. Lubricating the tool rake surface does not produce evident improvements, while positioning the MQL nozzle towards the flank surface determines a significant tool wear reduction. Elmunafi et al. [112] found that MQL can be a good technique in turning hard stainless steel using coated carbide cutting tools when machine at speed of 170 m/min and feed rate = 0.24 mm/rev. However, machining under the MQL technology seems to be limited by cutting temperature, because at high speed the oil mist may evaporate without lubricating the cutting zone.

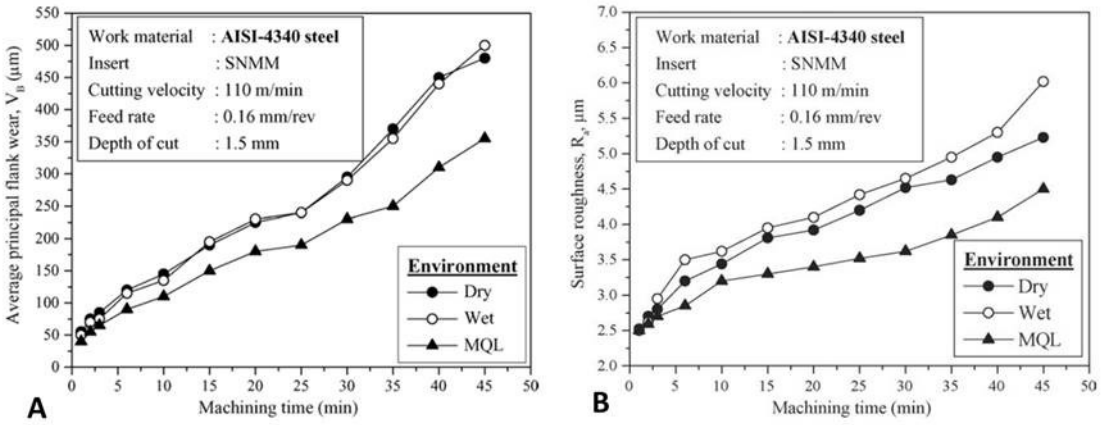

Figure 2.21. Progression of average principal flank wear and surface roughness [111].

Several work stated that although MQL is often used its low cooling capacity limits its application [94][113], especially when machining difficult-to-cut alloys such as titanium, cobalt or nickel alloys, where high dimensional accuracy and machined surface quality are mandatory, the conventional flood strategies still represent the best solution since they allow an efficient cooling of the cutting zone limiting the thermally-activated tool wear mechanisms responsible of the cutting edge alteration [114][115].

To improve the cooling effect of the MQL techniques two strategies have been recently proposed: one makes use of low-temperature fluids, such as Liquid Nitrogen (LN2), Carbon Dioxide (CO2) or cooled air, to provide a hybrid technology in which the tool flank face is lubricated and the rake one cooled simultaneously (techniques named as Minimum Quantity Cooling Lubrication (MQCL) [116]), while the other aims at improving the oil heat transfer characteristics thanks to specific additives [117].

A few literature works demonstrated the feasibility of the MQCL methods reporting important improvements with respect to pure cooling and pure lubricating strategies in case of hard machining of steel and DTC alloys. Pereira et al [118] tested the Minimum Quantity Lubrication in combination with the LN2 (CryoMQL_LN2) and CO2 (CryoMQL_CO2) respectively, in hard turning of AISI 302 stainless steel. The Figure 2.22 shows the tool life results using the dry cutting as reference, the other alternatives checked improve the tool wear behaviour.

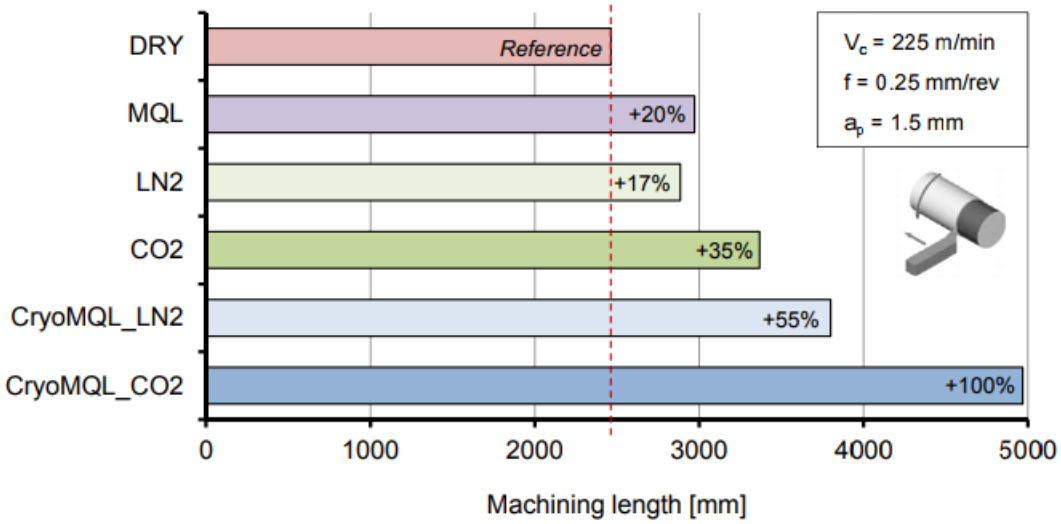

Figure 2.22 Tool life using different near-to-dry machining techniques on AISI 304 [118].

For example, using MQL the tool is capable of machining = 2900 mm before the end of the tool life that represent a percentage increase on tool life around 20%.Using CryoMQL techniques, results are notably better: 55% improvement in tool life using LN2+MQL and more than 100% using CO2+MQL (approximately double tool life). High temperatures during DRY machining imply lower tool life due to thermal effects on tool wear.

Maruda et al. [119] presented a comprehensive analysis of the effect of MQCL technique with phosphate ester-based EP/AW additive on the wear of P25 cemented carbide cutting tool in turning of AISI 1045 carbon steel. The authors reported that the tribofilm created when using this particular strategy reduces adhesion-diffusion and chemical wear as opposed to dry machining and pure MQCL method. The largest differences in wear between MQCL + EP/AW method and MQCL method were observed (ca. 34% for vc = 50 m/min and 27% for vc=350 m/ min), i.e., when high temperatures occur in the cutting zone. For low cutting speeds (vc=250 m/min), the differences between individual VBmax values and crater dimensions on the rake face did not exceed 12% flank wear

reduction. Zhang et al. [120] machined Inconel 718 in end-milling using as coolant in MQCL method cryogenic air cooling, also in this case a significantly tool wear rate reduction and a tool life extended were detected compared to the dry cutting.

The second solution, named Solid Lubricant (SL)-assisted MQL strategy, is nowadays receiving wider attention since it allows a drastic improvement of the fluid performances by controlling both the heat generation and the friction between the tool and workpiece without significant increase of the process costs, and, at the same time, it also avoids those issues related to the use of cryogenic temperatures as happens when using the aforementioned hybrid techniques. Various examples can be found with respect to the lubricant type, particles dimensions and concentration, developed on the basis of the metal alloy to be machined and the peculiar machining operation.

Graphite and molybdenum disulphide (MoS2) are the predominant materials used as solid lubricant, their tendency to create a solid thin lubricant layer onto the workpiece and tool material surfaces, parallel to the cutting direction prevent the surface contact resulting in the friction coefficient reduction. Dilbag et al. [121] reported as the surface roughness during hard turning of bearing steel with mixed ceramic tools was significantly reduced respect the dry condition. Also Reddy et al. [122] found a similar behaviour in milling of AISI 1045 steel using a coated carbide, the experimental findings revealed as the cutting forces, specific energy, surface quality and chip size were reduced. The studies conducted using WS_2, CaF_2, TiN, etc. testing both different machining process (grinding, turning, milling, etc.) and material (aluminium, steel, titanium etc.) confirmed the reduction of friction coefficient (tool wear) respect both the dry and pure MQL condition [123][124].

In the last years, thanks the rapid advances in nanotechnologies the use of nanoparticles as additives has become the most interesting solution in order to improve the cutting fluids properties. A Nanofluid, introduced for the first time by Choi [125], can be produced by dispersing a typical size of less than 100 nm of metallic or non-metallic nanoparticles or nanofibers in a base liquid such as water, ethylene, glycol or oil. A significant improvement in the transport properties, viscosity and heat transfer characteristics of the base fluid was observed, making the nanofluids a perfect candidate for the MQL techniques. Ay et al. [126] affirmed that during the cutting process the fluid's thermal properties play an important role because they affect the machining precision such as thermal expansion and surface roughness as well as tool wear. According to Teng et al. [127] and as well as the study of Ravikanth et al. [128]

demonstrated that the thermal conductivity of nanofluid depends strongly on the volume fraction and properties of nanoparticles added. For example as reported by Liu et al. [129] the use of Cu nanoparticles at 0.1% vol. increased the thermal conductivity of the pure fluids by 23.8%, while as reported by Vajjha et al.[130] the addiction of 6% in vol. of Al2O3 in base fluid produce an improvement of 22.4%.

Also the size, form and diameter of the added particles have a significant effect on heat transfer capacity [131][132], as concluded from Yoo et al.[133] in his investigation that the ratio of surface and volume of nanoparticles may be the primary factor that affects thermal conductivity of nanofluids. Sharma et al. [134] reported as the thermal conductivity, viscosity and density of nanofluids are improved with increase of Al2O3 concentration (see Figure 2.23), moreover reported as in turning of AISI 1040 steel the addiction of 1% of Al2O3 nanoparticles into the MQL fluid produced an improving in machining performance in terms of tool wear up to 63.9%, 44.9% and 5.27% with regard to dry, pure MQL and conventional wet condition, respectively.

Moura et al.[135] demonstrated as the application of solid lubricant for turning of Ti6Al4V has resulted in increase of tool life. Tool life improves dramatically due to the fact that the solid lubricant is able to penetrate to the chip-tool interface and perform both the lubrication and cooling functions, in particular the lubricant function reducing thus the frictional effects, compared to that of dry and wet machining.

Also the cutting temperatures influence the solid lubricant choice: below 500°C, graphite, transition metal dichalcogenides (e.g. molybdenum and tungsten disulphides) and polymers can represent the best solution, on the other hand, fluorides, oxides and sulphates (e.g. CaF_2, No, Cu, $CaSO_4$, etc.) proved to be good candidates to work at higher temperatures [136][137].

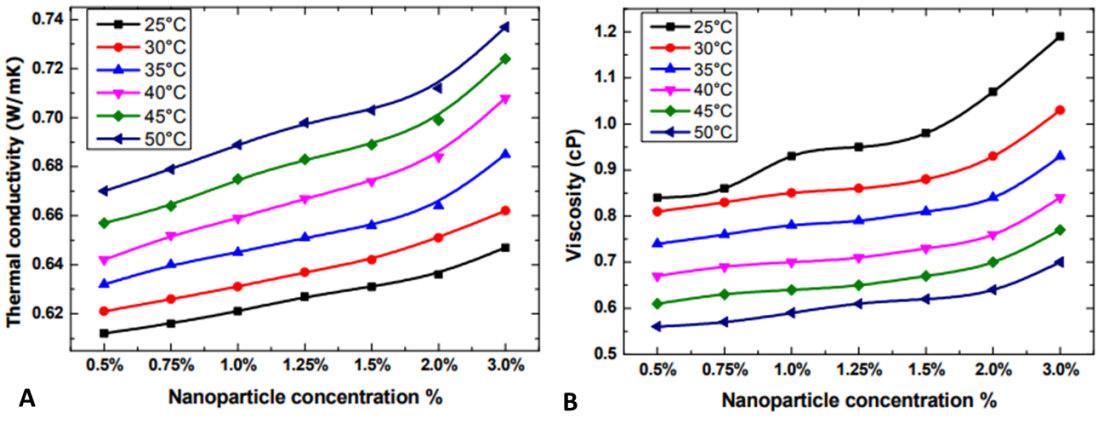

Figure 2.23. (A) Thermal conductivity w.r.t. nanoparticle concentration, (B) Viscosity of nanofluid with regards to. nanoparticle concentration [134].

2.4.2 Tool cutting coating

The second method to improve the DTC alloys machinability consists of adopting surface engineered tools: the scientific literature suggests that the tool inserts should exhibit characteristics of hot hardness (to maintain sharp and stable the geometry of the cutting edge at elevated temperatures), thermal shock resistance (not to be affected by the cyclic heating and cooling), low chemical affinity (to limit the Build-Up-Layer formation), oxidation resistance (to resist at the accelerate wear rate at elevated temperatures) and toughness (to withstand high cutting forces and mechanical socks) [138]. There are several groups of materials used for manufacturing cutting tools as shown in Figure 2.24, namely super-hard materials, ceramics, cermet, carbides and high speed steel.

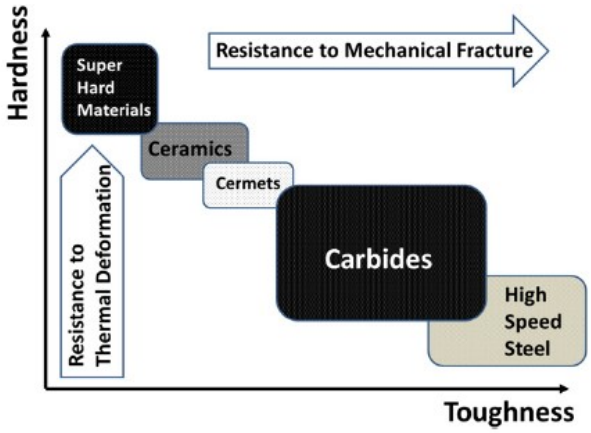

Figure 2.24. Material classification for manufacturing cutting tools**.**

The super hard materials such as diamond and cubic boron nitride present the highest hardness and thermal deformation resistance but also a low toughness and significant vulnerability for chipping making them suitable to machining carbon composites, hardened steel and high temperature alloys. At the bottom right side of the map the high speed steel have an excellent toughness and fracture resistance but their lower deformation resistance drastically reduce they use at few industrial cases in which is necessary avoid the chipping or premature breakage of the cutting edge during the machining operations.

The most common inserts used in machining are made of cemented carbide (WC) with cobalt as metal binder, its intermediate position in the hardness-toughness map guarantees a balanced combination of the required proprieties resulting in excellent wear resistance.

The WC/Co tools are thus suitable for machining an extensive variety of materials in a wide range of cutting conditions. However during machining of DTC alloys such as titanium or cobalt at the high cutting speeds the WC is subjected to a rapid deterioration due to its chemical reactivity that actives the adhesion and diffusion wear mechanisms [139]. The studies of the effects of the WC grains dimensions onto the tool wear resistance highlighted that finer grains improved the tool life with respect to coarser ones [140]. Another way to improve the surface characteristics of the cutting inserts is based on the use of coatings deposited by means of Chemical Vapour Deposition (CVD) and Physical Vapour Deposition (PVD) techniques, able to reduce both the friction coefficient, thanks to their self-lubricant properties, and the wear mechanisms since they present chemical inertness and high mechanical properties. Nowadays it is mainly CVD processes that are used for deposition of tool-coatings, although the main disadvantages of this technology are the high thermal loads imparted to the substrate as well as the thermal stresses in the interface due to the high temperatures during deposition ($T > 800°C$). The main characteristics of PVD process instead are low substrate temperature during deposition ($300°C< T < 500°C$), as well as a great flexibility of possible target materials. TiN, TiCN, TiC, TiAlN, Al_2O_3, TiB_2 are common materials used in single, multiple and nano-layers to enhance the DTC alloys machining performances: their influence on the tool life and surface integrity of the machined components have been extensively investigated, highlighting how the best solution does not exist, but it changes as a function of the machining operation (milling, turning,..), workpiece material, cutting parameters set (feed rate, cutting speed and depth of cut), and cooling strategy (dry, wet, MQL etc.). The coating properties are mainly influenced by two factors: the chemical composition and the structure. The possible coating architectures obtainable especially using the PVD techniques are monolithic, multi-layer and nanostructured coatings.

The proprieties of monolithic coatings depend almost exclusively from the used material (chemical composition, grain dimensions and anisotropy). The table 2.9 reports the main characteristics of common single-layer tool coatings.

A typical multi-layer coating consists of several monolithic coatings where each layer counters different wear mechanisms; the mechanical and thermal proprieties of the resultant coating exceed that of the sum of individual single-layer, with a significant enhancement of the tool performance in the target application. The number of the possible layer combinations is almost unlimited, the multi-layer coatings enable the generation of

more favourable characteristic combinations. The conceptual design of a coating to resist the combination of mechanical and thermal loads is presented in Figure 2.25: a multilayer in which each layer has good oxidation resistance, hardness, and thermo-chemical stability to minimize crater wear, that are separated by strong boundaries to delay and deflect propagation of the notch.

Table 2.9. Characteristics of most used coatings [141].

	Chemical stability	**Oxidation resistance**	**Room temperature hardness**	**Hot hardness**
Best	Al_2O_3	Al_2O_3	TiC	Al_2O_3
	TiAlN	TiAlN	TiCN	TiAlN
	TiN	TiN	Al_2O_3	TiN
	TiCN	TiCN	TiAlN	TiCN
Worst	TiC	TiC	TiN	TiC

To improve the interlayer cohesion and adhesion to the substrate reducing thus the delamination phenomenon, the multilayer often includes bonding layers.

As example in the Figure 2.26 the cross fracture image of Al2O3-coated cemented carbide is reported, the cobalt-enriched layer ensures higher toughness and fracture resistance, the TiC layer a good adhesion with the WC/Co substrate, the Al_2O_3 both the excellent high-temperature resistance and excellent protection against the adhesive and diffusive wear and lastly a TiN layer that is a wear indicator

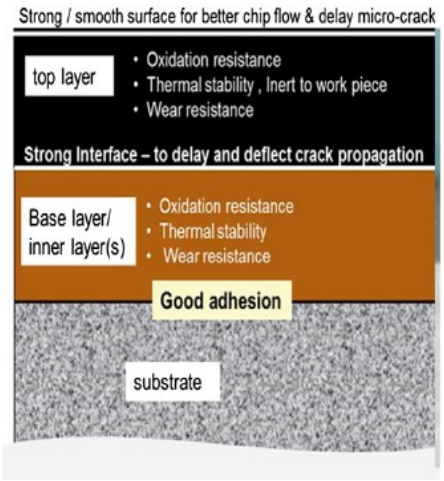

Figure 2.25. Conceptual design of the multilayer coating.

. The nano-layered films [142]and the nanocomposite films described by Veprek et al. [143] opened a new path to the design of coatings with tailor made properties. The properties of both coatings depend on their parent materials and their structures on a

nano-meter scale. For example the nanocomposites obtained embedding hard grains such as TiSiN, TiAlSiN or CrAlSiN with diameter less than 20 μm in an amorphous matrix thanks the formation of protective oxide layers highlights an astonishing high temperature strength and oxidation resistant [144], [145].

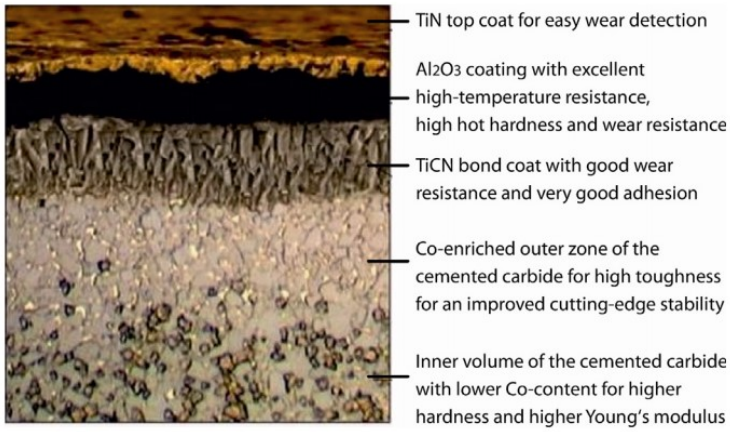

Figure 2.26. Multilayer composite of an Al2O3-coated index able insert made of graded cemented carbide. Source: Sandvick Coromant AB, Sweden

One example of nano-laminate coating is TiAlN/TiN multilayer that combines the hot hardness of TiAlN and the toughness of TiN [146]. Other multilayer coatings include dopants, such as Si and Cr for simultaneously enhance the hardness and toughness, the bulk of the coating is a TiAlN/ AlCrTiN nanolayer, with a top layer of AlCrN to improve chip flow, and another AlCrN layer at the interface, for good adhesion to the substrate (see Figure 2.27).

The effects of the different tool cutting coatings onto the machining performances were widely evaluated in several works present in literature. However, as the obtained results are linked to specific case study can their extrapolation results to be critical, for example varying the cutting parameter set or the cooling strategy the results could vary enormously. The following some interesting case studies are reported:

The Sahoo's [147] work deals with a comparative study on flank wear, surface roughness, tool life, volume of chip removal and economic feasibility in turning high carbon high chromium AISI D2 steel with multilayer MTCVD coated [TiN/TiCN/Al2O3/TiN] and uncoated carbide inserts under dry cutting. He observed that the chipping is the main wear mechanism for uncoated insert while the abrasion for the coated one. The high observed erosion wear resistance associated to the TiN layer (i.e. 3 times better than uncoated carbide insert) determined a tool life improvement approximately about 30 times and thus productivity increase. It can be seen that the total machining cost per part

using TiN coated inserts is considerably lower than that of uncoated carbide tools. Depending on the machine down time, considerable savings in machining costs using TiN coated inserts is 90.5% in machining, taking flank wear limit of 0.3 mm. The enhanced tool life due to the coating minimizes the downtime and therefore provides more savings.

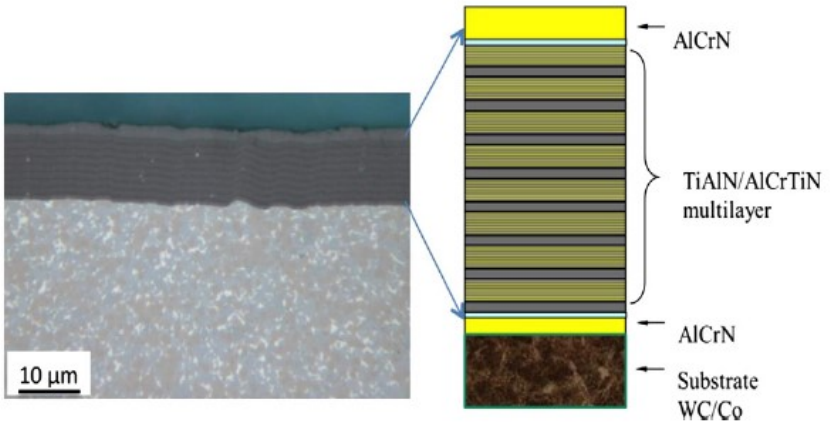

Figure 2.27. Schematic description and image of a tri-layer AlCrN/TiAlN/AlCrTiN coating.

Özel et al. [148] tested the performances of uncoated, TiAlN coated, CBN coated and multi-layer CBN + TiAlN coated tungsten carbide inserts during rough turning the Ti6Al4V alloy, evaluating the machinability in terms of cutting forces and tool wear. The results highlighted that CBN and TiAlN + CBN coated WC/CO inserts, although exhibited the largest cutting forces at the highest cutting speeds, showed favourable wear development. Tool wear zone measurements show that CBN coated WC/Co inserts present a smallest wear zone, consequently it may lead to reduction in tool wear dry machining of titanium alloyed Ti–6Al–4V material.

The relation of microstructure, mechanical properties and titanium cutting performance of the TiAlN, TiAlSiN and TiAlN/TiAlSiN coatings were evaluated by Sui et al. [149]. Their work reported that: (i) TiAlN/TiAlSiN composite coating present the highest hardness value. (ii) The addiction of Si element to the coating determined both a morphology coating change from columnar to nanocrystal and a grain size refining. This nanocrystal structure suppressed the propagation of cracks in the coating and makes the crack morphology form a type of relatively regular and straight, which means good fracture toughness. (iii) The main detected wear mechanisms in turning titanium are adhesion and chipping. The TiAlSiN coating thanks it dense structure, high hardness and good oxidation resistance produced the best results especially when high cutting speeds were used.

2.5 Ti6Al4V machinability

Titanium alloys are being extensively used in numerous fields such as aerospace, biomedical, military and petrochemical thanks to their excellent mechanical and physical properties, and high corrosion resistance at elevated operating temperature associated to their low density. On the other hand, they are classified as Difficult-To-Cut (DTC) alloy [17] due to their poor machinability attributable to the high temperature generated in the cutting zone as a consequence of their low thermal conductivity [150], strong chemical affinity with the conventional cutting tool materials [34], high stresses generated as a consequence of the short chip-tool contact length [151] and low Young's modulus, as well as due to the characteristic saw-tooth shape of the chip resulting from adiabatic plastic deformation [152].

A number of studies have been focused on investigating the dominant tool wear mechanism when machining Ti6Al4V alloys using tungsten carbide inserts while turning, highlighting that the adhesion, diffusion and abrasion are the main tool wear mechanisms. In particular, abrasion mainly involved the tool flank face, while adhesive and diffusive wear affected the tool rake face with the formation of the characteristic wear crater. Being the temperature the parameter that mainly influenced the tool wear, the application of the cooling technique resulted sufficient in this type of operation to guarantee acceptable tool wear resistance as well as product quality. The conventional strategies used to improve the machinability and reduce the process costs consist in adopting appropriate cutting fluids that, penetrating at the chip-tool and workpiece-tool contact areas, are able to effectively remove the generated heat (cooling effect), reduce the friction coefficient (lubrication effect), and assist in the chip flowing (flushing effect). In order to reduce the cutting fluids consuming and thus limiting its problems (operator health, disposal and cleaning costs) in the last years an innovative strategies have been developed, several research individuated in the low-temperature cooling techniques the best candidates to reduce the temperature fields and thus improve the Ti6Al4V alloy machinability.

Dhananchezian et al.[153] found that the cryogenic cooling based on the use of liquid nitrogen determined a substantial improvement through the control of the cutting zone temperature, respect to the wet condition used as baseline the percentage reduction of measured cutting forces, surface roughness and tool wear reached the 42%, 35% and 39% respectively. Similar results are highlighted also by Vonugopal et al. [154] and

Bermingham et al. [51] all agreed that such desirable control of tool wear can be attributed to more effective control of machining temperature under cryogenic cooling.

Despite the several advantages highlighted hitherto, the industrial application of this technology is limited due to the cryogenic coolant extremely low temperatures that could damage the mechanical parts of the CNC machine and cause thermal distortions that cannot be offset, with consequent loss of dimensional accuracy of the machined components, especially when finishing and semi-finishing operations are addressed. Islam et al. [155] published a paper concerned on the study of the dimensional accuracy achievable on cryogenically turned titanium parts comparing dry and wet conditions. He measured the geometrical discrepancies arising in external turning operations by setting three level of feed rate and three levels of cutting speeds usually using in rough machining. The geometrical discrepancies were quantified in terms of circularity and diameter errors comparing the final geometry with the nominal one.

With regard of the diameter errors, under dry and wet cooling they increased under low and medium cutting speed by increasing the feed rate. On the other hand, cryogenic cooling highlighted a different trend, when increasing the feed rate the diameter errors decreased. The measured circularity was the worst in the case of cryogenic cooling. In brief cryogenic cooling provided the least diameter error when combined with higher cutting speed and medium feed rate. The circularity was more affected by the cooling strategy, and it seemed that dry machining and a contribution of feed rate and cutting speed provided the best circularity due to the local softening and chip formation mechanism. Yasa et al. [156] in collaboration with the company TUSAS Engine Industries Inc. found that the excessive cooling of the workpiece generated geometrical distortions and that the dimensional tolerances were not respected, making necessary further machining operations. On the basis of this outcome, the company abandoned the cryogenic strategy and continued to use the standard flood cooling techniques.

[1] F. Spectrometry, R. Metals, I. Coupled, T. Alloys, and A. Bar, “Standard Specification for Wrought Titanium-6Aluminum-4Vanadium ELI (Extra Low Interstitial) Alloy for Surgical Implant Applications (UNS,” pp. 1–5, 2017.

[2] J. Sieniawski, W. Ziaja, K. Kubiak, and M. Motyka, *Microstructure and Mechanical Properties of High Strength Two-Phase Titanium Alloys*. 2013.

[3] G. Lutjering and J. C. Williams, *Titanium*. 2007.

[4] Y. Ohmori, K. Nakai, H. Ohtsubo, and M. Tsunofuri, “Formation of Widmanstätten Alpha Structure in a Ti–6Al–4V Alloy,” *Mater. Trans.*, vol. 35, pp. 238–246, 1994.

[5] L. Wanying, “Effect of Different Heat Treatments on Microstructure and Mechanical Properties of Ti6Al4V Titanium Alloy,” *Rare Met. Mater. Eng.*, vol. 46, no. 3, pp. 634–639, 2017.

[6] R. Pederson, “Microstructure and Phase Transformation of Ti-6Al-4V,” 2002.

[7] R. Boyer, E. W. Collings, and G. Welsch, *Materials Properties Handbook: Titanium Alloys*. ASM International, 1993.

[8] R. Boyer, E. W. Collings, and G. Welsch, *Materials Properties Handbook: Titanium Alloys*.

[9] B. Dutta and F. H. S. Froes, “The Additive Manufacturing (AM) of titanium alloys,” *Met. Powder Rep.*, vol. 72, no. 2, pp. 96–106, 2017.

[10] L. E. Murr *et al.*, “Microstructure and mechanical behavior of Ti-6Al-4V produced by rapid-layer manufacturing, for biomedical applications,” *J. Mech. Behav. Biomed. Mater.*, vol. 2, no. 1, pp. 20–32, 2009.

[11] B. Vrancken, L. Thijs, J.-P. Kruth, and J. Van Humbeeck, “Heat treatment of Ti6Al4V produced by Selective Laser Melting: Microstructure and mechanical properties,” *J. Alloys Compd.*, vol. 541, no. 0, pp. 177–185, 2012.

[12] L. Facchini, E. Magalini, P. Robotti, A. Molinari, S. Höges, and K. Wissenbach, “Ductility of a Ti-6Al-4V alloy produced by selective laser melting of prealloyed powders,” *Rapid Prototyp. J.*, vol. 16, no. 6, pp. 450–459, 2010.

[13] L. Facchini, E. Magalini, P. Robotti, A. Molinari, and L. Facchini, “Microstructure and mechanical properties of Ti-6Al-4V produced by electron beam melting of pre-alloyed powders,” *Rapid Prototyp. J.*, 2010.

[14] X. Tan *et al.*, “Graded microstructure and mechanical properties of additive manufactured Ti – 6Al – 4V via electron beam melting,” *Acta Mater.*, vol. 97, pp. 1–16, 2015.

[15] M. Geetha, A. K. Singh, R. Asokamani, and A. K. Gogia, “Ti based biomaterials , the ultimate choice for orthopaedic implants – A review,” *Prog. Mater. Sci.*, vol. 54, no. 3, pp. 397–425, 2009.

[16] M. A. Gepreel and M. Niinomi, “Biocompatibility of Ti-alloys for long-term implantation,” *J. Mech. Behav. Biomed. Mater.*, vol. 20, pp. 407–415, 2013.

[17] E. O. Ezugwu and Z. M. Wang, “Titanium alloys and their machinability a review,” *J. Mater. Process. Technol.*, vol. 68, no. 3, pp. 262–274, 1997.

[18] E. P. Degarmo, J. T. Black, and R. A. Kohser, *Materials and Processes in*

Manufactring, 9th ed. 2003.

[19] B. Vijaya Ramanath and R. Kesavan, *Manufacturing Technology - II*. Laxmi Publications, 2006.

[20] B. M. Kramer and B. F. von Turkovich, "A Comprehensive Tool Wear Model," *CIRP Ann. - Manuf. Technol.*, vol. 35, no. 1, pp. 67–70, 1986.

[21] Y. Huang, Y. K. Chou, and S. Y. Liang, "CBN tool wear in hard turning : a survey on research progresses," *Int. J. Adv. Manuf. Technol.*, pp. 443–453, 2007.

[22] M. C. Shaw, *Metal cutting principles*, Second. 2008.

[23] S. Pervaiz, A. Rashid, I. Deiab, and M. Nicolescu, "Influence of Tool Materials on Machinability of Titanium- and Nickel-Based Alloys : A Review," *Mater. Manuf. Process.*, pp. 219–252, 2014.

[24] E. M. Trent and P. K. Wright, *Metal cutting*, Fourth edi. 2000.

[25] A. Devillez, F. Schneider, S. Dominiak, D. Dudzinski, and D. Larrouquere, "Cutting forces and wear in dry machining of Inconel 718 with coated carbide tools," vol. 262, pp. 931–942, 2007.

[26] F. Klocke, G. Eisenblatter, and T. Krieg, "Machining: wear of tools," *Encycl. ¨ Mater. Sci. Technol.*, pp. 4708–4711, 2008.

[27] N. Fang and P. Dewhurst, "Slip-line modeling of built-up edge formation in machining," vol. 47, pp. 1079–1098, 2005.

[28] J. M. Brion, B. Sander, G. Pierson, J. Lepage, and J. von Stebut, "Mechanisms of built-up layer formation on turning tools: Influence of tool and workpiece," *wear*, vol. 154, pp. 225–239, 1992.

[29] A. Gonza, M. Marcos, M. S. Carrilero, R. Bienvenido, and J. M. Sa, "A SEM and EDS insight into the BUL and BUE differences in the turning processes of AA2024 Al – Cu alloy," vol. 42, pp. 215–220, 2002.

[30] J. Salguero, M. Batista, M. Marcos, and A. Go, "Analysis of the evolution of the Built-Up Edge and Built-Up Layer formation mechanisms in the dry turning of aeronautical aluminium alloys," vol. 302, pp. 1209–1218, 2013.

[31] M. Alvarez, A. Gomez, J. Salguero, M. Batista, M. Huerta, and M. Marcos, "SOM-SEM-EDS identification of tool wear mechanisms in the dry-machining of aerospace titanium alloys," *Adv. Mater. Res.*, vol. 107, pp. 77–82, 2010.

[32] M. D. Acunto, "Wear and diffusive processes," vol. 36, pp. 553–558, 2003.

[33] A. Molinari and M. Nouari, "Modeling of tool wear by diffusion in metal cutting," vol. 252, pp. 135–149, 2002.

[34] D. Jianxin, L. Yousheng, and S. Wenlong, "Diffusion wear in dry cutting of Ti-6Al-4V with WC/Co carbide tools," *Wear*, vol. 265, no. 11–12, pp. 1776–1783, 2008.

[35] C. Ramirez, A. I. Ismail, C. Gendarme, M. Dehmas, E. Aeby-gautier, and G. Poulachon, "Understanding the di ff usion wear mechanisms of WC-10 % Co carbide tools during dry machining of titanium alloys," *Wear*, vol. 390–391, no. February, pp. 61–70, 2017.

[36] Z. N. Farhat, "Wear mechanism of CBN cutting tool during high-speed machining

of mold steel," vol. 361, pp. 100–110, 2003.

[37] S. Y. Liang, "Modeling of CBN Tool Flank Wear Progression in Finish," vol. 126, no. February 2004, pp. 98–106, 2017.

[38] D. Zhu, X. Zhang, and H. Ding, "Tool wear characteristics in machining of nickel-based superalloys," *Int. J. Mach. Tools Manuf.*, vol. 64, pp. 60–77, 2013.

[39] J. A. Olortegui-yume, P. Y. Kwon, and M. Engineering, "Crater Wear Evolution in Multilayer Coated Carbides During Machining Using Confocal," 2007.

[40] J. Hua and R. Shivpuri, "A Cobalt Diffusion Based Model for Predicting Crater Wear of Carbide Tools in Machining Titanium Alloys," *J. Eng. Mater. Technol.*, vol. 127, no. 1, p. 136, 2005.

[41] ASM, *ASM Metals Handbook, Machining, ASM International, vol.16,*. Ohio, USA, 1989.

[42] M. Sanchez-Carrilero and M. Marcos, *Parametric Relationships in Machining*. 1994.

[43] D. T. Quint, "Technology Perspective on CVD and PVD Coated Metal-Cutting Tools," pp. 7–20, 1994.

[44] ISO3685.1993, "Tool life testing with single-point turning tools, 1993."

[45] M. Binder, F. Klocke, and B. Doebbeler, "Simulation Modelling Practice and Theory An advanced numerical approach on tool wear simulation for tool and process design in metal cutting," *Simul. Model. Pract. Theory*, vol. 70, pp. 65–82, 2017.

[46] S. Sun, M. Brandt, and J. P. T. Mo, "Evolution of tool wear and its effect on cutting forces during dry machining of Ti-6Al-4V alloy," vol. 228, no. 2, pp. 191–202, 2014.

[47] S. Thamizhmanii and S. Hasan, "Relationship between Flank wear and Cutting Force on the Machining of Hard Martensitic Stainless Steel by Super Hard Tools," vol. III, 2010.

[48] M. Y. Noordin, V. C. Venkatesh, S. Sharif, S. Elting, and A. Abdullah, "Application of response surface methodology in describing the performance of coated carbide tools when turning AISI 1045 steel," vol. 145, pp. 46–58, 2004.

[49] A. Kumar and B. Sahoo, "Experimental investigations on machinability aspects in finish hard turning of AISI 4340 steel using uncoated and multilayer coated carbide inserts," *Measurement*, vol. 45, no. 8, pp. 2153–2165, 2012.

[50] M. Armendia, A. Garay, L. Iriarte, and P. Arrazola, "Comparison of the machinabilities of Ti6Al4V and TIMETAL ® 54M using uncoated WC – Co tools," vol. 210, pp. 197–203, 2010.

[51] M. J. Bermingham, J. Kirsch, S. Sun, S. Palanisamy, and M. S. Dargusch, "New observations on tool life, cutting forces and chip morphology in cryogenic machining Ti-6Al-4V," *Int. J. Mach. Tools Manuf.*, vol. 51, no. 6, pp. 500–511, 2011.

[52] M. Armendia, A. Garay, A. Villar, M. A. Davies, and P. J. Arrazola, "High bandwidth temperature measurement in interrupted cutting of difficult to machine materials," *CIRP Ann. - Manuf. Technol.*, vol. 59, no. 1, pp. 97–100, 2010.

[53] A. Kus, Y. Isik, and M. C. Cakir, “Thermocouple and Infrared Sensor-Based Measurement of Temperature Distribution in Metal Cutting,” pp. 1274–1291, 2015.

[54] A. Hase, H. Mishina, and M. Wada, “Correlation between features of acoustic emission signals and mechanical wear mechanisms,” *Wear*, vol. 292–293, pp. 144–150, 2012.

[55] M. Wada and M. Mizuno, “Study on friction and wear utilizing acoustic emission. Relation between friction and wear mode and acoustic emission signals,” *J. Japan Soc. Precis. Eng.*, vol. 55, no. 4, pp. 673–678, 1989.

[56] C. Ferrer, F. Ã. Salas, M. Pascual, and J. Orozco, “Discrete acoustic emission waves during stick – slip friction between steel samples,” *Tribiology Int.*, vol. 43, no. 1–2, pp. 1–6, 2010.

[57] A. Hase, M. Wada, and T. Koga, “The relationship between acoustic emission signals and cutting phenomena in turning process,” pp. 947–955, 2014.

[58] V. Baranov, E. Kudryavtsev, G. Sarychev, and V. Schavelin, *Acoustic emission in friction*, 1st ed. Oxford, 2007.

[59] I. Marinescu and D. A. A. Ã, “A critical analysis of effectiveness of acoustic emission signals to detect tool and workpiece malfunctions in milling operations,” vol. 48, pp. 1148–1160, 2008.

[60] L. Henrique, A. Maia, A. Mendes, W. Luiz, W. Falco, and A. Rocha, “A new approach for detection of wear mechanisms and determination of tool life in turning using acoustic emission,” *Tribiology Int.*, vol. 92, pp. 519–532, 2015.

[61] A. Garg, J. Siu, L. Lam, and L. Gao, “Power consumption and tool life models for the production process,” *J. Clean. Prod.*, vol. 131, pp. 754–764, 2016.

[62] B. S. Prasad and M. P. Babu, “Correlation between vibration amplitude and tool wear in turning : Numerical and experimental analysis,” *Eng. Sci. Technol. an Int. J.*, vol. 20, no. 1, pp. 197–211, 2017.

[63] M. Siddhpura and R. Paurobally, “A review of chatter vibration research in turning,” *Int. J. Mach. Tools Manuf.*, vol. 61, pp. 27–47, 2012.

[64] Y. Fan, Z. Hao, and M. Zheng, “Study of surface quality in machining nickel-based alloy,” pp. 2659–2667, 2013.

[65] “Tool life and surface integrity in turning titanium alloy,” vol. 118, pp. 231–237, 2001.

[66] S. M. Darwish, “The impact of the tool material and the cutting parameters on surface roughness of supermet 718 nickel superalloy,” vol. 97, pp. 10–18, 2000.

[67] D. Umbrello, “Investigation of surface integrity in dry machining of Inconel 718,” pp. 2183–2190, 2013.

[68] A. Thakur, A. Mohanty, and S. Gangopadhyay, “Applied Surface Science Comparative study of surface integrity aspects of Incoloy 825 during machining with uncoated and CVD multilayer coated inserts,” *Appl. Surf. Sci.*, vol. 320, pp. 829–837, 2014.

[69] E. Capello, “Residual stresses in turning Part I : Influence of process parameters,” vol. 160, pp. 221–228, 2005.

[70] P. Dahlman, F. Gunnberg, and M. Jacobson, “The influence of rake angle , cutting feed and cutting depth on residual stresses in hard turning,” vol. 147, pp. 181–184, 2004.

[71] J. C. Outeiro, J. C. Pina, R. M. Saoubi, F. Pusavec, and I. S. Jawahir, “CIRP Annals - Manufacturing Technology Analysis of residual stresses induced by dry turning of difficult-to-machine materials,” vol. 57, pp. 77–80, 2008.

[72] F. Pusavec, H. Hamdi, J. Kopac, and I. S. Jawahir, “Surface integrity in cryogenic machining of nickel based alloy—Inconel 718,” *J. Mater. Process. Technol.*, vol. 211, no. 4, pp. 773–783, 2011.

[73] J. D. P. Velásquez, A. Tidu, B. Bolle, P. Chevrier, and J. Fundenberger, “Sub-surface and surface analysis of high speed machined Ti – 6Al – 4V alloy,” vol. 527, pp. 2572–2578, 2010.

[74] G. Rotella, O. W. Dillon, D. Umbrello, and L. Settineri, “The effects of cooling conditions on surface integrity in machining of Ti6Al4V alloy,” pp. 47–55, 2014.

[75] E. O. Ezugwu, Z. M. Wang, and A. R. Machado, “The machinability of nickel-based alloys : a review,” vol. 86, pp. 1–16, 1999.

[76] Y. Sun, B. Huang, D. A. Puleo, J. Schoop, and I. S. Jawahir, “Improved Surface Integrity from Cryogenic Machining of Ti-6Al-7Nb Alloy for Biomedical Applications,” *Procedia CIRP*, vol. 45, pp. 63–66, 2016.

[77] N. Jouini, P. Revel, P. Mazeran, and M. Bigerelle, “The ability of precision hard turning to increase rolling contact fatigue life,” *Tribiology Int.*, vol. 59, pp. 141–146, 2013.

[78] B. Zou, M. Chen, C. Huang, and Q. An, “Study on surface damages caused by turning NiCr20TiAl nickel-based alloy,” *J. Mater. Process. Technol.*, vol. 209, pp. 5802–5809, 2009.

[79] J. M. Zhou, V. Bushlya, and J. E. Stahl, “An investigation of surface damage in the high speed turning of Inconel 718 with use of whisker reinforced ceramic tools,” *J. Mater. Process. Tech.*, vol. 212, no. 2, pp. 372–384, 2012.

[80] A. Ginting and M. Nouari, “Surface integrity of dry machined titanium alloys,” *Int. J. Mach. Tools Manuf.*, vol. 49, no. 3–4, pp. 325–332, 2009.

[81] S. Anton, S. Andreas, and B. Friedrich, “Heat Dissipation in Turning Operations by Means of Internal Cooling,” *Procedia Eng.*, vol. 100, pp. 1116–1123, 2015.

[82] Beuth-Verlag., “51385 DIN - Lubricants—Processing Fluids for Forming and Machining of Materials—Terms.” 2013.

[83] E. Brinksmeier, D. Meyer, A. G. Huesmann-cordes, and C. Herrmann, “Metalworking fluids — Mechanisms and performance,” *CIRP Ann. - Manuf. Technol.*, vol. 64, no. 2, pp. 605–628, 2015.

[84] A. Aggarwal, H. Singh, P. Kumar, and M. Singh, “Optimization of multiple quality characteristics for CNC turning under cryogenic cutting environment using,” vol. 5, pp. 42–50, 2007.

[85] F. Klocke and G. Eisenblatter, “Dry Cutting,” *Ann. CIRP*, vol. 46, no. 2, pp. 519–526, 1997.

[86] F. Pusavec, P. Krajnik, and J. Kopac, “Transitioning to sustainable production –

Part I : application on machining technologies," *J. Clean. Prod.*, vol. 18, no. 2, pp. 174–184, 2010.

[87] S. Y. Hong and Y. Ding, "Micro-temperature manipulation in cryogenic machining of low carbon steel," vol. 116, pp. 22–30, 2001.

[88] S. Y. Hong and Y. Ding, "Cooling approaches and cutting temperatures in cryogenic machining of Ti-6Al-4V," *Int. J. Mach. Tools Manuf.*, vol. 41, no. 10, pp. 1417–1437, 2001.

[89] S. Y. Hong, "Economical and Ecological Cryogenic Machining," vol. 123, no. May 2001, pp. 331–338, 2017.

[90] A. Y. L. Yong, K. H. W. Seah, and M. Ã. Rahman, "Performance evaluation of cryogenically treated tungsten carbide tools in turning," vol. 46, pp. 2051–2056, 2006.

[91] N. Altan, A. Çiçek, M. Gülesin, and O. Özbek, "Effect of cutting conditions on wear performance of cryogenically treated tungsten carbide inserts in dry turning of stainless steel," *Tribiology Int.*, vol. 94, pp. 223–233, 2016.

[92] F. Pusavec *et al.*, "Sustainable machining of high temperature Nickel alloy e Inconel 718 : part 2 e chip breakability and optimization," *J. Clean. Prod.*, vol. 87, pp. 941–952, 2015.

[93] J. Rech and J. Kopaˇ, "Cryogenic machining as an alternative turning process of normalized and hardened AISI 52100 bearing steel," *J. Mater. Process. Technol.*, vol. 212, pp. 2609–2618, 2012.

[94] Y. Sun, B. Huang, D. A. Puleo, and I. S. Jawahir, "Enhanced Machinability of Ti-5553 Alloy from Cryogenic Machining : Comparison with MQL and Flood-cooled Machining and Modeling," *Procedia CIRP*, vol. 31, pp. 477–482, 2015.

[95] K. A. Venugopal, S. Paul, and A. B. Chattopadhyay, "Growth of tool wear in turning of Ti-6Al-4V alloy under cryogenic cooling," vol. 262, pp. 1071–1078, 2007.

[96] A. A. Khan and M. I. Ahmed, "Improving tool life using cryogenic cooling," vol. 6, pp. 149–154, 2007.

[97] M. J. Bermingham, S. Palanisamy, D. Kent, and M. S. Dargusch, "A comparison of cryogenic and high pressure emulsion cooling technologies on tool life and chip morphology in Ti – 6Al – 4V cutting," *J. Mater. Process. Technol.*, vol. 212, no. 4, pp. 752–765, 2012.

[98] B. D. Jerold and M. P. Kumar, "Experimental investigation of turning AISI 1045 steel using cryogenic carbon dioxide as the cutting fluid," *J. Manuf. Process.*, vol. 13, no. 2, pp. 113–119, 2011.

[99] C. MacHai and D. Biermann, "Machining of -titanium-alloy Ti-10V-2Fe-3Al under cryogenic conditions: Cooling with carbon dioxide snow," *J. Mater. Process. Technol.*, vol. 211, no. 6, pp. 1175–1183, 2011.

[100] O. Çakır, M. Kıyak, and E. Altan, "Comparison of gases applications to wet and dry cuttings in turning," vol. 154, pp. 35–41, 2004.

[101] B. D. Jerold and M. P. Kumar, "Experimental comparison of carbon-dioxide and liquid nitrogen cryogenic coolants in turning of AISI 1045 steel," *Cryogenics.*, vol.

52, no. 10, pp. 569–574, 2012.

[102] S. Sun, M. Brandt, S. Palanisamy, and M. S. Dargusch, “Effect of cryogenic compressed air on the evolution of cutting force and tool wear during machining of Ti – 6Al – 4V alloy,” *J. Mater. Process. Tech.*, vol. 221, pp. 243–254, 2015.

[103] S. Sun, M. Brandt, and M. S. Dargusch, “Machining Ti – 6Al – 4V alloy with cryogenic compressed air cooling,” *Int. J. Mach. Tools Manuf.*, vol. 50, pp. 933–942, 2010.

[104] R. B. Da Silva *et al.*, “Tool wear analysis in milling of medium carbon steel with coated cemented carbide inserts using different machining lubrication / cooling systems,” *Wear*, vol. 271, no. 9–10, pp. 2459–2465, 2011.

[105] A. Attanasio, M. Gelfi, C. Giardini, and C. Remino, “Minimal quantity lubrication in turning: Effect on tool wear,” *Wear*, vol. 260, no. 3, pp. 333–338, 2006.

[106] B. L. Tai, D. A. Stephenson, R. J. Furness, and A. J. Shih, “Minimum Quantity Lubrication (MQL) in Automotive Powertrain Machining,” *Procedia CIRP*, vol. 14, pp. 523–528, 2014.

[107] N. Boubekri, V. Shaikh, P. R. Foster, N. Boubekri, V. Shaikh, and P. R. Foster, “A technology enabler for green machining : minimum quantity lubrication (MQL),” 2014.

[108] D. Adler, W.-S. Hii, D. Michalek, and J. Sutherland, “Examining the role of cutting fluids in machining and efforts to address associated environmental/health concerns,” *Mach. Sci. Technol*, vol. 10, pp. 23–58, 2006.

[109] K. Weinert, I. Inasaki, J. W. Sutherland, and T. Wakabayashi, “Dry Machining and Minimum Quantity Lubrication,” *CIRP Ann. - Manuf. Technol.*, vol. 53, no. 2, pp. 511–537, 2004.

[110] P. S. Sreejith, “Machining of 6061 aluminium alloy with MQL, dry and flooded lubricant conditions,” *Mater. Lett.*, vol. 62, no. 2, pp. 276–278, 2008.

[111] N. R. Dhar, M. Kamruzzaman, and M. Ahmed, “Effect of minimum quantity lubrication (MQL) on tool wear and surface roughness in turning AISI-4340 steel,” vol. 172, pp. 299–304, 2006.

[112] M. Handawi, S. Elmunafi, D. Kurniawan, and M. Y. Noordin, “Use of Castor Oil as Cutting Fluid in Machining of Hardened Stainless Steel with Minimum Quantity of Lubricant,” *Procedia CIRP*, vol. 26, pp. 408–411, 2015.

[113] B. C. Behera, S. Ghosh, and P. V Rao, “Wear behavior of PVD TiN coated carbide inserts during machining of Nimonic 90 and Ti6Al4V superalloys under dry and MQL conditions,” *Ceram. Int.*, vol. 42, no. 13, pp. 14873–14885, 2016.

[114] I. Deiab, S. W. Raza, and S. Pervaiz, “Analysis of lubrication strategies for sustainable machining during turning of titanium ti-6al-4v alloy,” *Procedia CIRP*, vol. 17, pp. 766–771, 2014.

[115] A. E. Diniz, J. R. Ferreira, and F. T. Filho, “Influence of refrigeration/lubrication condition on SAE 52100 hardened steel turning at several cutting speeds,” *Int. J. Mach. Tools Manuf.*, vol. 43, no. 3, pp. 317–326, 2003.

[116] O. Pereira, P. Català, A. Rodríguez, T. Ostra, J. Vivancos, and A. Rivero, “The use of hybrid CO 2 + MQL in machining operations,” *Procedia Eng.*, vol. 132, pp.

492–499, 2015.

[117] P. V. Krishna, R. R. Srikant, and D. N. Rao, “Solid lubricants in machining,” *J. Eng. Tribol.*, vol. 225, no. 4, pp. 213–227, 2011.

[118] J. Barreiro and L. N. L, “Cryogenic and minimum quantity lubrication for an eco-ef fi ciency turning of AISI 304,” vol. 139, pp. 440–449, 2016.

[119] R. W. Maruda, G. M. Krolczyk, E. Feldshtein, P. Nieslony, B. Tyliszczak, and F. Pusavec, “Tool wear characterizations in finish turning of AISI 1045 carbon steel for MQCL conditions,” *Wear*, vol. 372–373, pp. 54–67, 2017.

[120] S. Zhang, J. F. Li, and Y. W. Wang, “Tool life and cutting forces in end milling Inconel 718 under dry and minimum quantity cooling lubrication cutting conditions,” vol. 32, 2012.

[121] S. Dilbag and P. V. Rao, “Performance improvement of hard turning with solid lubricants,” *Int. J. Adv. Manuf. Technol.*, vol. 38, no. 5–6, pp. 529–535, 2008.

[122] N. S. K. Reddy and P. V. Rao, “Experimental investigation to study the effect of solid lubricants on cutting forces and surface quality in end milling,” vol. 46, pp. 189–198, 2006.

[123] F. J. Clauss, *Solid Lubricants and Self-Lubricating Solids*. 1972.

[124] R. R. Moura, M. B. Silva, Á. R. Machado, and W. F. Sales, “The effect of application of cutting fl uid with solid lubricant in suspension during cutting of Ti-6Al-4V alloy,” *Wear*, vol. 332–333, pp. 762–771, 2015.

[125] S. U. S. Choi, “Enhancing thermal conductivity of fluids with nanoparticles,” *ASME Fed 231*, pp. 99–105, 1995.

[126] H. Ay and W. J. Yang, “Heat transfer and life of metal cutting tools in turning,” vol. 41, no. 3, 1998.

[127] T. Teng, Y. Hung, T. Teng, H. Mo, and H. Hsu, “The effect of alumina / water nano fl uid particle size on thermal conductivity,” *Appl. Therm. Eng.*, vol. 30, no. 14–15, pp. 2213–2218, 2010.

[128] R. S. Vajjha and D. K. Das, “Experimental determination of thermal conductivity of three nanofluids and development of new correlations,” *Int. J. Heat Mass Transf.*, vol. 52, no. 21–22, pp. 4675–4682, 2009.

[129] M. S. Liu, M. C. C. Lin, C. Y. Tsai, and C. C. Wang, “Enhancement of thermal conductivity with Cu for nanofluids using chemical reduction method,” *Int. J. Heat Mass Transf.*, vol. 49, no. 17–18, pp. 3028–3033, 2006.

[130] R. S. Vajjha and D. K. Das, “A review and analysis on influence of temperature and concentration of nanofluids on thermophysical properties , heat transfer and pumping power,” *Int. J. Heat Mass Transf.*, vol. 55, no. 15–16, pp. 4063–4078, 2012.

[131] Y. Xuan and Q. Li, “Heat transfer enhancement of nano ¯ uids,” vol. 21, pp. 58–64, 2000.

[132] B. X. Wang, L. P. Zhou, and X. F. Peng, “A fractal model for predicting the effective thermal conductivity of liquid with suspension of nanoparticles,” *J. Heat Mass Transf.*, vol. 46, pp. 2665–2672, 2003.

[133] D. Yoo, K. S. Hong, and H. Yang, “Study of thermal conductivity of nanofluids for the application of heat transfer fluids,” vol. 455, pp. 66–69, 2007.

[134] A. Kumar, R. Kumar, A. Rai, and A. Kumar, “Characterization and experimental investigation of Al 2 O 3 nanoparticle based cutting fluid in turning of AISI 1040 steel under minimum quantity lubrication (MQL),” *Mater. Today Proc.*, vol. 3, no. 6, pp. 1899–1906, 2016.

[135] R. R. Moura, M. B. Silva, Á. R. Machado, and W. F. Sales, “The effect of application of cutting fl uid with solid lubricant in suspension during cutting of Ti-6Al-4V alloy,” vol. 333, pp. 762–771, 2015.

[136] F. A. Essa, Q. Zhang, and X. Huang, “Investigation of the effects of mixtures of WS2 and ZnO solid lubricants on the sliding friction and wear of M50 steel against silicon nitride at elevated temperatures,” *Wear*, vol. 374–375, pp. 128–141, 2017.

[137] J. F. Yang, Y. Jiang, J. Hardell, B. Prakash, and Q. F. Fang, “Influence of service temperature on tribological characteristics of self-lubricant coatings: A review,” *Front. Mater. Sci.*, vol. 7, no. 1, pp. 28–39, 2013.

[138] G. T. Smith, *Cutting tool technology*. London, 2008.

[139] R. Komanduri and W. R. Reed, “Evaluation of carbide grades and a new cutting geometry for machining titanium alloys,” *wear*, vol. 92, no. 1, pp. 113–123, 1983.

[140] A. Jawaid, C. H. Che-haron, and A. Abdullah, “Tool wear characteristics in turning of titanium alloy Ti-6246,” *J. Mater. Process. Technol.*, vol. 92–93, pp. 329–334, 1999.

[141] K. Bobzin, “High-performance coatings for cutting tools,” *CIRP J. Manuf. Sci. Technol.*, vol. 18, no. 2017, pp. 1–9, 2018.

[142] S. A. Barnett, M. H. Fracombe, and J.A. Vossen, *Physics of Thin Films*. New York: Academic press.

[143] S. Veprek, “New development in superhard coatings : the superhard nanocrystalline-amorphous composites,” pp. 449–454, 1998.

[144] A. Vennemann, H. Stock, J. Kohlscheen, S. Rambadt, and G. Erkens, “Oxidation resistance of titanium – aluminium – silicon nitride coatings,” vol. 175, pp. 408–415, 2003.

[145] T. Al, N. Si, L. Zhu, M. Hu, W. Ni, and Y. Liu, “High temperature oxidation behavior of Ti 0.5 Al5 N coating,” *Vaccum*, vol. 86, no. 12, pp. 1795–1799, 2012.

[146] S. Kalidas, R. E. Devor, and S. G. Kapoor, “Experimental investigation of the effect of drill coatings on hole quality under dry and wet drilling conditions,” vol. 148, pp. 117–128, 2001.

[147] A. Kumar and B. Sahoo, “A comparative study on performance of multilayer coated and uncoated carbide inserts when turning AISI D2 steel under dry environment,” *Measurement*, vol. 46, no. 8, pp. 2695–2704, 2013.

[148] M. Sima, A. K. Srivastava, and B. Kaftanoglu, “Investigations on the effects of multi-layered coated inserts in machining Ti – 6Al – 4V alloy with experiments and finite element simulations,” *CIRP Ann. - Manuf. Technol.*, vol. 59, no. 1, pp. 77–82, 2010.

[149] X. Sui *et al.*, “Relationship of microstructure , mechanical properties and titanium

cutting performance of TiAlN / TiAlSiN composite coated tool," *Ceram. Int.*, vol. 42, no. 6, pp. 7524–7532, 2016.

[150] H. A. Abdel-aal, M. Nouari, and M. El Mansori, "Influence of thermal conductivity on wear when machining titanium alloys," *Tribiology Int.*, vol. 42, pp. 359–372, 2009.

[151] N. Narutaki, A. Murakoshi, S. Motonishi, and H. Takeyama, "Study on Machining of Titanium Alloys," *CIRP Ann. - Manuf. Technol.*, vol. 32, no. 1, pp. 65–69, 1983.

[152] F. Ducobu and E. Filippi, "Numerical contribution to the comprehension of saw-toothed Ti6Al4V chip formation in orthogonal cutting," *Int. J. Mech. Sci.*, vol. 81, pp. 77–87, 2014.

[153] M. Dhananchezian and M. P. Kumar, "Cryogenic turning of the Ti – 6Al – 4V alloy with modified cutting tool inserts," *Cryogenics (Guildf).*, vol. 51, no. 1, pp. 34–40, 2011.

[154] K. A. Venugopal, S. Paul, and A. B. Chattopadhyay, "Tool wear in cryogenic turning of Ti-6Al-4V alloy," *Cryogenics (Guildf).*, vol. 47, pp. 12–18, 2007.

[155] M. N. Islam, J. M. Anggono, A. Pramanik, and B. Boswell, "Effect of cooling methods on dimensional accuracy and surface finish of a turned titanium part," pp. 2711–2722, 2013.

[156] E. Yasa, S. Pilatin, and O. Çolak, "Overview of cryogenic cooling in machining of Ti alloys and a case study," *J. Prod. Eng.*, vol. 15, no. June, pp. 1–9, 2012.

Chapter 3

Experimental procedure

3.1 Approach

The most consolidated approach to investigate the materials machinability is through the conduction of machining test under proper cutting conditions. These tests offer the chance to quantify important phenomenon that are peculiar aspects of this kind of material characterization such as the tool wear, surface integrity, the cutting temperature etc.

As a consequence, the scientific approach followed in this thesis is solidly based on the conduction of machining tests adopting real industrial conditions and equipment.

As a first step, the dry and flood cooling techniques commonly used in many industrial application were tested in semi-finishing turning of Ti6Al4V wrought alloy using insert and the cutting parameters recommended by the tool manufacturer for this specific cutting process, these conditions were considered as reference for the following experimental campaigns. An innovative approach to measure the tool crater wear that is suitable in

particular for all the sticky materials as titanium was proposed and applied.

In the second activity carried out in this work an innovative cooling and lubricating technologies were developed, implemented and tested comparing the new experimental findings with those previously obtained to verify the effects of such innovation.

After that different insert coatings were tested using the most interesting cooling technologies such as LN2 and cooled N2 at -100°C. Also the influences of the Ti6Al4V microstructure in machining process were considered, the machinability results were correlate with the main thermal and mechanical proprieties considered responsible to the tool degradation.

In this chapter all the experimental methods used to characterize the machinability of the Ti6Al4V alloy are presented and the experimental apparatus and the cooling/lubricating lines described. In details the chapter is divided in three sections, namely the material characterization, turning tests and post-machining analysis.

Even dough the machining tests conducted for all the analysis presented in this thesis were carried out in different moments, having used the same experimental set-up and procedure for all the tests, it is introduced and described only in this chapter to avoid repetitions in the following part of the work.

3.2 Material characterization

The metal alloy object of investigation in this thesis is the alpha-beta Ti6Al4V titanium alloy produced by different technologies, namely the Additive Manufacturing technologies (Electron Beam Melting and Direct Metal Laser Sintering) and the conventional wrought one.

The Ti6Al4V nominal chemical composition (in wt %) according to the ASTM F1472 standard [1] is given in Table 3.1. The high purity (extra-low interstitial), with specified limits on iron and interstitial elements such carbon and oxygen make it suitable for biomedical application, particularly for implantable components thanks to its high biocompatibility.

Table 3.1. Chemical composition of the Ti6Al4V alloys [1]

Chemical composition (wt %)							
Al	V	C	Fe	O	N	H	Ti
6	4	0.03	0.1	0.15	0.01	0.003	Bal

Along with the chemical composition, the manufacturing process plays a major role in determining the microstructural features (see Figure 3.1) and, consequently, the alloy mechanical and thermal properties in the as-received state. Facchini et al. [2] analysed the microstructure of the EBM Ti6Al4V and identified an acicular microstructure consisting of alpha phase fine lamellae with 7% of beta phase (Fig.1A). On the other hand, the high undercooling typical of the DMLS technology promotes the formation of a martensitic structure composed by alpha prime phase with typical needles (Fig.1B); since this kind of microstructure is of limited practical application, post-building heat treatments are necessary to transform it into a biphasic alpha + beta microstructure (Fig.1C) suitable for structural products. Vracken et al. [3] and Facchini et al. [4] determined that the new lamellae nucleated and grew along the martensitic grain boundaries maintaining the previous orientation, being the grain size dependent on the heat treatment temperature, soaking time and cooling rate. The wrought Ti6Al4V alloy is obtained through hot working followed by annealing: the thermo-mechanical process produces a recrystallized equiaxed structure composed by alpha grains with 8% of beta phase at the grain boundaries (Fig.1D).

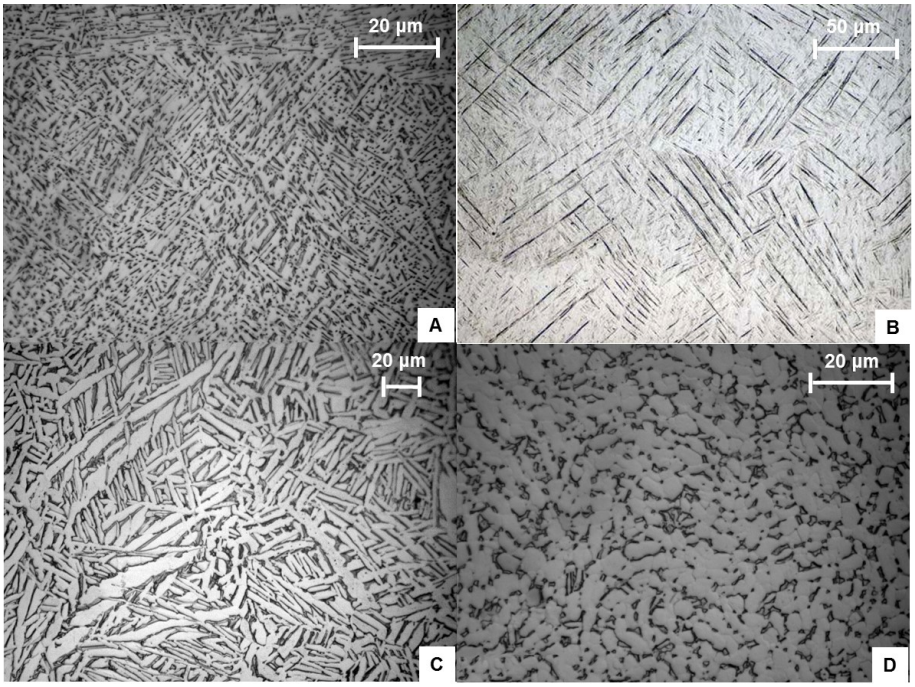

Figure 3.1. Ti6Al4V microstructure in the as-received conditions: (A) EBM, (B) DMLS, (C) heat-treated DMLS, (D) wrought.

The EBM material was produced using an ARCAM^{TM} Q10 machine in cylindrical bars with a diameter of 50 mm and length of 230 mm, while for the realization of the DMLS

material an EOS^{TM} EOSINT M270 machine was used. In the latter case the samples were again cylindrical bars of diameter of 40 mm and length of 150 mm. The wrought material was supplied in annealed state by Sandvik^{TM} in bars with a diameter of 50 mm.

The main mechanical properties of the Ti6Al4V in the different as-received conditions at room temperature are reported in Table 3.2. The yield strength values are in the range between 835 and 995 MPa, while there are no substantial differences in the elastic modulus values.

Despite the different microstructures, the EBM and the heat treated DMLS Ti6Al4V exhibit comparable mechanical properties, while the DMLS alloy, due to its martensitic microstructure and the residual stresses induced by the rapid cooling, presents the highest yield strength and the lowest elongation. The new microstructure generated during the post-building heat treatment shows an improved ductility of the heat-treated DMLS alloy, as the elongation increases of about 30% while the yield strength decreases of about 15%.

Table 3.2 Mechanical properties of the Ti6Al4V in the as-received conditions at room temperature *Sandvik Bioline datasheet [5] and **Facchini et al.[4].

Ti6Al4V	E (GPa)	UTS (MPa)	Y_S (MPa)	Elongation (%)
Wrought*	118	940	870	15.0
EBM**	114 ± 5	915 ± 10	830 ± 5	13.1 ± 0.4
DMLS**	110 ± 5	1095 ± 10	990 ± 5	8.1 ± 0.3
Heat-treated DMLS**	117 ± 1	915 ± 5	835 ± 5	10.6 ±0.6

3.3 Machining tests

The semi-finishing turning tests were carried out on a Mori-Seiki^{TM} NL1500 CNC lathe using carbide inserts CNMG 120404 supplied by Sandvik^{TM} with a radius of 0.4 mm and clearance angles of 0°, respectively. The cutting inserts were clamped in a PCLNR 2020K 12 Sandvik^{TM} Coromant tool holder with an approach angle of 95°.

In this study four different commercial insert made of WC (substrate composition: 93 % WC and 7% Co) commonly used for machining DTC alloys were tested, namely an uncoated insert (H13A), an insert coated with a single layer of (Ti,Al)N (GC 1105), and two inserts coated with a multi-layer (Ti,Al)N–(Al,Cr)2O3 deposited through Chemical Vapour Deposition CVD (GC 1125) and Physical Vapour Deposition PVD (GC 1115).

The cutting parameters range advised by the manufacturer to machine Ti6Al4V is indicated in Table 3.3.

Being the insert geometry the same the feed rate and depth of cut were chosen equal for each type of insert, namely 0.2 mm/rev and 0.25 mm, respectively. Whereas, as concerns the cutting speeds, the maximum values recommended by the tool manufacturer were chosen (see Table 3.3). A fresh cutting edge was used for each trial, and 15 minutes were considered as turning time. The turning tests were repeated three times for each cutting condition to assure the results repeatability.

Table 3.3. Cutting parameters.

Cutting parameters		**GD 1125**	**H13A**	**GD 1115**	**GD 1105**
Depth of cut (mm)	Range	0.15-2.5	0.15-2.5	0.15-2.5	0.15-2.5
	Adopted value	0.25	0.25	0.25	0.25
Feed rate (mm/rev)	Range	0.1-0.3	0.1-0.3	0.1-0.3	0.1-0.3
	Adopted value	0.2	0.2	0.2	0.2
Cutting speed (m/min)	Range	25-35	30-40	40-65	50-80
	Adopted value	35	40	65	80

In order to improve the titanium machinability in this thesis several cooling, lubricating and hybrid strategies were tested using the dry cutting and the wet conditions as baseline, in details all tested technologies are summarized in Figure 3.3. For each of them a dedicated line was designed and installed on to the CNC lathe.

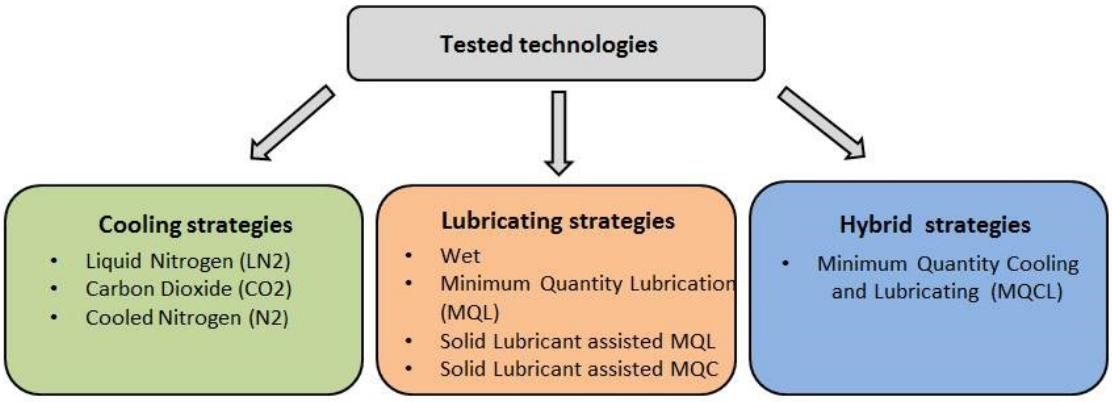

Figure 3.3. Cooling, lubricating and hybrid technologies tested in this work.

The most efficient methods to inhibit or reduce the temperature effect during the machining process consist to applied cryogenic or low-temperature fluids in the cutting

zone. In according to the literature review three distinct coolants were tested, namely Liquid Nitrogen (LN2), Carbon Dioxide and gaseous Nitrogen (N2) cooled at different temperatures in the range between 0, -150°C, the Figure 3.4 and 3.5 show the developed cooling apparatus implemented in the CNC lathe, for the LN2 and cooled N2 fluids respectively.

The LN2 apparatus consists of three sub-systems, namely a Dewar in which the LN2 is stored and maintained at controlled pressure and temperature, a control unit including solenoid valves and safety systems that allow to stop the flow in case of emergency, and a distribution system made of special plates mounted on the lathe turret designed to deliver the LN2 onto the cutting zone. A lot of technical attention was paid to the nozzle systems, according to the literature findings the proposed experimental set-up consists of two flow of LN2 direct on to the rake and flank face by means of external copper nozzles with internal diameter of 0.9 mm. The position and the direction of the nozzles with the respect the tool faces were optimized after several rough turning trials conducted on wrought Ti6Al4V workpieces. A high vacuum insulated pipe leads the LN2 directly from the Dewar to the distribution system at a pressure of 15±0.5 bar, resulting in mass flow of 0.9 kg/min that corresponding at 4 Lt/min of flow rate. The mass flow was measured by laying the Dewar on a balance and measuring the mass reduction in a fixed time unit.

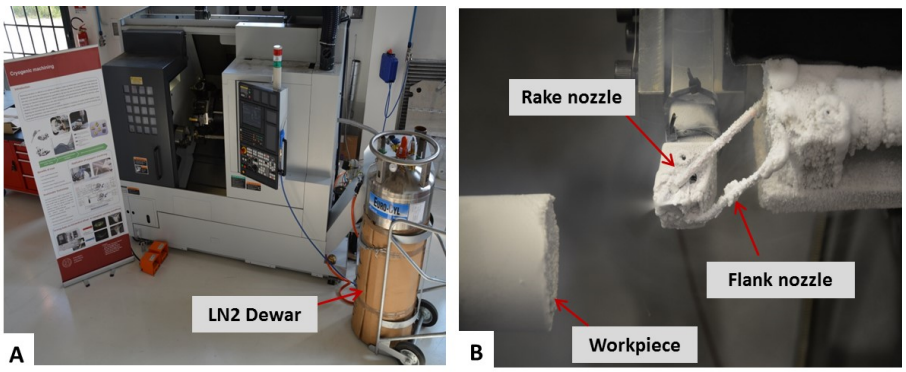

Figure 3.4. Experimental apparatus for LN2 technologies: (A) overall view of the equipment, (B) detail of the cutting zone.

The control unit and distribution system developed for the LN2 turned out to be suitable also for the management of the gaseous CO2. Only the Dewar was substituted with another able to resist at higher pressure since the CO2 must be storage in liquid phase at the pressure of 57 bar. The fluid was applied by means the same distribution system used for the LN2 turning tests onto the cutting zone at 57 bar with flow rate of 2,3 Lt/min.

Unlike the previous case, in which the cryogenic fluid remains always in the liquid state, the CO2 when is fused with the ambient air at the exit of the nozzle immediately becomes a gas determining a drastic temperature decrease down to -78.5°C that makes possible the formation of CO2 solid state called snow.

The last tested cooling strategy is based on the use of low temperature N2 cooled through an experimental apparatus called Cryofluid™ patented by Air Liquide™ Service Italy. The N2 was cooled to different temperatures in the range between 0° and -150°C within an insulated chamber where Liquid Nitrogen (LN2) was mixed with the N2 until reaching the desired temperature. As soon as the desired temperature was reached, it was kept constant for the whole test using an internal PLC controller to manage the flow rates of the two fluids. The output pressure of the cooled N2 was set constant at 2.5 bar. In order to provide the right amount of coolant, a single nozzle with internal diameter of 6 mm was fixed onto the tool holder so as to direct the flow to the tool rake face being this area the most exposed to the thermally-activated wear mechanisms.

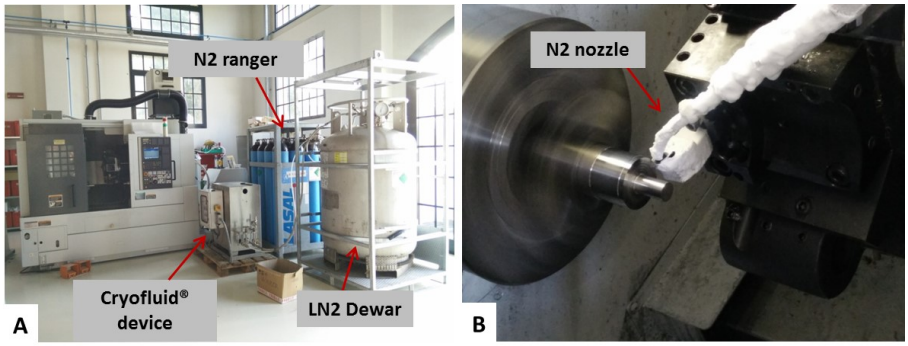

Figure 3.5. Experimental apparatus for Cryofluid™ technologies: (A) overall view of the equipment, (B) detail of the cutting zone.

The reduction of the friction coefficient represents another efficient solution to improve the machinability since limit the abrasive wear and therefore also the heat produced during the cutting process. In this work several technique were considered, the conventional flood strategies commonly used in many industrial machining process was compared with the Minimum Quantity Lubrication (MQL) and Solid Lubricant assisted techniques.

The wet strategy made use of the commercial semi-synthetic cutting fluid Monroe™ Astro-Cut HD XBP mixed with water obtaining a 5% emulsion coolant that was supplied

at a pressure of 2 bar by exploiting the lubricating embedded apparatus provided in the CNC lathe

For the MQL case a modular air/oil system called Miquel™ patented by Dropsa was used. The system is composed by a pressurized tank, a mixing control module and a Venturi's nozzle. The lubricant contained in the tank is pressurised by the air pressure (4-7 bar) and sent to the mixing module through an internal pipe. The module is equipped with a self-compensation valve which maintains constant the Δp between the inflowing oil pressure and outflowing pressure. A coaxial tube to transport separately the misting air and the lubricant to the Venturi's nozzle was used. Inside the nozzle the lubricant is atomized in tiny particles by the air flow forming an aerosol at a pressure of 2 bar. The air consumption is around 50 Nl/min while is possible set the oil flow rate within the range 20-500 ml/h. To guarantee a sustainability machining, reducing the cleaning and disposal cost, a Berecut MQL A20 vegetable biodegradable oil supplied by Bechem™ was adopted. Preliminary turning tests individuated the oil flow rate of 200 ml/h as the minimum value able to guarantee efficient cutting zone lubrication; lastly the nozzle spray was directed onto the tool flank face being the zone main subject to the abrasive wear mechanism.

To improve the lubrication effect of the pure MQL technology during the turning process a Solid Lubricant assisted technique was tested, the adopted solution consisted in increasing the lubricating effect of the MQL oil by adding 5% in weight of PTFE particles (Munzing™ LUBARIT 267); since the additives had an average dimension less than 5 μm, the same devices and procedure used in the pure MQL tests were applied.

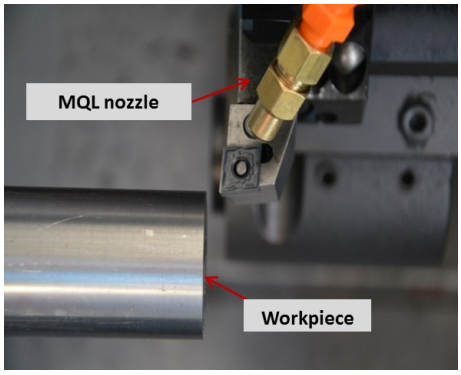

Figure 3.5. Experimental set-up for the MQL and LS assisted MQL technologies.

The operating principle of the SL-assisted MQC strategy is similar to that described for the MQL technique, with the sole difference that the solution is water based instead of

being oil based. The high cooling capacity of the water, due to its high density and heat capacity, make it a suitable coolant to reduce the temperature field produced during the cutting process. On the other hands its low lubricating capacity is not sufficient to limit efficiently the friction and thus the tool abrasion responsible to the cutting edge alteration. To overcame this problem a graphite lamellar particles (commonly used as lubricant during the stamping process) were used as additive, the solutions was prepared following the producer's recommendations [7]: the demineralized water was enriched with stable colloidal graphite particles with dimensions in the range between 0.6 and 0.8 μm (Henkel^{TM} Bonderite L-GP Aquadaq 22%). at different graphite percentage 5%, 10% and 15% in weight.

A dedicated Venturi's nozzle (see Figure 3.6) was used to deliver the solution to the tool cutting edge, at a pressure of 7 bar and flow rate of 4 l/h. To prevent the graphite sedimentation, the solution was maintained in agitation during the whole test. On the basis of the very low cutting fluid consumption (two orders of magnitude lower than the conventional wet one); this strategy can be regarded as a minimal cooling technique.

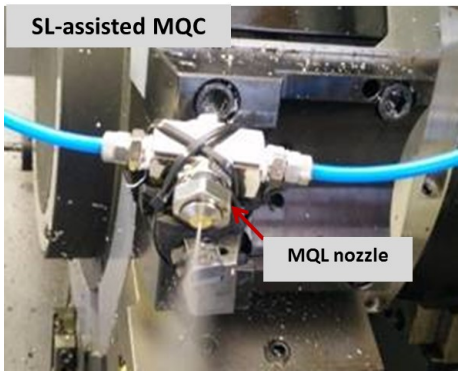

Figure 3.6. Experimental set-up for SL - assisted MQC technology.

The tool failure generally is caused by the simultaneously combination of different wear mechanisms, the best results may occurs using a hybrid cooling/lubricating strategies capable to reduce both the temperature and the friction. Two different technologies were developed, namely Minimum Quantity Cooling Lubrication (MQCL) and a SL-assisted Minimum Quantity Cooling (SL-assisted MQC).

The MQCL strategy allows improving the cooling capacity of the MQL technology using a low temperature cutting fluids. The first experimental campaign was aimed to individuate the correct nozzles position using LN2 as coolant and a MQL aerosol as lubricant. In particular, two solutions were proposed: the first made use LN2 supplied on

the tool rake face and the MQL aerosol on the tool flank face (Figure 3.7A), while in the second the nozzle positions were reversed, with the LN2 onto the flank face and the MQL aerosol cooling the rake face (Figure 3.7B).

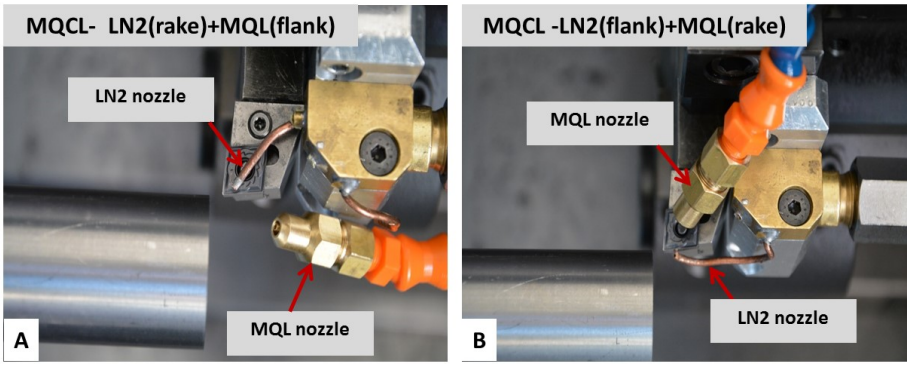

Figure 3.7. Experimental set-up for: (A) hybrid strategy with LN2 and CO2 on the rake face and MQL on the flank face, (B) hybrid strategy with LN2 on the flank face and MQL on the rake face.

On the basis of experimental evidences, the best solution consists to cooling the rake face and lubricating the flank face, this particular nozzles position was considered as the optimal solution and therefore used also in the second study in which the LN2 was substituted with the CO2.

3.4 Post machining analysis

3.4.1 Tool wear

In order to evaluate the main tool wear mechanisms in the tested cutting conditions a preliminary qualitative analysis of the tool rake wear was carried out by using a FEI QUANTA 450^{TM} Scanning Electron Microscope (SEM) equipped with the Everhart Thornley Detector (ETD) and Backscattered Electrons Detector (BSED). The workpiece material adhered on the worn tools was evaluated by means of an Energy Dispersive X-ray Spectroscopy (EDX) analysis, whereas a quantitative evaluation of the wear was carried out using a Sensofar Plu-Neox^{TM} optical 3D profiler. To evaluate the extent of the tool damage, the 2D profiles of the worn tool rake faces were compared with the unworn one. The 2D profiles were obtained in a fixed central position of the rake face from the 3D optical profiler images: using as baseline the change of the insert slope at the rake face, specifically designed to improve the chip breaking, it was possible to efficiently align the insert profiles. The maximum crater depth was measured following the approach shown in Figure 3.8. The tool profiles were rotated to make them aligned with the X-axis:

the difference between the minimum value of the worn tool and the equivalent value of the unworn tool profile corresponds to the maximum crater depth.

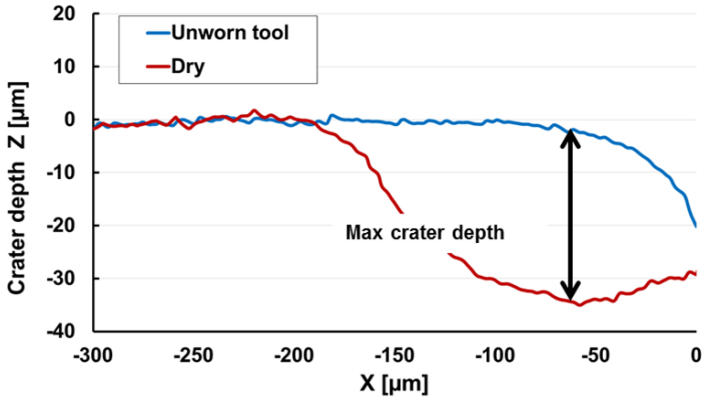

Figure 3.8. Measuring approach to evaluate the tool maximum crater depth.

On the other hand, the flank wear was quantified in accordance with the ISO 3685:1993 standard [8] measuring the notch flank wear (VBc) on the SEM images. According to the standard, a limit value of 0.3 mm must not be exceeded; nonetheless in fields such as the aerospace and biomedical ones this value is reduced to 0.1 mm in order to guarantee a better surface integrity.

3.4.2 Surface integrity

The Ti6Al4V alloy surface integrity was evaluated in terms of surface roughness and topography, surface defects, altered layers, nano-hardness and residual stresses.

The surface finishing (roughness and topography) was measured along the cutting direction by means of a Sensofar^{TM} Plu-Neox optical 3D profiler in according to the ISO 4287:1996 standard [9], fixing the cut-off filter and the measuring length at 0.25 mm and 1.25 mm, respectively, 5 readings at different points of machined surface were taken for each experiment and an average reading was used for comparative analysis.

Microstructural analysis was performed to evaluate the main effect of the turning process on the material microstructures alteration. The machined samples were cut using a metallographic disc cutter, hot mounted using a Struers hot mounting press and then grinded and polished according to procedure outlined in Table 3.4 by using an automatic Struers grinding machining. After the polishing procedure the samples were prepared following the standard metallographic procedure [10], using the Kroll's etching to evidence the microstructure, than cleaned by using soup and water than methanol. The machined altered layer was quantified on the basis acquired using the FEI ^{TM} QUANTA

450 Scanning Electron Microscope (SEM) equipped with the Back Scattered Electron (BSE) detector.

Table 3.4. Polishing procedure for microstructural analysis.

Step	Surface	Abrasive type	Speed (rpm)	Force (N)	Time (s)
Grinding	Si-C paper	Gr.120	300	150	240
-	-	Gr.320	-	-	-
-	-	Gr.500	-	-	-
-	-	Gr.800	-	-	-
-	-	Gr.1200	-	-	-
-	-	Gr.400	-	-	-
Polishing	MD-Chem	70% Hydrogen peroxide – 30% Colloidal silica	150	60	240

The residual stresses were determined with CuKα-radiation using the (2,1,3) interference lines. The analysis was based on the $\sin^2\psi$-method [11] for which the lattice spacings d were measured at five ψ-angles between −35° and +35°. A Young's modulus of E=114 GPa and a Poisson's ratio of ν=0.237 were used for the calculation of the residual stresses from the observed lattice strains. The samples for X-ray analysis were degreased in an ultrasonic bath and fixed on a holder. The measurements were performed using a Spider ^{TM} X GNR portable diffractometer working at 30 KV and 90 μA. The counting time for each of the five measures at the different ψ-angles was 500 s. The depth distribution of the residual stresses was determined by electrolytic removal of thin surface layers and subsequent X-ray measurements. The electrolytic polishing was performed using as electrolyte a solution containing 90 ml of water, 730 ml of ethanol, 100 ml of butoxyethanol and 78 ml of perchloric acid working at 50 V for one minute and maintaining the temperature of the electrolyte at 20 °C.

The nano-hardness and Young's modulus analyses carried out by means of nano-indentation tests were conducted only for the most relevant cases, namely for the samples machined under LN2 and CO2 cooling conditions, as well as in dry cutting. In order to acquire reliable nano-indentation data and distinguish the two phases, namely the α and β phases present in Ti6Al4V, the surface of the three samples was ground again, gently polished using diamond paste to mirror finish and finally polished with Oxide Polishing Suspension (OPS) [12].The nano-indentations were carried out using a HYSITRON TI

950 TriboIndenter™ at controlled displacement equal to 450 nm using a Berkovich indenter tip on a high load transducer, while the load was continuously monitored. The displacement was chosen based on the Ti6Al4V average grain size, in order to consider both phases, as shown through a scanning of the surface in Fig. 3.9b. The width of the indentation was varied from 3 to 4.5 µm. Owing to these dimensions and in order to study as many distances from the surface as possible, a particular test grid was elaborated with a minimum distance of 7 µm between the indents [13],[14].Several grids were performed on the surface of the samples and, in order to obtain reference values, one grid was carried out at the centre of the dry sample. The grid consisted of a system of 20 alternated lines of 5 indentations shifted by 5 µm on the y-axis (perpendicular to the surface) and by 10 µm on the x-axis (Fig. 3.9a). The first row was positioned at 6 µm from the sample edge to avoid indentations on the resin. Due to the roughness variation in the sample depending on the phases present in the analysed zone, some indentations failed or could not reach the 450 nm displacement.

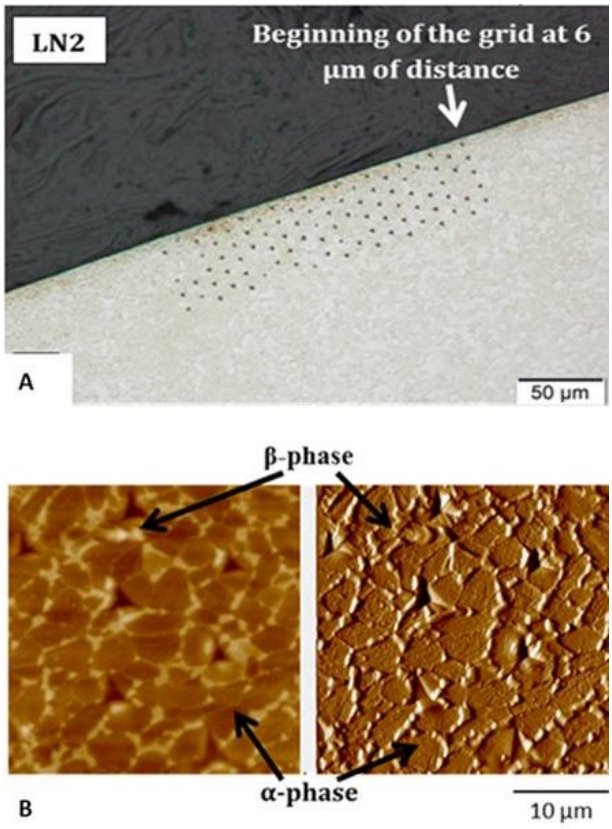

Figure 3.9. A) Grid on the LN2 sample with an evident work hardened surface with indication of the grid first point from the surface; B) Scan (Imaging mode) of the same grid, in two modes (topography on the left and gradient mode on the right).

Only indentations with a displacement of 450 nm were evaluated. Three grids per sample were taken in different positions with a potential total of 300 points, which became 195 effective points after being filtered by the criteria. All these effective points were divided per the ten considered distances from the surface and an average value per distance was obtained for each sample. Moreover, the reference value (average value of 90 effective points from the grid carried out in the center of dry sample) is given for each property in the relative graph. Randomly distributed larger α or β-zones can increase or decrease the properties upon hitting the indenter and consequently this slightly affects the data variance. However, the measured data characterize the general mechanical behavior of the surface.

[1] F. Spectrometry, R. Metals, I. Coupled, R. Metals, T. Alloys, and A. Bar, “Standard Specification for Wrought Titanium-6Aluminum-4Vanadium Alloy for Surgical Implant Applications (UNS R56400) 1,” pp. 1–5, 2017.

[2] L. Facchini, E. Magalini, P. Robotti, A. Molinari, and L. Facchini, “powders Users who downloaded this article also downloaded : Microstructure and mechanical properties of Ti-6Al-4V produced by electron beam melting of pre-alloyed powders,” 2010.

[3] B. Vrancken, L. Thijs, J.-P. Kruth, and J. Van Humbeeck, “Heat treatment of Ti6Al4V produced by Selective Laser Melting: Microstructure and mechanical properties,” *J. Alloys Compd.*, vol. 541, no. 0, pp. 177–185, 2012.

[4] L. Facchini, E. Magalini, P. Robotti, A. Molinari, S. Höges, and K. Wissenbach, “Ductility of a Ti-6Al-4V alloy produced by selective laser melting of prealloyed powders,” *Rapid Prototyp. J.*, vol. 16, no. 6, pp. 450–459, 2010.

[5] Sandvik Bioline Ti6Al4V ELI materials datasheet, “No Title.”.

[6] A. Bordin, S. Bruschi, A. Ghiotti, and P. F. Bariani, “Analysis of tool wear in cryogenic machining of additive manufactured Ti6Al4V alloy,” *Wear*, vol. 328–329, pp. 89–99, 2015.

[7] Henkel, “Bonderite L-GP AQUADAG ACHESON graphite dispersion in water-technical process bulletin,” *2013*.

[8] ISO3685.1993, “Tool life testing with single-point turning tools, 1993.”

[9] ISO4287:1197, “Geometrical product specifications (GPS) - Surface texture: profile method - terms, definitions and surface texture parameters.”

[10] ASTME407-70, “Standard test method for microetching metals and alloys,1989.”

[11] M. E.Fitzpatrick, P. H. A. T. Fry, F. A. Kandil, J. Shackleton, and L. Suominen, “Determination of residual stresses by X-ray diffraction,” *Natl. Phys. Lab. Teddingt.*, 2005.

[12] Struers, “Metallographic preparation of titanium Application Notes.” 2015.

[13] Y. Murakami and M. Itokazu, “Elastic-plastic analysis of a triangular pyramidal identation,” *Int. J. solids sructures*, vol. 34, no. 30, pp. 4005–4018, 1997.

[14] B. Jung, H. Lee, and H. Park, “Effect of grain size on the indentation hardness for polycrystalline materials by the modified strain gradient theory,” *Int. J. Solids Struct.*, vol. 50, pp. 2719–2724, 2013.

Chapter 4.

Effects of different cooling/lubricating strategies onto the Ti6Al4V wrought machinability

4.1 Introduction

In the recent years, the concept of environmental sustainability has driven the manufacturing companies towards the adoption of more environmental friendly cutting fluids that allow both the minimization of the process chain costs and the improvement of the material machinability. An innovative approach to enhance the machining performance is to reduce the cutting temperature using high-pressure air, liquid coolants or through the application of low-temperature fluids. The use of Liquid Nitrogen (LN2) and Carbon Dioxide (CO2) as low-temperature coolants is becoming particularly attractive because they are clean, safe and non-toxic, and do not present any environmental issue. Several studies investigated the use of both the LN2 and CO2 in machining titanium alloys, showing significant improvements in the tool life compared to

the dry cutting, which, in turn, allows using higher Material Removal Rates. Overall, the cooling solutions adopting low-temperature coolants determine significant improvements, but their lubricating capacity is not comparable yet with the one obtainable in case of adoption of conventional cutting fluids. An alternative strategy, nowadays widely accepted thanks to its economic competitiveness, is represented by the Minimum Quantitative Lubrication (MQL), which consists in spraying an aerosol made of biodegradable oil micro-particles to the cutting zone. The supply and disposal costs are reduced because the flow rate is between 50 ml/h and 250 ml/h, which are several orders of magnitude lower than the traditional lubrication that has a flow rate of tens of litres per hour. In this case its low cooling capacity insufficient to eliminate the temperature generated during the cutting process responsible to the thermally activated mechanism represents the critical issues that limiting its use especially in the machining of DTC alloys. To improve the cooling effect of the MQL techniques two strategies have been recently proposed: one makes use of low-temperature fluids, such as LN2, CO2 or cooled air, to provide a hybrid technology in which the tool flank face is lubricated and the rake one cooled simultaneously (techniques named as Minimum Quantity Cooling Lubrication (MQCL), while the other aims at improving the oil heat transfer characteristics thanks to specific additives. The latter solution, named Solid Lubricant (SL)-assisted MQL strategy, is nowadays receiving wider attention since it allows a drastic improvement of the fluid performances by controlling both the heat generation and the friction between the tool and workpiece without significant increase of the process costs, and, at the same time, it also avoids those issues related to the use of cryogenic temperatures as happens when using the aforementioned hybrid techniques. In this chapter the abovementioned strategies were developed and tested in order to verify their machinability effects during the semi-finishing of Ti6Al4V titanium alloy. As reference the dry cutting and wet conventional strategies were used as baseline.

4.2 Cooling strategies

The aim of this section is to investigate the tool wear mechanism and modes coated tungsten carbide inserts and the surface integrity of the machined product when turning a wrought Ti6Al4V under different low-temperature cooling strategies in semi-finishing cutting conditions (see Table 4.1). In details three coolants were tested as cutting fluids, namely Liquid Nitrogen, Liquid Carbon Dioxide and cooled N2. While the techniques

based on the use of LN2 and LCO2 were widely investigated, the cooled N2 represents a novelty. For this reason different tests were conducted in order to evaluate the temperature effects on the Ti6Al4V machinability and identify the cooling condition that guaranteed the best performances.

Table 4.1. Experimental plan for the turning tests.

Material	**Cutting parameters**			**Tested technologies**
-	**Depth of cut (mm)**	**Feed rate (mm/rev)**	**Cutting speed (m/min)**	-
Wrought	0.25	0.2	80	LN2 – CO2 – Cooled N2

4.2.1 Tool wear

In order to evaluate the tool wear mechanisms in the tested cutting conditions a preliminary qualitative analysis of the tool rake and flank faces wear was carried out by using a FEI QUANTA 450^{TM} Scanning Electron Microscope (SEM) equipped with the Everhart Thornley Detector (ETD) and Backscattered Electrons Detector (BSED). The workpiece material adhered on the worn tools was evaluated by means of an Energy Dispersive X-ray Spectroscopy (EDX) analysis, whereas the crater depth was quantitatively measured in a fixed central position of the tool rake face using a Sensofar Plu-Neox^{TM} optical 3D profiler.

Figure 4.1 shows the SEM images of the tool rake faces after 15 minutes of turning the Ti6Al4V under different cooling strategies.

A more detailed SEM analysis of the tool rake faces highlighted adhesion of the workpiece material on the cutting edge and abrasion of the insert coating as the main wear mechanisms (see Figure 4.2).

Adhesive wear can be due to the adhesion of the workpiece material on the cutting edge, determining the formation of the Built-Up-Edge (BUE) or Built-Up-Layer (BUL), and to the chip sliding onto the tool rake face that causes the welding of the chip.

The BUE formation is commonly associated to the mechanical adhesion forces at the tool-workpiece interface; on the contrary, the BUL is formed as a consequence of the BUE plastic deformation onto the tool rake face due to the high pressure generated by the chip sliding: this adhered layer protects the tool substrate from the abrasive wear, but it activates the diffusion mechanism responsible of the crater wear formation [1][2].

Regardless of the tested conditions, the above mentioned mechanisms were detected, as shown as example in Fig. 4.2 in case of the cooled N2 at -100°C cut wrought sample.

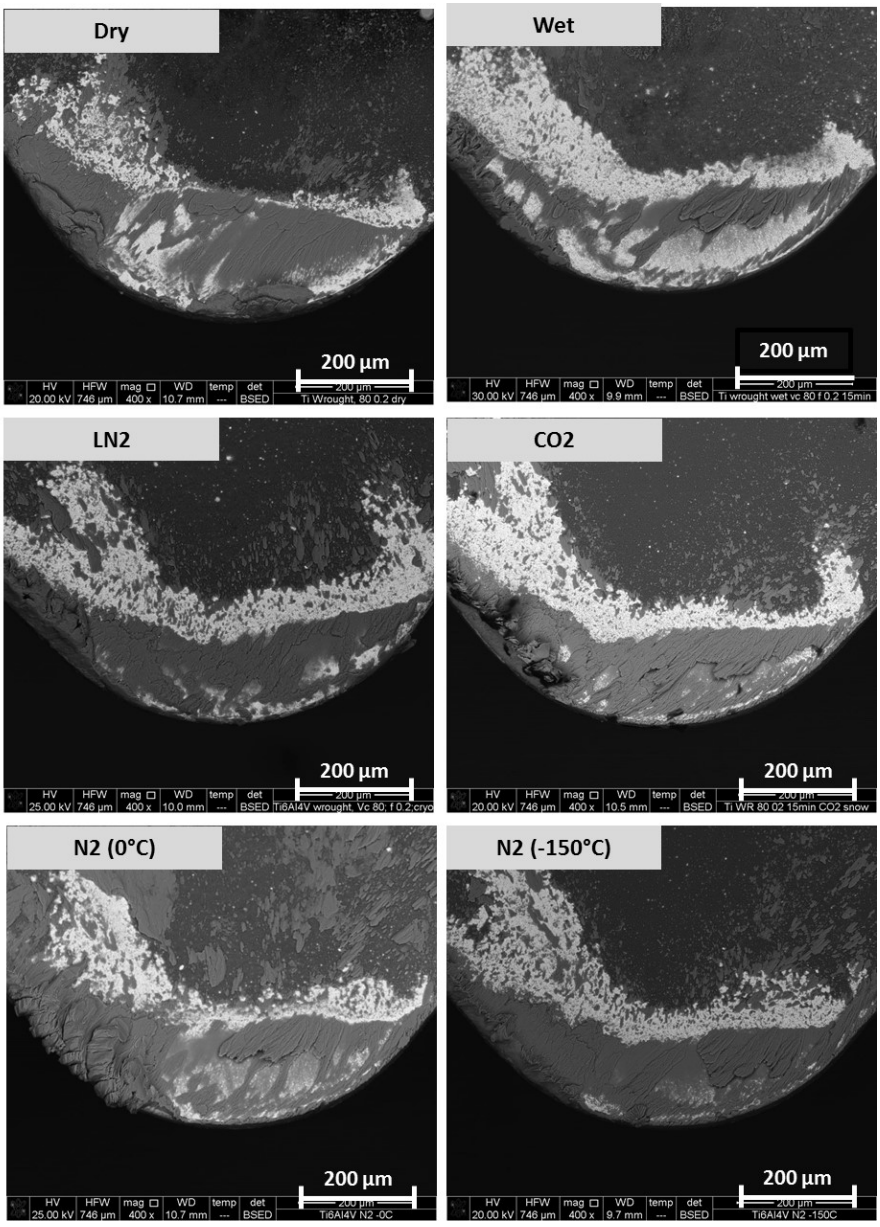

Figure 4.1. SEM images of the worn tool rake faces after 15 minutes of turning under the different cooling strategies

Also the EDX analysis on different zones of the tool rake face (marked with a spot in Figure 4.3) after cutting under cryogenic cooling gives clear evidence of the occurrence of the adhesion mechanism. According to the data reported in Table 4.2, the spot #1 shows high concentration of titanium, aluminium and vanadium that are the main Ti6Al4V elements, indicative of the BUL and chip welding, whereas the spot #2 indicates higher concentration of tungsten and cobalt, namely the chemical elements of the tool substrate, proving the occurrence of the tool coating abrasion. The quantification

of the adhered layer is commonly carried out through the measurements of the chip contact length (sticking zone) onto the tool rake face; however, the crater wear present in many samples did not make possible this type of analysis, as the chip sliding direction was altered by the loss of the tool geometrical tolerances.

The qualitatively analysis of the rake tool face demonstrated as regardless of adopted technologies, adhesion and abrasion are the most significant wear mechanisms.

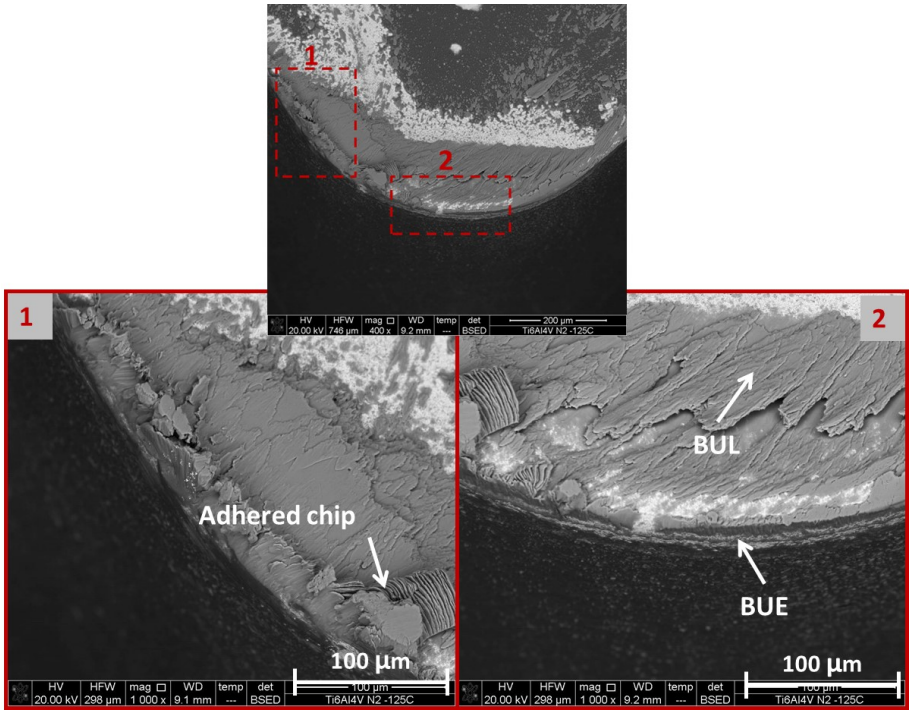

Figure 4.2. Adhesive wear mechanisms after 15 minutes of turning Ti6Al4V under cooled N2 at -150°C.

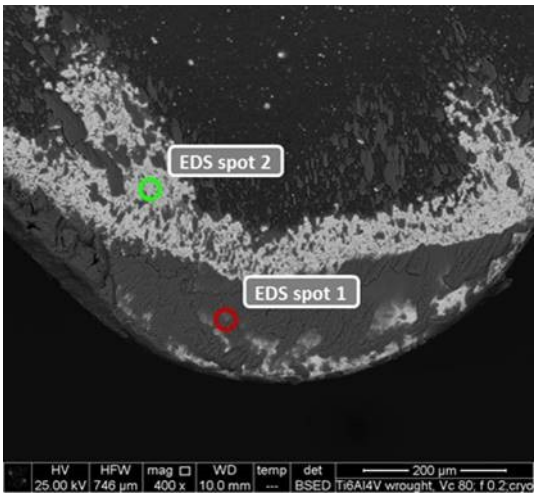

Figure 4.3. Tool rake face after 15 minutes of turning the wrought Ti6Al4V under cryogenic cooling.

Table 4.2. EDS results (% wt) for the spots marked in Fig. 7.

# Spot	W	Co	Ti	Al	V
1	10.19	0.64	77.31	5.76	6.1
2	86.63	6.79	4.22	1.95	0.41

Another typical wear mechanism associated to titanium machining is the formation of a crater wear onto the tool rake face, which, in most cases, represents the major cause of accelerated and catastrophic tool failure [3]. The pauperization of the tool matrix elements, primarily the cobalt, as a result of the diffusion process between the tool substrate and adhered workpiece material (BUL), determines the embrittlement of the tool that facilitates the removal process (abrasion and pull-out of the WC grains) associated to the chip flowing. Being the latter a thermally-activated process, those cutting parameters that favour the temperature increase play a key role. In fact, several works demonstrated how the cutting speed represented the most influencing parameter [4], while it was shown that the addition of cryogenic cutting fluids permitted to completely inhibit the crater wear formation.

Figure 4.4 shows the 2D tool rake profiles after machining when using N2 cooled in the temperature range between 0°C and -150°C: the blue line represents the unworn insert, whereas the red, orange, light blue and green ones the profiles of the tool rake faces worn at 0°, -50°, -100° and -150°C, respectively.

Figure 4.5, instead, reports the comparison between the wet and dry case used as references, CO2, LN2 and cooled N2 at -100°C conditions.

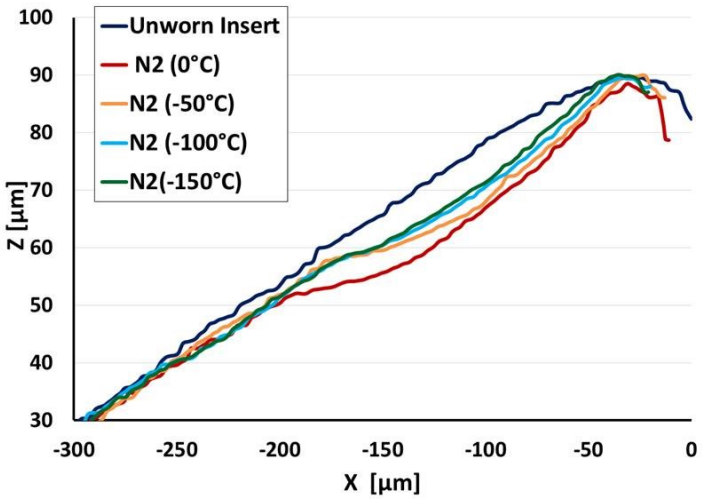

Figure 4.4. 2D profiles of the tool rake face when using N2 cooled at different temperatures.

The values reported in Table 4.3 highlight that the deepest crater was measured in dry machining, while among the cooling strategies the maximum crater was reached when using the N2 at 0°C, even if it must be noted that the wet case presents a negligible difference while the improvement when using the LN2 is just about 10%. On the other hand, when using N2 cooled at temperatures in the range between -25°C and -75°C, the depths of the wear crater became comparable to those obtained when using the LN2 and slightly better than in the case of wet cutting. When using N2 cooled below -75°C, the improvements are not significant, being -150°C the N2 working temperature giving the lowest crater depth, but with already a significant reduction of the crater wear at -100°C. The use of CO2 as cutting fluids did not produce crater.

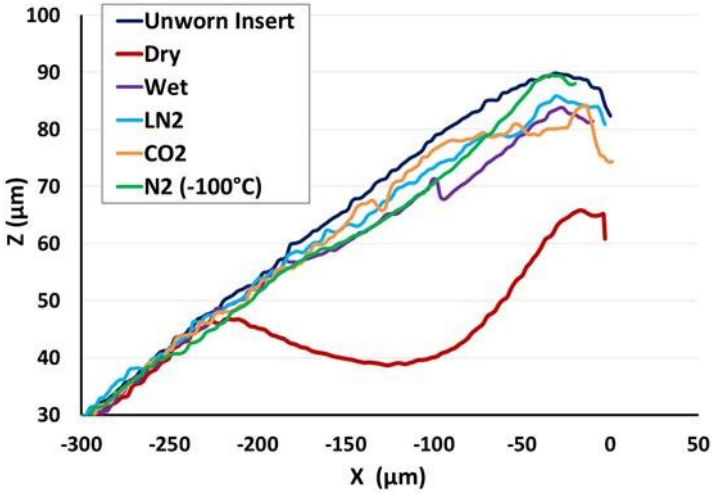

Figure 4.5. 2D profiles of the tool rake face when using conventional cutting fluid, LN2, CO2, N2 cooled at -100°C, and dry cutting.

The low temperatures generated thanks to the LN2, N2 at -100°C and CO2 adduction to the cutting zone can be considered sufficient to completely eliminate the heat generated during the cutting process, inhibiting the diffusion phenomenon and, therefore, reducing the cratering phenomenon. Fig. 4.4 highlights that the tested low-temperature coolants induced very similar tool wear profiles: in both cases the crater wear was completely eliminated, with the detection of only the uniform erosion of the insert notch. The use of cooled N2 compared to the LN2 and CO2 caused a lower geometrical loss of the cutting edge, although in all cases the profile shape is very similar to the one of the unworn insert.

Table 4.3 Wear crater depth as a function of the adopted cooling strategies (measurement uncertainty equal to 6%).

Cooling strategy	Crater depth (µm)
Dry	32.73
Wet	8.31
LN2	7.55
CO2	-
N2 (0°C)	8.41
N2 (-25°C)	7.87
N2 (-50°C)	8.09
N2 (-75°C)	7.69
N2 (-100°C)	6.17
N2 (-125°C)	6.21
N2 (-150°C)	4.94

The tool life criterion is usually defined in terms of flank wear: according to the ISO 3685 standard [5], the mean abraded layer thickness called VBc (white areas visible in Figure 4.6 for two cooling conditions) must not exceed the value of 0.3 µm for turning operations, but this limit, in case of finishing operations on difficult-to-cut alloys, is reduced to 0.1 µm in order to guarantee an acceptable surface quality.

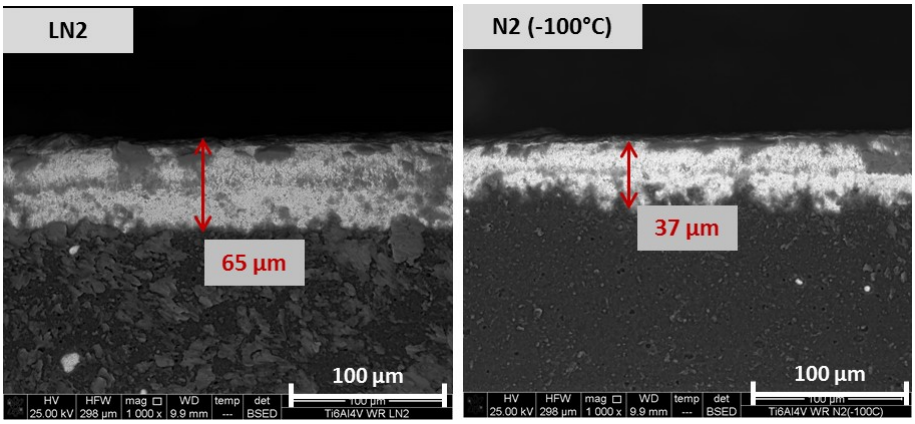

Figure 4.6. Tool flank wear after 15 min of turning when using LN2 and N2 cooled at -100°C.

As shown in Figure 4.7, this condition is always respected, being the fixed limit never exceeded. Also in this case the maximum flank wear was detected in dry cutting, the

value was estimated around 84 μm. Surprisingly the second highest value was measured when adopting the LN2 cooling, which showed a percentage increase of about 30% with respect to the wet condition. On the contrary, the use of cooled N2 always determined an improvement compared to the wet cases: the best result was highlighted at -100°C at which the abraded layer reduction reached the 26% with respect to the conventional lubrication, and 43% with respect to the LN2 cooling. However, as it can been in Figure 4.7, the N2 temperature did not significantly influence the VBc value: in fact, the maximum difference was detected between the N2 cooled at a 0°C and the N2 cooled at -100°C, with a flank wear reduction of 19%, however, such slight improvement does not economically justify the costs associated to the use of cooled N2 at -100°C. Lastly the CO2 produced an intermediate case between the LN2/wet and the cooled N2, amounting to 55 μm.

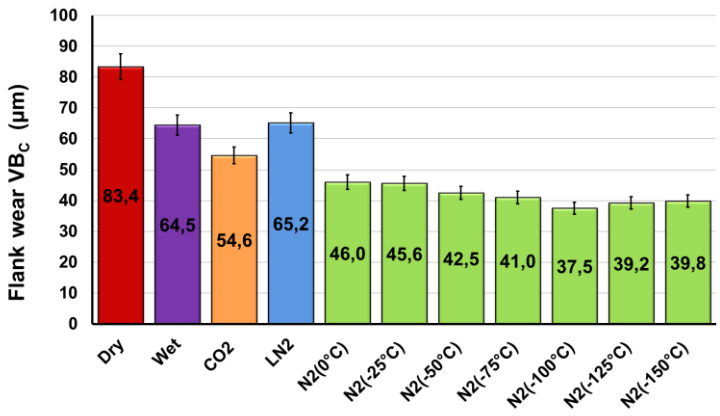

Figure 4.7. Flank wear VBc as a function of the adopted cooling strategies.

4.2.2 Surface integrity

Machining operations are renowned to affect the service life of the machined products altering their surface topography as well as mechanical and metallurgical characteristics within the machining-altered surface layers as described in details by Ginting et al [6] and Che-Haron et al. [7] under dry cutting conditions. In this work, the machined surface integrity was evaluated in terms of deformed layer width, surface finish as well as typology of surface defects.

The average values of the surface roughness Ra obtained from five measurements at different points of the machined surface for each cooling condition are reported in Table 4.4. The best surface finishing was found when applying the LN2 whereas the worst one was measure under dry condition. Two distinct roughness ranges as a function of

temperature were highlighted when using the cooled N2. In details, from 0°C to -50°C the surface roughness oscillated between 1.32 and 1.26 μm while it was close to 1.15 μm in the range between -75°C and -150°C, being the latter value very close to the one measured for the wet condition. The results obtained for the CO2 and cooled N2 did not present significant differences compared to the wet case used as baseline.

The surface quality was further evaluated analysing the surface topography of the machined samples. Figure 4.10 shows the 2D and 3D profiles for the wet, LN2 and some cooled N2 conditions.

Table 4.4. Average values of the surface roughness as a function of the adopted cooling strategies.

	Ra (μm)	**STD (μm)**
Dry	1.32	0.053
Wet	1.163	0.024
CO2	1.208	0.019
LN2	1.044	0.026
N(0°C)	1.281	0.037
N(-25°C)	1.327	0.019
N(-50°C)	1.261	0.049
N(-75°C)	1.157	0.038
N(-100°C)	1.1465	0.027
N(-125°C)	1.153	0.031
N(-150°C)	1.1438	0.054

The dry and wet samples do not present any irregularities due to the material improved plasticity as a consequence of the high temperatures generated during the cutting process. The effect of drastic cooling is visible in the 2D profile for the LN2 and CO2 cases where double feed-marks topography is evident. The only other samples that presented such discontinuous surfaces were those machined using the N2 cooled at -100°C and -150°C, with the irregularities localized on the feed peaks for the former and along the slope feed for the latter. Lastly, the use of N2 up to temperature of -75°C produces surfaces similar to that obtained under wet conditions.

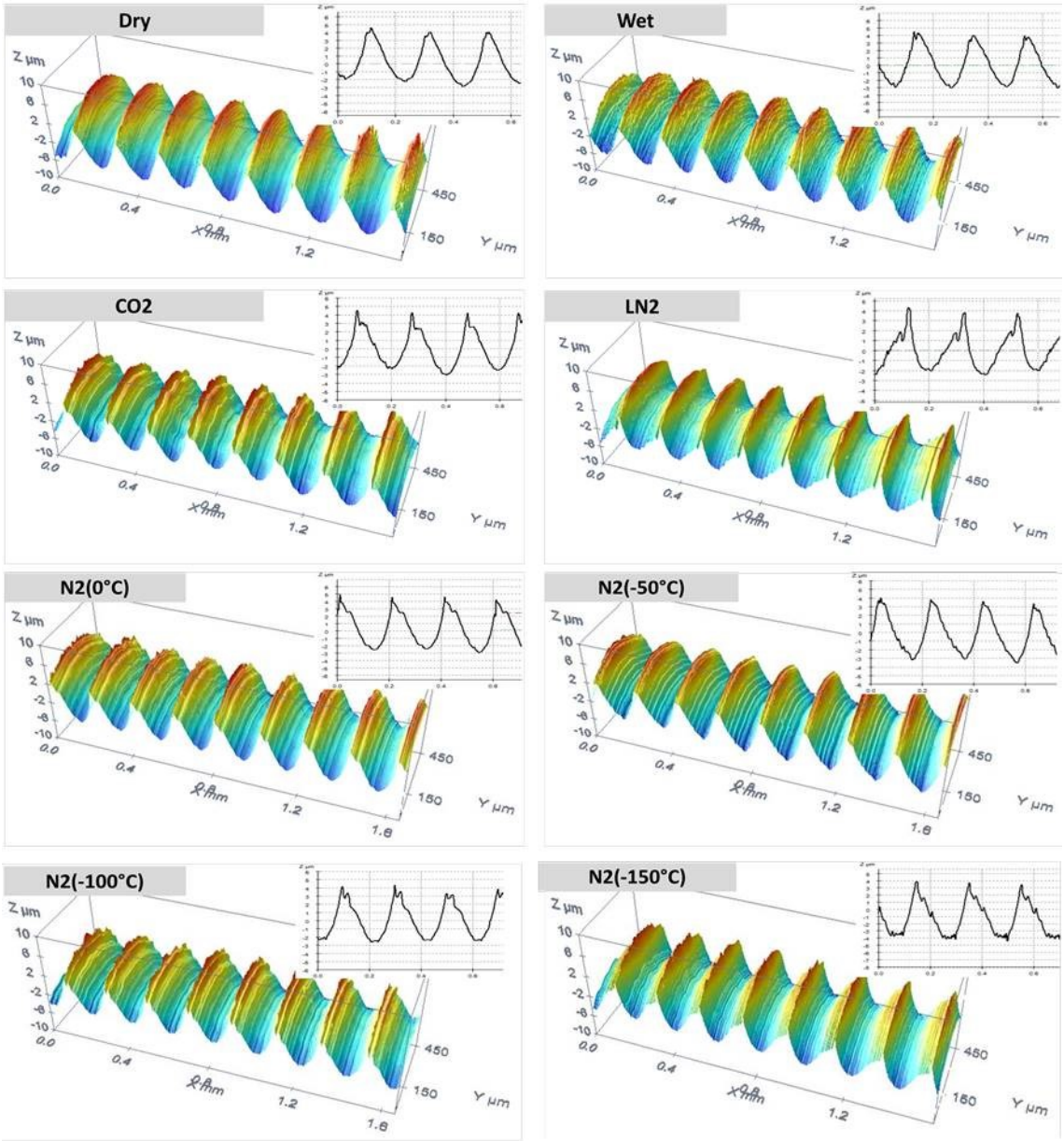

Figure 4.8. 3D and 2D surface topographies of samples machined under different cooling strategies

An SEM qualitative analysis was carried out to identify the main surface defects produced during turning under the adopted cooling strategies. An overview of the main typologies is shown in Figure 4.9, where two distinct defect categories can be defined on the basis of their formation mechanism. The first category is relevant to defects that formed as a consequence of the high temperatures generated in the cutting zone due to the Ti6Al4V low thermal conductivity and high mechanical resistance: examples of these defects are micro-particles welded on the machined surface (these can be either chip fragments or portions of built-up edge) and material side flow. The sample machined in dry condition and under conventional lubrication showed this type of defects in highest

density and with the highest average dimension with respect to the other cooling conditions. The use of low temperature coolants determined a substantial reduction of these defects: the cleanest surfaces, almost free from adhered material and side flow, were obtained using LN2 and N2 cooled at -100°C and -150°C.

The second category includes defects generated as a consequence of the drop of the alloy plasticity due to the very low temperatures: examples are feed marks irregularities, tears and wrinkles inside the feed-marks valleys, as shown by the sample machined under LN2 and CO2 cooling.

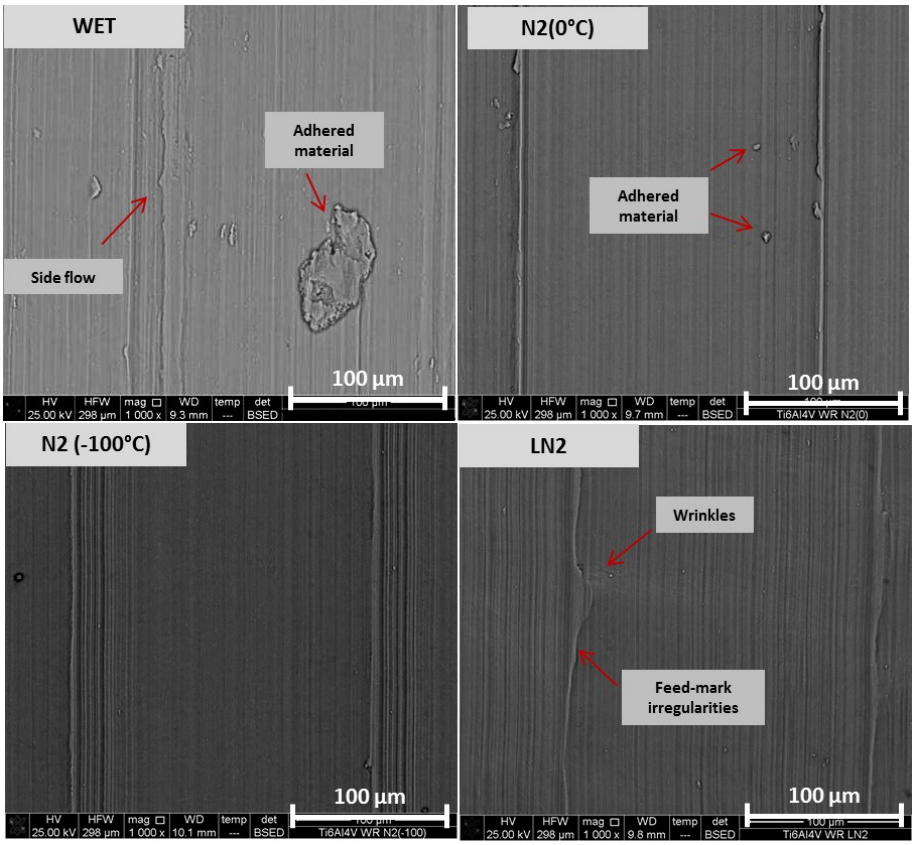

Figure 4.9. Main typologies of surface defects detected on samples machined under different cooling strategies.

Figure 4.10 shows an example of typical sub-surface microstructural alterations as a consequence of turning, consisting of grains heavily deformed along the cutting direction. The effect of the use of different coolants onto the deformed layer thickness is shown in Figure 4.11: the reported values are the average ones obtained from five SEM measurements in different areas of the investigated sample.

The use of LN2 and the dry condition produced an altered layer of about 9.93 µm and 10.3 µm, that represent in this analysis the highest measured values, 27% and 21% respectively higher than the one measured in case of wet cutting. Surprisingly, the use of

cooled N2 was ameliorative compared to the baseline cases, except when using N2 cooled at 0°C. A progressive improvement was found in the temperature range between 0 and -50°C, within which the deformed layer thickness was reduced from 8.8 µm to 6.2 µm with a percentage reduction equal to 29.7%. On the contrary, for temperatures lower than -50°C, the measured values remained almost constant, even if they were significantly lower than the one measured in case of LN2 cooling. Compared to the conventional lubrication case, the N2 cooled at 0°C did not produce any improvement, whereas already at -25°C there was a significant reduction, with the best result detected when cooling the N2 at -125°C).

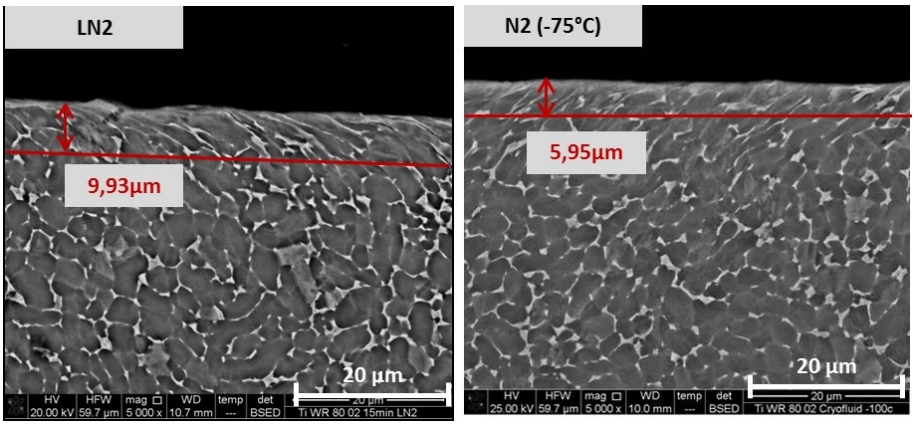

Figure 4.10. Examples of sub-surface microstructures after 15 minutes of turning with indication of the deformed layer**.**

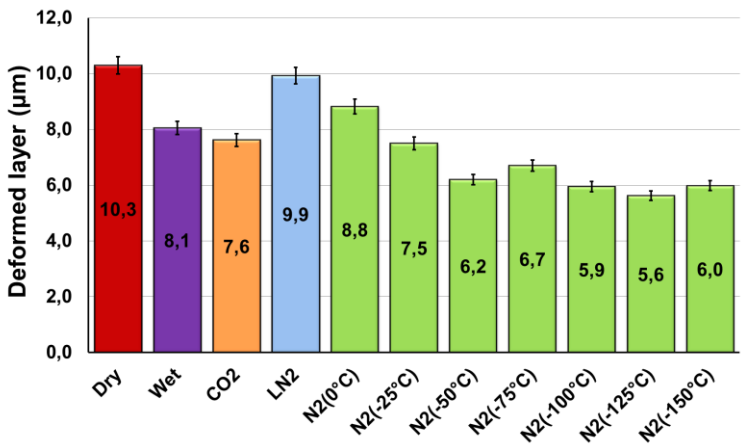

Figure 4.11. Thickness of the deformed layer as a function of the adopted cooling strategies

The axial residual stresses depth profiles measured on the workpiece surface are shown in Fig. 4.12. In this analysis the first measured points (at the surface) must not considered since the surface topography is not suitable for the X-Ray measurements and hence may be subject to measuring errors.

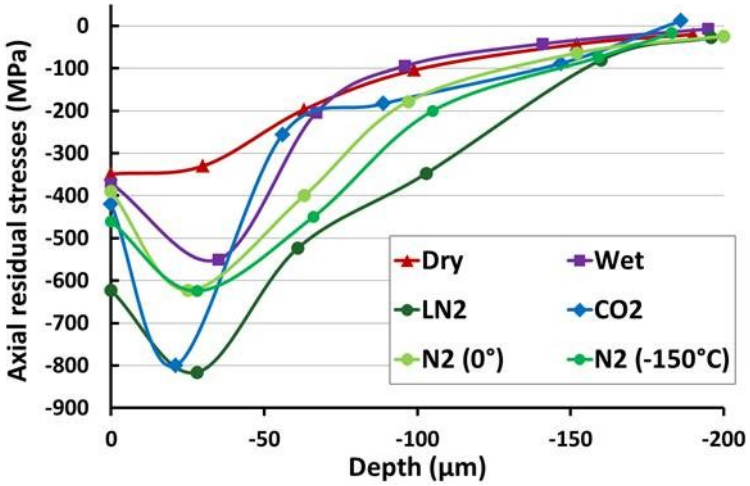

Figure 4.12. Axial residual stresses as a function of the adopted cooling strategies (measurement uncertainty equal to 8%).

In this type of analysis only the most interesting cooling condition were evaluated, namely the dry cutting, wet, LN2, CO2, N2 at -100°C and N2 at -150°C. A residual compression stress state was evidenced for all the tested strategies, but with the highest values found for the LN2 and CO2 conditions while the worst one for the dry cutting, -816 MPa, -800 MPa and -330 MPa, respectively. The cooled N2 strategy instead produced intermediate values, slightly higher than those measured for the wet case, with a percentage difference of about 11.8%.

The application of the cryogenic coolants induced a general thickening of the compressive surface residual stress layer. A proof of that is reported in Table 4.5, in which if a threshold value of -300 MPa is considered for the axial stress, the corresponding abscissa is shifted towards deeper position for the tested cooling strategies with respect to the dry condition.

Table 4.5. Minimum values of residual stresses and layer thickness considering a threshold value of -300 MPa.

Strategies	Min. residual stresses (MPa)	Gain (%)	Layer depth > 200MPa (µm)	Gain (%)
Dry	- 330 ±	-	-33.0	-
Wet	- 550 ±	+66.6	-58.0	+75.7
LN2	- 816 ±	+147.3	-113.0	+242
CO2	- 800 ±	+142.4	-53.6	+62.4
N2 (0°C)	- 623 ±	+88.8	-78.1	+136.6
N2 (-150°C)	- 624 ±	+89.0	-89.2	+170.3

The deepest layer was measured for the sample machined under LN2 in which the thickness reached about 113 μm. Regardless by the adopted temperature value, the use of cooled N2 determined the formation of a thinner layer about 80 μm, while the CO2 outcome was similar to the conventional wet one. It is worth to notice that the technique based on CO2 produced one of the highest values of compressive residual stresses but it dropped quickly, while the LN2 presented a thicker layer with higher compressive values.

The Young's modulus and nano-hardness of the three samples, namely dry, LN2 and CO2, are shown in Fig. 4.13 and Fig. 4.14, respectively. The reference value (average value of the grid evaluated at the sample center) is given for each property.
The nano-hardness analyses (see Table 4.6 and Fig. 4.13) highlighted that the adopted strategies determined microstructural alterations, increasing the surface nano-hardness with respect to the reference condition (4.33 ± 0.38 GPa). However, the difference in properties existing between the two phases of the Ti6Al4V led to a quite large deviation standard (see Table 4.6) that did not permit further considerations about the nano-hardness evolution.

Table 4.6. Nano-hardness values for the samples machined under different cooling strategies.

Distance from the surface (μm)	**Nano-hardness (GPa)**		
	Dry	**LN2**	**CO2**
6	4.585 ± 0.088	4.823 ± 0.519	4.791 ± 0.358
11	4.791 ± 0.096	4.840 ± 0.438	4.821 ± 0.511
16	4.758 ± 0.221	4.924 ± 0.597	4.802 ± 0.477
21	4.868 ± 0.145	4.969 ± 0.642	4.634 ± 0.453
26	4.957 ± 0.228	4.729 ± 0.506	4.573 ± 0.566
31	4.783 ± 0.232	4.693 ± 0.674	4.609 ± 0.446
36	4.934 ± 0.173	4.706 ± 0.421	4.699 ± 0.452
41	4.797 ± 0.377	4.374 ± 0.429	4.547 ± 0.504
46	4.921 ± 0.173	4.447 ± 0.503	4.491 ± 0.498
51	4.719 ± 0.101	4.531 ± 0.288	4.397 ± 0.431

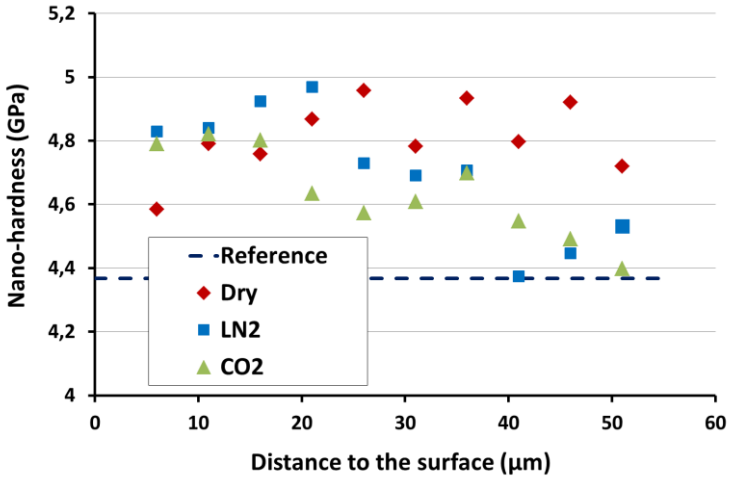

Figure 4.13. Nano-hardness profiles for the samples machined under different cooling strategies (average measurement uncertainty equal to 10%).

As concerns the Young's modulus, appreciable differences are evident between the dry sample and the other two samples (Fig. 4.14). In order to smooth the uncertainties associated with the Ti6Al4V biphasic microstructure, the values of the Young's modulus were normalized using the reference one obtained at the center of the dry sample, namely 127 GPa.

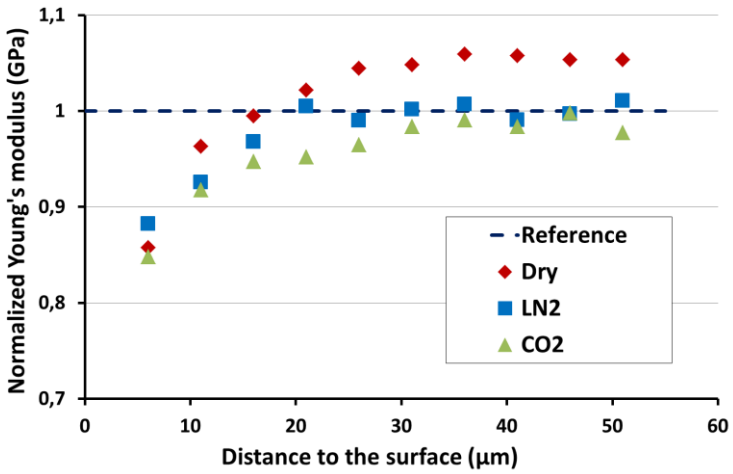

Figure 4.14. Young's modulus behaviour for the samples machined under different cooling strategies with the bulk value as reference.

The highest difference was measured for the sample machined under CO2 cooling: at 6 µm from the machined surface, the elastic modulus was 15% lower than the bulk value. In case of dry and LN2 cooled samples, the reduction reached 14% and 11%, respectively. However, in both cases, the initial values rapidly increased moving away from the surface: at approximately 30 µm from the machined surface, the LN2 and CO2

cooled samples presented the same value measured for the bulk material, while the dry cut sample showed a relative increase in the normalized Young's modulus of 5% with respect to the reference value.

4.2.3 Discussion

The aforementioned experimental results showed as the cooling technology based on the use of gaseous N2 cooled at around -100 °C produced the best performances in terms of both tool wear and surface integrity. In order to explain this unexpected experimental evidence, a detailed analysis of the fluids properties was carried out. Since the improvements of most of the measured parameters (i.e. adhesion mechanisms, hardening layer,..) are directly linked to the temperature reduction, the fluids cooling capacity was chosen to be calculated in order to provide the information necessary to explain the effects of the different cooling technologies on the Ti6Al4V machinability. In the following, the analytical modelling of the fluids the cooling capacity is presented and the correlation with the Ti6Al4V machinability is discussed. Since the CO2 presents some critical issues associate to its thermodynamic phase transformation, only the LN2 and cooled N2 were evaluated in term of cooling capacity.

4.2.3.1 Analytical modelling

The temperature at which the coolant is delivered to the cutting zone is not the only parameter affecting the Ti6Al4V machinability: if this were so, the tool wear and machined surface integrity for the N2 condition cooled at -150°C should be close to those obtained for the LN2.

Besides temperature, also the pressure of coolant application p and nozzles area A, which were different between the tested cooling strategies, affect the Ti6Al4V machinability. In order to take into account all the relevant parameters, and merge them into one single parameter characteristic of the applied cooling strategy, the cooling capacity defined according to Eq. (4.1) and expressed in (kW), was used in this study.

$$\dot{Q} = \dot{m}Q \tag{4.1}$$

Where $\dot{m}$ represents the mass rate (kg/s), and Q the heat exchanged by the system with the environment (kJ).

It is worth to note that the fluid cooling capacity expressed in terms of thermal power combines the most relevant process parameters, namely temperature, pressure and flow rate, with the physical characteristics of the coolant (see Table 4.7).

Table 4.7. Experimental set-up parameters and physical characteristics of LN2 and gaseous N2.

	Δp (bar)	**A (m^2)**	**ρ (kg /m^3)**
LN2 (-196°)	15	$1.27x10^{-6}$	808.5
N2 (-100°C)	2.5	$2.83x10^{-5}$	3.528

The evaluation of the cooling capacity started with the calculation of the heat required by either the gas or the fluid to pass from its initial state inside the ranger (namely its pressure and temperature) to the environmental one at 1 bar and 20°C. This step was subdivided in two distinct stages: in the first one an isothermal transformation was applied determining a pressure change through the fluid expansion (Eq. (4.2)), while in the second one a isobaric transformation at 1 bar was applied to cause a heating from the N2 initial temperature to the room one, which was fixed at 20°C (Eq. (4.3)). In this analysis the work done to the system during the isothermal expansion was considered negligible.

$$N2\,{}^{Tin.}_{pin.} \xrightarrow[process]{isothermal} N2\,{}^{Tin.}_{1bar.} \tag{4.2}$$

$$N2\,{}^{Tin.}_{1bar.} \xrightarrow[process]{isobaric} N2\,{}^{20°C}_{1bar.} \tag{4.3}$$

From the first thermodynamics principle in an isobaric transformation the heat exchanged with the environment (Q in Eq. (4.1)) corresponds to the enthalpy difference ΔH (kJ/kg) between the initial and final states: for the adopted cooling strategies the literature values are reported in Table 7.

Afterwards, the mass rate $\dot{m}$ was calculated, using two different formulations for the LN2 and the N2.

For incompressible fluids as the LN2 is, $\dot{m}$ is defined as the product between the flow rate and the density (Eq. (4.4)), using for the latter the value reported in Table 6.

$$\dot{m} = \dot{q}\rho \tag{4.4}$$

The flow rate $\dot{q}$ was determined according to Eq. (4.5) by multiplying the nozzle area A with the outlet coolant speed v_c (m/s) calculated by means of the Bernoulli simplified

equation (Eq. (4.6)), hypothesizing null the losses along the cooling line. In detail, P_{in} and P_{out} represent the pressure inside the chamber and the atmospheric pressure, respectively, while ρ is the fluid density (kg/m^3).

$$\dot{q} = Av_c \tag{4.5}$$

$$v_c^2 = \frac{2(P_{in}-P_{out})}{\rho} \tag{4.6}$$

Substituting the Eq. (4.5) and Eq. (4.6) in Eq. (4.1), the following formula was obtained:

$$\dot{Q} = \dot{q}\rho(Q) = A\sqrt{2\,\Delta p\,\rho}\,(\Delta H) \tag{4.7}$$

The parameters that influence the cooling capacity of fluids as the LN2 can be subdivided into two categories: the first one is linked to the fluid thermo-physical properties, namely the density, specific heat capacity, and specific heat of vaporization, while the second to the experimental setup parameters, namely the applied pressure and nozzle area.

For gases instead, assuming the process inside the chamber as stationary being in this case the gas composed only by the N2, Eq. (4.8) was used for the gas outflow from a pipe.

$$\dot{m} = ACp_0\sqrt{\frac{PM\,\Upsilon}{T_0\,R}\left(\frac{2}{\Upsilon+1}\right)^{(\Upsilon+1)(\Upsilon-1)}} \tag{4.8}$$

where A represents the nozzle area (m^2), C is a constant equal to 0.8 for the critical outflow [8], p_0 and T_0 are the pressure and the temperature inside the chamber, respectively, PM the N2 molecular weight, R the universal gas constant, and lastly Υ a constant linked to the atomic structure of the gas that assumes the value of 1.4 being N2 a diatomic gas.

Eq. (4.9) expresses the thermal power for gaseous phases.

$$\dot{Q} = ACp_0\sqrt{\frac{PM\,\Upsilon}{T_0\,R}\left(\frac{2}{\Upsilon+1}\right)^{(\Upsilon+1)(\Upsilon-1)}}\,(\Delta H) \tag{4.9}$$

On the basis of the procedure above described, the cooling capacities of the LN2 and N2 cooled at different temperatures were calculated and are shown in Figure 4.15 and reported in Table 4.8 as well.

The results highlight how the LN2 presents much higher cooling capacity than the N2, even cooled at -150°C. This very significant difference is mainly due to the LN2 high density and high enthalpy difference between the initial and final conditions as a consequence of the specific heat of vaporization, despite the system adducting the LN2 has a smaller nozzles area than the one of the cooled N2. Furthermore, it must be noted that the reduction of the N2 temperature from 0° to -150°C leads to a cooling capacity increase from 0.18 to 2.36 kW, but still one order of magnitude less than the LN2 one.

Table 4.8. Heat, mass rate and cooling capacity values calculated for the adopted coolants (*ΔH was calculated using NIST website [9]).

Coolant	ΔH* (kJ/kg)	ṁ (kg/s)	$\dot{Q}$ (kW)
LN2 (-196°C)	425.61	0.058	24.7
N2 (-150°C)	176.53	0.0134	2.36
N2 (-125°C)	150.24	0.0122	1.83
N2 (-100°C)	124.06	0.0112	1.39
N2 (-75°C)	97.95	0.0105	1.03
N2 (-50°C)	71.88	0.0099	0.71
N2 (-25°C)	45.83	0.0094	0.43
N2 (0°C)	19.79	0.0089	0.18

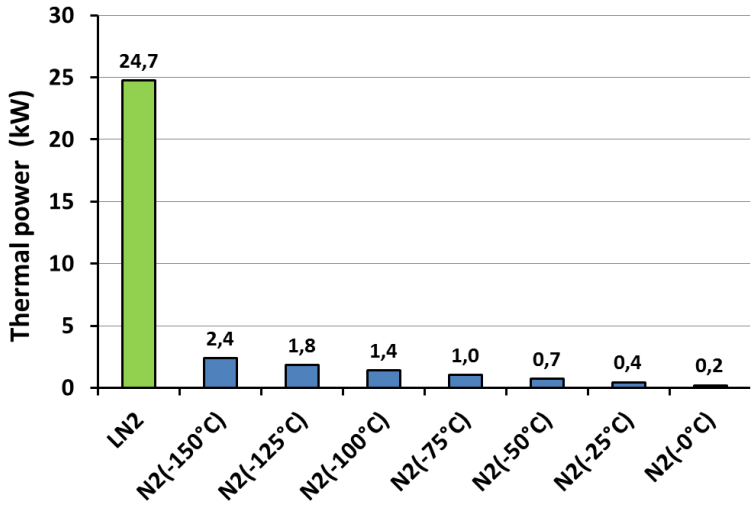

Figure 4.15. Cooling capacity defined as thermal power for the adopted coolants.

4.2.3.2 Correlation with Ti6Al4V machinability

As described in paragraph 3, the main wear mechanisms detected during semi-finishing turning of Ti6Al4V were adhesion/diffusion, responsible of the cratering phenomenon, and abrasion, both temperature dependent, although with different effects.

The experimental analysis highlighted that the crater depth did not vary substantially when using LN2 or N2 cooled under -25°C. Since the crater wear is a combination of thermally activated process, the addition of these coolants to the cutting zone was sufficient to completely eliminate the heat generated during the cutting process inhibiting the diffusion phenomenon and, therefore, reducing the adhesion. The removed material is to be attributed to the sole abrasive action due to the chip sliding on the tool rake face. At 0°C, instead, the fluid cooling capacity was not sufficient to remove completely the generated heat, determining a crater similar in terms of depth to that found when using the conventional lubricating strategy.

As regards the flank wear the mechanical properties of the material to be machined played a predominant role. The highest VBc measured for the LN2 case can be ascribed to the material hardening induced by its elevated cooling capacity. The best results in terms of flank wear reduction were highlighted in the case of N2 cooled at -100°C, which presented a cooling capacity sufficient to limit the material adhesion without causing an excessive material hardening.

Also the parameters that characterized the machined surface integrity showed a correlation with the tested cooling strategies. The very high cooling capacity of the LN2 affected significantly the deformed layer as a consequence of the excessive reduction of the material plasticity.

The drop of the material ductility linked to the product thermal contraction due to the LN2 use during the cutting process can be the cause of formation of both jagged surface (double feed-marks) and surface defects, such as wrinkles and feed-marks irregularities. Although machined using N2 cooled at -150°C, the sample surface did not present characteristic defects detected for the previous case; again, these different outcomes can be ascribed to the very different cooling capacities of the two coolants. Defects, as adhered and smeared material that were typical of dry and wet turning, were progressively eliminated reducing the coolants temperature, since the thermal component responsible of either the welding or plastic deformation was inhibited.

Different considerations can be drawn to explain the evolution of the residual stresses. The main mechanisms responsible of their formation are the mechanical stress field, which induces the plastic deformation of the surface layer, and the thermal load, which affects the cutting zone. As reported in literature, the former phenomenon induces a compressive state of stress in the machined material, while the developed temperature field, being responsible of the material thermal dilatation, determines a tensile state of stress. The resulting residual stress state is the sum of these two contributions. The experimental evidences highlighted that in all the machined samples a surface compressive state of stress was present, proving that the plastic deformation represented the main contribution regardless the adopted cooling strategies. However, the use of low-temperature coolants, able to reduce the thermal effects, determined an increase of the surface compressive value. The highest surface compressive stress was measured when using the LN2 characterized by the highest cooling capacity.

The Young's modulus is affected and the thickness of the affected layer varies as a consequence of the adopted cooling strategies. The CO2 sample appears to be more perturbed with an alteration of the 15% at 6 μm to the surface and with the larger affected range (31 μm). The reference value obtained from the centre of the dry sample (127± 4.37 GPa) is in accordance with the literature in similar alloys [10]-[12].The difference between the Young's modulus given by the supplier (118 GPa in Table 1) and the value obtained from nano-indentation is consistent with other studies reporting on both macro and nano-properties [10],[11].As concerns the surface properties evaluated by nano-indentation, both the Young's modulus and nano-hardness resulted modified with respect to the bulk material, with some uncertainties due to the biphasic microstructure of the Ti6Al4V alloy. In view of the similar trends in the Young's modulus, it was chosen to normalize it. This revealed a significant alteration onto the samples surface as a consequence of the adopted cooling strategies. The reference value obtained at the centre of the dry cut sample (127 GPa) is in accordance with literature values of similar alloys obtained using nano-indentation [10]-[12]. However, it is worth to underline that the difference between the Young's modulus given by the supplier (114 GPa in Table 1) and the value obtained from nano-indentation is consistent with other studies reporting both macro and nano-properties. In accordance with the literature, the nano-hardness of the surfaces exhibited higher values in comparison with the reference value (4.33 ± 0.38

GPa) [13]. These alterations may be correlated to the machining process that induced material hardening.

On the basis of the experimental evidences, the N2 cooled at -100°C represents the best cooling strategy as it presented the lowest VBc value (flank wear), a crater depth comparable to that obtained using LN2, and an improved surface quality in terms of surface topography, surface defects and altered layer. Moreover, the lower cooling capacity of the cooled N2 reduces both the thermal stresses induced onto the mechanical components that may damage the lathe and mandrel mechanism, and the thermal distortion onto the tool holder with consequent loss of dimensional accuracy of the machined components especially when finishing and semi-finishing operations are addressed. It is worth to note that the N2 cooled at -150°C produced very similar results, as its cooling capacity is very close to the one of the N2 cooled at -100°C: therefore, to reduce the process cost, to lower the thermal stresses of the mechanical components and to improve the operator safety, the optimal choice is the N2 cooled at -100°C.

4.3 Lubricating strategies

In this paragraph the experimental results of innovative minimal techniques, based on Minimum Quantity Lubrication (MQL) and Minimum Quantity Cooling (MQC) strategies are reported.

An aqueous solution added with different graphite percentages, namely 5%, 10% and 15%, was used as SL-assisted MQC technique, whereas vegetable MQL oil enriched with 5% in weight of PTFE particles provided the SL-assisted MQL technique. As baseline, dry cutting, conventional wet strategy and pure MQL were used. The effects on the tool wear were analysed in terms of crater and nose wear while the machined surface quality was assessed considering the surface topography, surface defects and altered layer. The Table 4.9 shows the experimental set-up adopted for the turning tests.

Table 4.9. Experimental plan for the turning tests.

Material	**Cutting parameters**			**Tested technologies**
-	**Depth of cut (mm)**	**Feed rate (mm/rev)**	**Cutting speed (m/min)**	-
Wrought	0.25	0.2	80	MQL – SL assisted MQC – SL assisted MQL

4.3.1 Tool wear

The SEM images of the tool rake face after 15 minutes of turning highlight the presence of adhered material (BUL and BUE) onto the tool rake face (see Figure 4.16) regardless the adopted lubricating techniques. An EDS analysis carried out by the authors in a previous paragraph (see §4.2.1) proved in fact that the adhered grey material was titanium while the white zones were the insert substrate made by tungsten carbide.

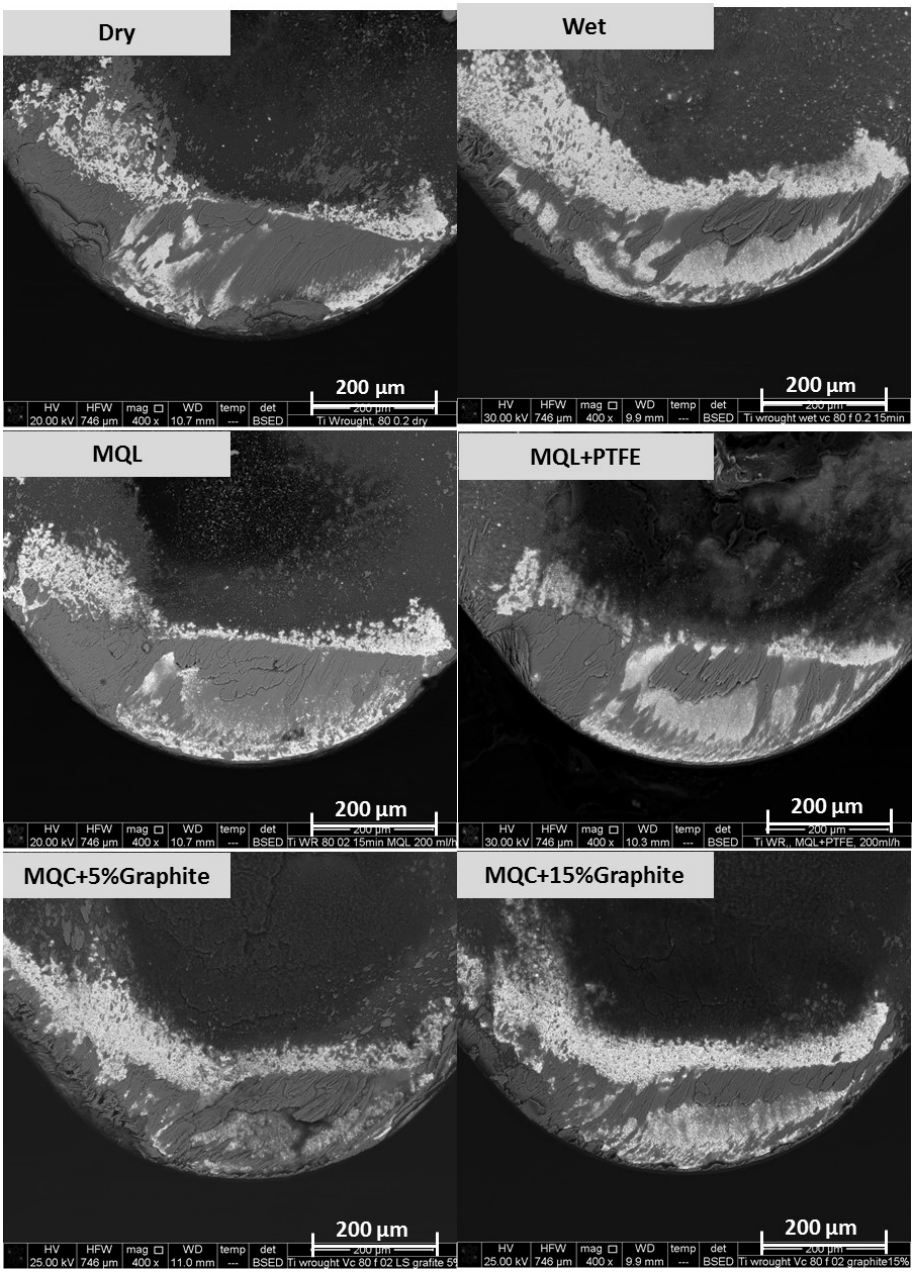

Figure 4.16. SEM images of the tool rake face after 15 minutes of turning under the adopted lubricating/cooling strategies.

In the case of the SL-assisted techniques, deposits of the used additives were found immediately over the abraded area (their chemical composition from the EDS analysis is

reported in Table 4.10). Also the 2D profiles of the tool rake face obtained using the optical profiler highlighted their presence as shown in the Figure 4.17, where the green and light blue lines represent the worn tool profiles under SL-assisted MQC and MQL technologies using graphite and PTFE, respectively. These residues developed as a consequence of the chip flowing on the tool rake face that tended to press the solid particles of the lubricant solution into the tool rake face depression designed to facilitate the chip breaking. The EDS analyses revealed the presence of carbon, silicon and oxygen in the deposit onto the rake face of the tool used under SL-assisted MQC technique, whereas carbon and fluoride were found when using the SL-assisted MQL technique: these are the elements of which graphite and PTFE are constituted, respectively

Table 4.10. Chemical composition (% wt) of the adhered material found in the tool rake face depression for the SL-assisted techniques.

	C	Si	O	F	Ti
MQC+Graphite	65.58	21.78	12.36	-	0.28
MQL+PTFE	36.81	-	-	63.19	-

The graph in Figure 4.17 B shows the profiles closer to the cutting edge at higher magnification. To evaluate the extent of the crater wear, the 2D profiles of the worn tool rake faces were compared with the unworn one, and the recorded depth values are reported in Table 4.11.

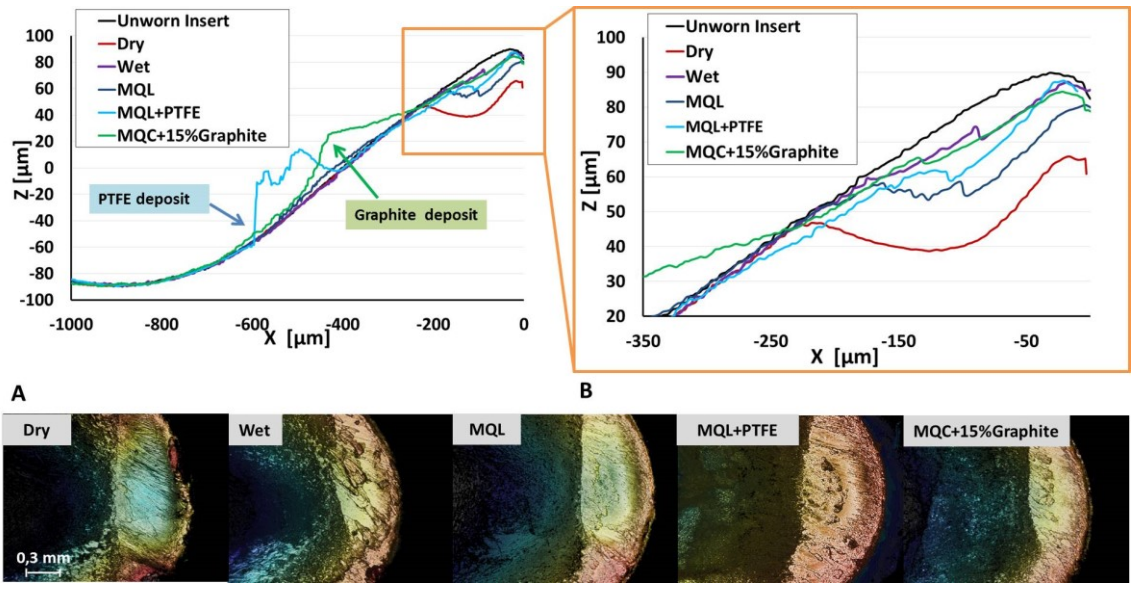

Figure 4.17. Tool rake faces under the adopted lubricating/cooling strategies: (A) overall 2D profiles, (B) zoom of the zone of the worn cutting edge, and (C) 3D images.

A maximum crater depth of about 32 μm was reached under dry cutting conditions. The lowest depth was found for the conventional wet strategy, even if the use of the SL-assisted MQC strategy with 15% of graphite produced similar results with a reduction in the crater depth of around 75% with respect to the dry case; the use of lower graphite percentages (5% and 10%) determined a slightly deeper crater.

The results obtained with the strategies based on the MQL technique did not produce advantages comparable with those found using the wet and SL-assisted MQC strategies, as the percentage improvements compared to dry cutting conditions were equal to 41.5% and 50% for the pure MQL and for the MQL added with PTFE, respectively.

Table 4.11 Crater depth as a function of the adopted lubricating/cooling strategies (measurement uncertainty equal to 6%).

Lubricating/cooling strategy	Crater depth (μm)
Dry	32.73
Wet	8.31
MQL	19.12
MQC + 5% Graphite	12.22
MQC + 10% Graphite	11.69
MQC + 15% Graphite	8.76
MQL + PTFE	16.11

A uniform abrasion of the flank face without formation of the wear notch was found in all the conditions regardless the tested strategies as shown in the SEM images of Figure 4.18. After 15 minutes of turning no chipping caused by the BUE instability was found on the worn cutting edge despite of the significant presence of adhered material. Fig. 4.19 clearly shows that the adopted strategies had a substantial effect on the tool nose wear expressed as VBc value (width of the abraded layer). It may be noted that the highest VBc was measured for the dry and wet cases, with values of 83.9 and 65.3 μm, respectively. The pure MQL and the SL-assisted MQC strategies determined similar outcomes, without any significant difference by changing the graphite content, with an average VBc value of around 47 μm. On the contrary, the use of MQL added with PTFE particles determined a significant improvement compared to the pure MQL technique: the VBc value varied from 53.9 μm to 38.1 μm with a percentage reduction equal to 29%

making the MQL added with PTFE the best condition in terms of nose wear reduction. Lastly, unlike what found on the tool rake face, no additive deposits were highlighted on the tool flank face.

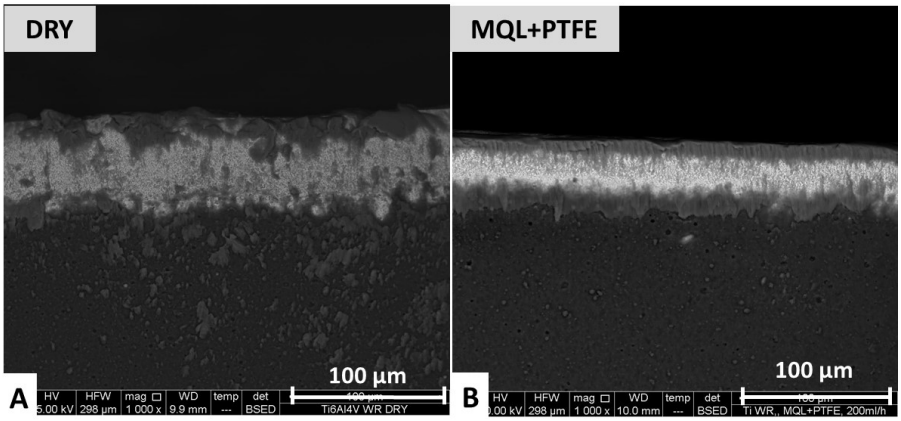

Figure 4.18. Tool flank face after 15 minutes of turning under: (A) dry cutting, and (B) SL-assisted MQL.

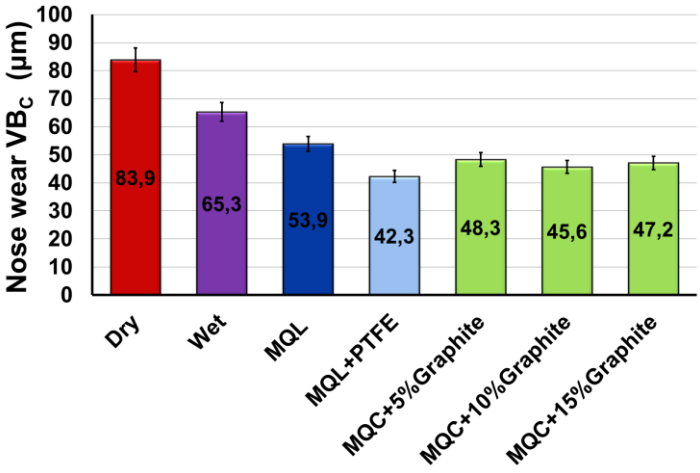

Figure 4.19. Flank wear VB_c as a function of the adopted lubricating/cooling strategies.

4.3.2 Surface Integrity

The alternative lubricating/cooling strategies proposed in this study determined a surface topography similar to the one obtained using a conventional wet strategy (see Figure. 4.20). In all the tested conditions, the 2D profiles presented the same trend without those irregularities or pronounced double feed-marks typical of other innovative cooling strategies as the cryogenic one. The values of the average surface roughness Ra reported in Table 4.12 confirmed this, with a maximum difference of about 25% between the best and worst cases. The dry case presented the worst result, whereas the best surface finish was obtained in case of wet cutting and MQL with PTFE particles.

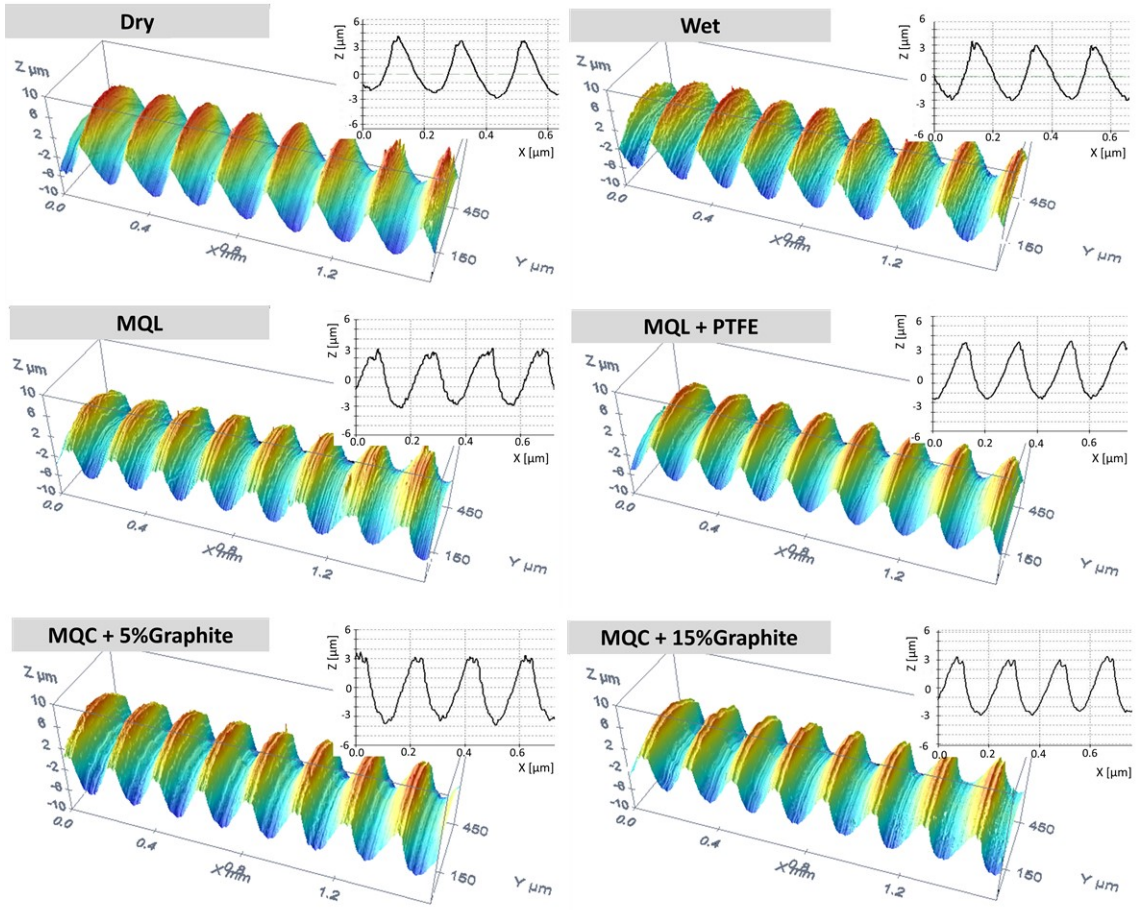

Figure 4.20. 3D topographies and 2D profiles of the surfaces machined under the adopted lubricating/cooling strategies.

Table 4.12. Average roughness Ra as a function of the adopted lubricating/cooling strategies.

Lubricating/cooling strategy	Ra (µm)	STD (µm)
Dry	1.431	0.053
Wet	1.163	0.024
MQL	1.315	0.017
MQC + 5% Graphite	1.328	0.026
MQC + 10% Graphite	1.217	0.031
MQC + 15% Graphite	1.239	0.015
MQL + PTFE	1.146	0.025

The SEM analysis carried out on the surface of the dry cut sample confirmed the presence of material side flow, long grooves and micro-particles adhered on the machined surface, as shown in Figure 4.21 A where the aforementioned defects are present both at high density and with large dimension. These types of defects were

promoted by the high cutting temperatures that determined an increase of the workpiece material plasticity and, therefore, a higher tendency to material welding. They are also present in the case of SL-assisted MQL and MQC strategies even if to a much less extent: from Figure 4.21 B and 4.21 C it can be noted how the machined surfaces are much cleaner, almost free from adhered material and grooves. No deposit or adhered particles of either graphite or PTFE were found onto the surfaces of the samples machined using the SL-assisted strategies.

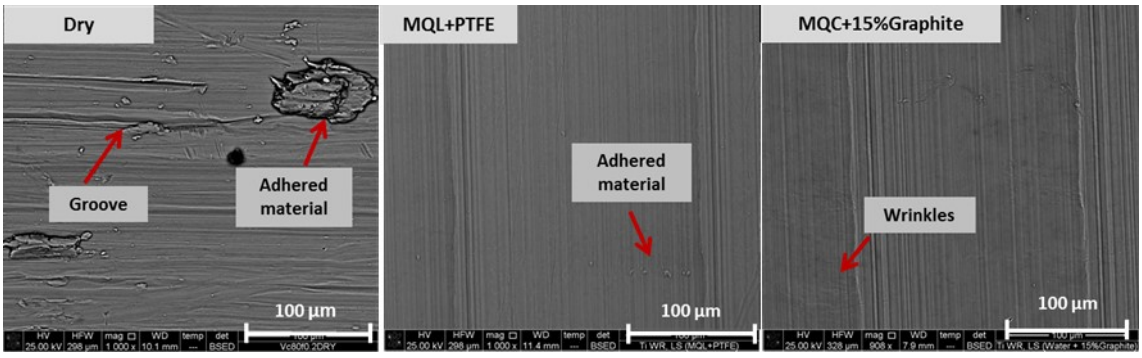

Figure 4.21. Main typologies of surface defects detected on samples machined under: (A) dry cutting, (B) SL-assisted MQL, and (C) SL-assisted MQC strategies

Lastly, the machining-altered layer was evaluated, as the high cutting forces and temperatures involved during the cutting process may determine microstructural alterations of the workpiece material besides the characteristic deformation of the grains along the cutting direction. The effect of the use of different fluids onto the thickness of the deformed layer is shown in Figure 4.22, the reported values representing the average of 5 measurements conducted on SEM images of the machined surfaces in different areas.

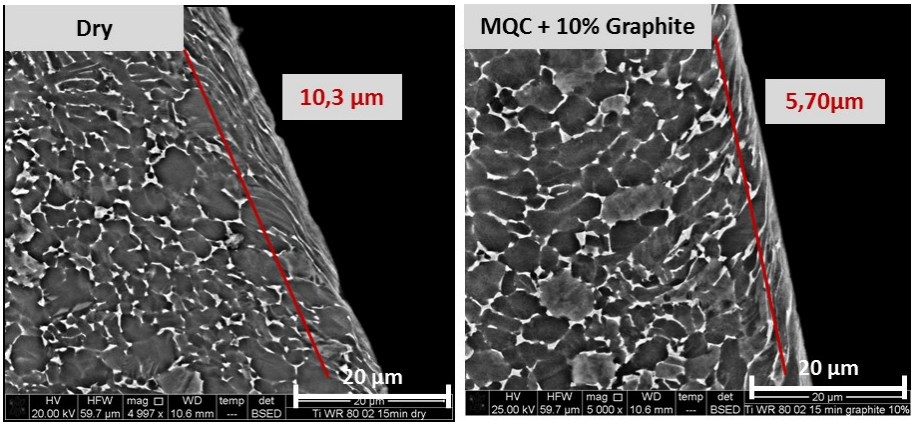

Figure 4.22. Examples of sub-surface microstructure after 15 minutes of turning with indication of the deformed layer.

Dry cutting induced the highest microstructural alteration with a layer thickness of around 10.3 μm, while wet and pure MQL strategies led to a thickness reduction of 21.3% and 12.7%, respectively. A significant improvement was found using MQC with graphite, with the best performance found in case of 15% of graphite, where a reduction of 44% was found compared to the dry case. The use of MQL enriched with PTFE determined a layer thickness comparable to that of the wet case, but without the relevant improvements of the MQC cases (Figure 4.23).

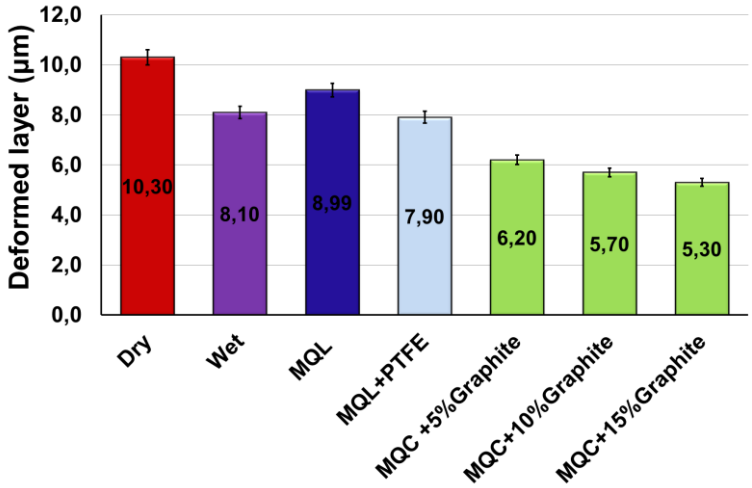

Figure 4.23. Thickness of the deformed layer as a function of the adopted lubricating/cooling strategies.

4.3.3 Discussion

4.3.3.1 Cutting fluid characteristics

An ideal cutting fluid should provide both cooling and lubricating functions. To this regard, the experimental results presented and discussed in § 4.3 are here analysed taking into account the different physical parameters of the cutting fluids: to a first approximation, the cooling capacity can be associated to the heat capacity of the fluid while the lubricating capacity can be linked to its viscosity [14]. Table 4.11 reports the abovementioned parameters: for the aqueous solutions the water heat capacity was considered while for the MQL techniques the heat capacity provided by the manufacturer, considering not significant the effect of the additives in both cases. The dynamic viscosity was instead measured for all the tested cutting fluids by means of a Brookfield^{TM} viscometer according to the procedure presented in [15] and by setting the impeller speed at 50 rpm.

The techniques based on MQL presented the highest values of viscosity, with an additional increase of 9% when using PTFE particles. An interesting behaviour was detected for the SL-assisted MQC techniques, where the dynamic viscosity did not increase linearly with the graphite content. The measured values passed from 28.9 cP to 43.9 cP using solutions at 5% and 10% of graphite, respectively, while a further increase to 15% of graphite did not show the same effect, as the viscosity value remained almost constant with respect to the previous cases at about 45 cP.

The conventional wet emulsion presented an extremely low value of viscosity, out of the lowest limit of the viscometer measurement range and therefore not reported in Table 4.13.

Among the tested techniques the conventional cutting fluid presented the highest cooling capacity thanks to both the water high heat capacity and its high flow rate while had the lowest lubricating capacity, since its viscosity could not be measured with the available viscometer unlike the other fluids; the opposite situation was instead assessed for the MQL cases, which, being minimal lubrication strategies, did not present a significant cooling effect. The MQC techniques guaranteed both the functions: the water allowed dissipating the heat generated during the cutting process while the graphite particles reduced the friction. Despite the flow rates higher than those used in the MQL cases, the MQC strategies may be still considered as minimal techniques when compared to the conventional wet cutting, being their flow rates lower of two orders of magnitude.

Table 4.13. Physical parameters of the tested cutting fluids.

Cutting fluid	Density (kg/ m^3)	Flow rate (l/h)	Dynamic viscosity (cP)	Heat capacity (J/ kg K)
Conventional	1050	225	-	4186
MQL	840	0.2	110	1790
MQL + PTFE	845	0.2	120	1790
MQC + 5% Graphite	1004.7	4	28.9	4186
MQC + 10% Graphite	1009.5	4	42.9	4186
MQC + 15% Graphite	1014.2	4	45.5	4186

4.3.3.2 Correlation with Ti6Al4V machinability

During turning of Ti6Al4V the tool is subjected to different wear mechanisms that often overlap, being diffusion and adhesion the main mechanisms responsible of the crater wear formation onto the tool rake face and abrasion, which is the main cause of the nose wear occurrence.

Conventional wet cutting and SL-assisted MQC techniques produced very similar outcomes in terms of crater dimension, although there are several differences between the two approaches. The high cooling capacity of the conventional flood strategy was determined by the use of water at high flow rate, condition that compensated its lowest viscosity. The same effects were possible by drastically reducing the flow rate but increasing the lubricating effect with the addition of graphite particles as it happened when applying the SL-assisted MQC strategies.

The MQL oil presented a low heat removal capacity, being the wear crater depth reduction of about 15% thanks to the PTFE addition attributable to the sole viscosity increase with the consequent reduction of the abrasion mechanism since its cooling capacity remained unchanged.

On the other hand, the abrasion of the tool flank face is mainly associated to the lubricating capacity of the cutting fluid that must be able to reduce both the friction coefficient and the welding mechanisms on the cutting edge leading to the chipping phenomenon. The best result was measured for the MQL oil added with PTFE that presented the highest dynamic viscosity among the tested cutting fluids. Very similar VBc values were found for the tool that worked under MQC techniques regardless the graphite percentage: in these cases the water cooling effects compensated the viscosity reduction with respect to the MQL cases since the material adhesion was limited.

In contrast to what observed for the cratering phenomenon, the increase of graphite content did not produce a significant reduction in terms of abraded layer width although a dynamic viscosity change was measured. The different behaviour can be probably ascribed to the particles difficulty in reaching the cutting zone being the MQC nozzle direction almost orthogonal to the rake tool face.

It must be noticed that the high flow rate and, consequently, the sole high heat dissipation capacity of the conventional cutting fluid was not sufficient to assure nose wear values comparable to the ones of the other tested conditions, meaning that its lubricating capacity was insufficient.

Different considerations pertain to the surface integrity analysis as the experimental results highlighted a less dependence to the cutting fluids characteristics. As concerns the surface roughness, having fixed the cutting parameters, it mainly depended on the tool wear, therefore the dry and pure MQL conditions that both presented the deepest crater on the tool rake face were the worst cases; the other cases presented similar surface finishes being the tool wear comparable. The differences between the adopted lubricating/cooling strategies in terms of surface defects were minimal, as all the machined samples presented surfaces free from the typical defects of dry cutting (welded and smeared material and flow lines). Lastly, only the SL-assisted MQC strategies produced a significant improvement in terms of machining-altered layer reduction, whereas the use of pure cooling and lubricating techniques did not lead to the same results.

4.4 Hybrid strategies

It was proved that the adoption of hybrid lubricating/cooling strategies is a viable alternative to the conventional ones, leading to a drastic reduction of the crater wear as well as good surface integrity given an optimized positioning of the lubricant/coolant nozzles. A commercial Minimum Quantity Lubrication (MQL) system was implemented together with Liquid Nitrogen (LN_2) and Carbon Dioxide (CO_2) distribution systems designing the position of the nozzles to optimize the lubrication and cooling effects.
In particular, the tool rake face, being mainly interested by the temperature increase due to the cutting process, was cooled by means of low-temperature coolants (LN2 or CO2), while the flank face, more prone to the abrasion, and was lubricated using the MQL technique.
The material, cutting parameters and strategies used are summarized in Table 4.14.

Table 4.14. Experimental plan for the turning tests.

Material	**Cutting parameters**			**Tested technologies**
-	**Depth of cut (mm)**	**Feed rate (mm/rev)**	**Cutting speed (m/min)**	
Wrought	0.25	0.2	80	MQCL (LN2/MQL) – MQCL (CO2/MQL)

4.4.1 Tool wear

Figure 4.24 and Figure 4.25 show the worn tool profiles for the hybrid strategies, using the LN2 and the CO2 in combination with the MQL technique, respectively. Both the graphs further highlight that the cratering phenomenon mainly depends on the temperature: the tool profiles when applying the hybrid technologies are, in fact, similar to those found when using only the low-temperature coolants.

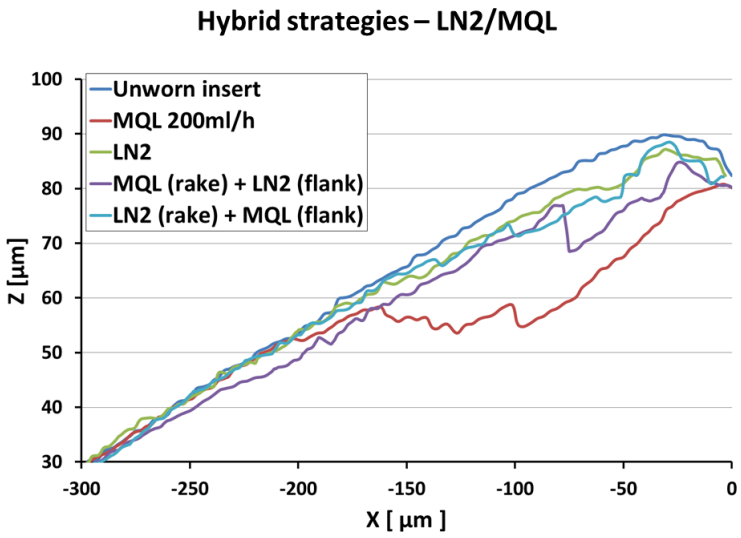

Figure 4.24. 2D profiles of the tool rake face when using LN2 and MQL for the hybrid strategy

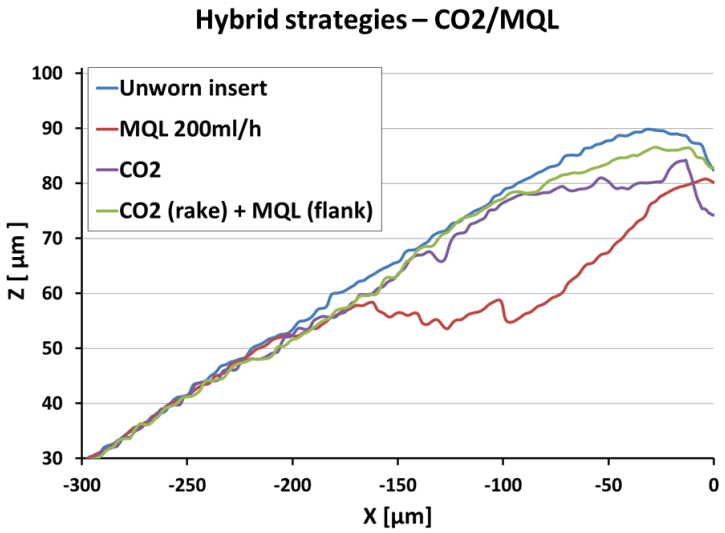

Figure 4.25. 2D profile of the tool rake face when using CO2 and MQL for the hybrid strategy.

Furthermore, the position of the nozzles influences the tool wear: when using the LN2, the choice of cooling the flank face through the LN2 and directing the MQL nozzle to the tool rake face determined an increase of the crater wear compared to both the reverse

situation and the sole LN2 application, although a significant improvement persists compared to the sole MQL. On the other hand, a net improvement was found for the hybrid CO2/MQL strategy in which the MQL adduction to the flank face greatly reduced the erosion of the cutting edge bringing it close to the unworn tool geometry.

For each condition, the maximum crater depth was measured by subtracting the worn tool profile to the unworn one, and its position evaluated with respect to the cutting edge (the results are reported in Table 4.14). The percentage reduction of the crater depth compared to the dry cutting reaches 41,5% for the MQL technique, 74.6% for the wet cutting, and 76.9% for the pure LN2 cooling. For the hybrid strategies implying the use of LN2, no significant differences compared to the use of the conventional cutting fluid were measured, whereas the use of CO2, both solely and in combination with the MQL, completely eliminated the crater wear. The crater wear is generally formed at the interface between the sliding and sticking zones at the chip-tool interface where the temperature reaches its maximum value [22]. The measurement of the distance between the cutting edge and the deepest point of the crater provides information about how the chip contact length is influenced by the different lubricating/cooling strategies: based on the values reported in Table 4.15, it can be affirmed that the use of low-temperature coolants, besides the reduction of the crater depth, tends to move the crater closer to the cutting edge regardless the nozzles position.

Table 4.15. Depth and position of the wear crater as a function of the adopted lubricating/cooling strategies (measurement uncertainty equal to 6%).

	Max crater depth (µm)	**Crater distance from the cutting edge (µm)**
Dry	32.728	126.4
Wet	8.305	93.41
MQL-200ml/h	19.126	97.75
LN2	7.556	57.78
CO2	-	-
LN2(rake) + MQL(flank)	8.853	58.61
LN2(flank) + MQL(rake)	8.259	75.06
CO2(rake) + MQL(flank)	-	-

The crater distance to the cutting edge is about 126 μm in case of dry cutting, 95 μm for the lubricating strategies, and 60 μm for the cooling strategies, including the hybrid technique LN2/MQL with the MQL directed to the tool flank face. On the contrary, in the LN2/MQL strategy with the MQL adduction to the rake face, the crater distance from the cutting edge increases to a value closer to the pure lubricating strategies (75 μm).

Figure 4.26 clearly shows that the lubricating/cooling strategy and the delivery method have substantial effects on the tool flank wear. As expected, the highest value of the average flank wear was measured in case of dry cutting as a consequence of the generated temperature increase in the cutting zone that facilitates the material adhesion. The use of both the conventional cutting fluid and the MQL aerosol determined a reduction of the flank wear of about 33% compared to the dry cutting condition. On the contrary, the use of the sole LN2 did not assure the same results, as a consequence of the low temperatures that inhibited the adhesive mechanisms but did not have acceptable lubricating effects. A different behaviour can be observed when applying the CO2: even if the temperature effect is the same of the LN2 one, the observed reduction of the flank wear may be attributed to the high pressure of the CO2 adduction that reduced the adhesion. All the investigated hybrid strategies induced a flank wear comparable to the one of the conventional cutting fluid. The best result was obtained in case of the hybrid CO2/MQL strategy, which gave a measured VB_C value around 50 μm, leading to an improvement of about 17% and 9% with respect to the sole LN2 and CO2 application, respectively. In case of the hybrid strategies making use of the LN2, the position of the nozzles did not significantly influence the flank wear.

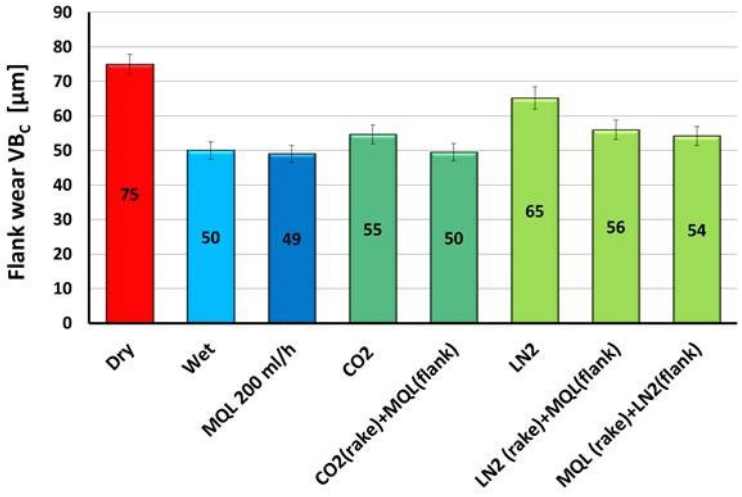

Figure 4.26. Flank wear VB_c as a function of the adopted lubricating/cooling strategies.

4.4.2 Surface Integrity

On the basis of the roughness values reported in Table 4.16, it can affirm that the best surface finishing was found when applying the sole LN2 while the worst ones were measured in case of dry machining and MQL, being the highest difference quantifiable in about 27%.

Table 4.16. Average values of the surface roughness Ra as a function of the adopted lubricating/cooling strategies.

	Ra (μm)	**Standard deviation (μm)**
Dry	1.431	0.053
Wet	1.163	0.024
MQL-200ml/h	1.315	0.017
LN2	1.044	0.026
CO2	1.208	0.019
LN2 (rake) + MQL (flank)	1.207	0.042
LN2 (flank) + MQL (rake)	1.224	0.02
CO2(rake) + MQL(flank)	1.197	0.032

The low surface finish found for the dry and MQL conditions may be due to the tool severe wear that causes the loss of the cutting edge geometry as well as to the tool wear adhesion that may damage the machined surface. For the hybrid strategies, regardless the adopted low-temperature coolant, no significant differences were detected, the Ra values ranging from 1.197 to 1.224 μm, close to the values obtained in case of application of the sole CO2.

Further examinations of the surface quality were carried out analysing the surface topography of the machined samples. Figure 4.27 shows the 2D and 3D profiles for the dry, wet, MQL, CO2, LN2 and LN2/MQL conditions. The effect of the severe cooling is visible in the 2D profiles of the samples machined using the low-temperature coolants, where a discontinuous surface was detected along the feed mark slopes, probably caused by the drop of material ductility due to the low temperature during the cutting process. The addition of MQL onto the tool flank determined the slipping of these irregularities close to the feed mark peaks, but without substantial differences in the profile shape

compared to the dry cutting case. The combined strategies produced surface topography similar to the one obtainable with the conventional cutting fluid application.

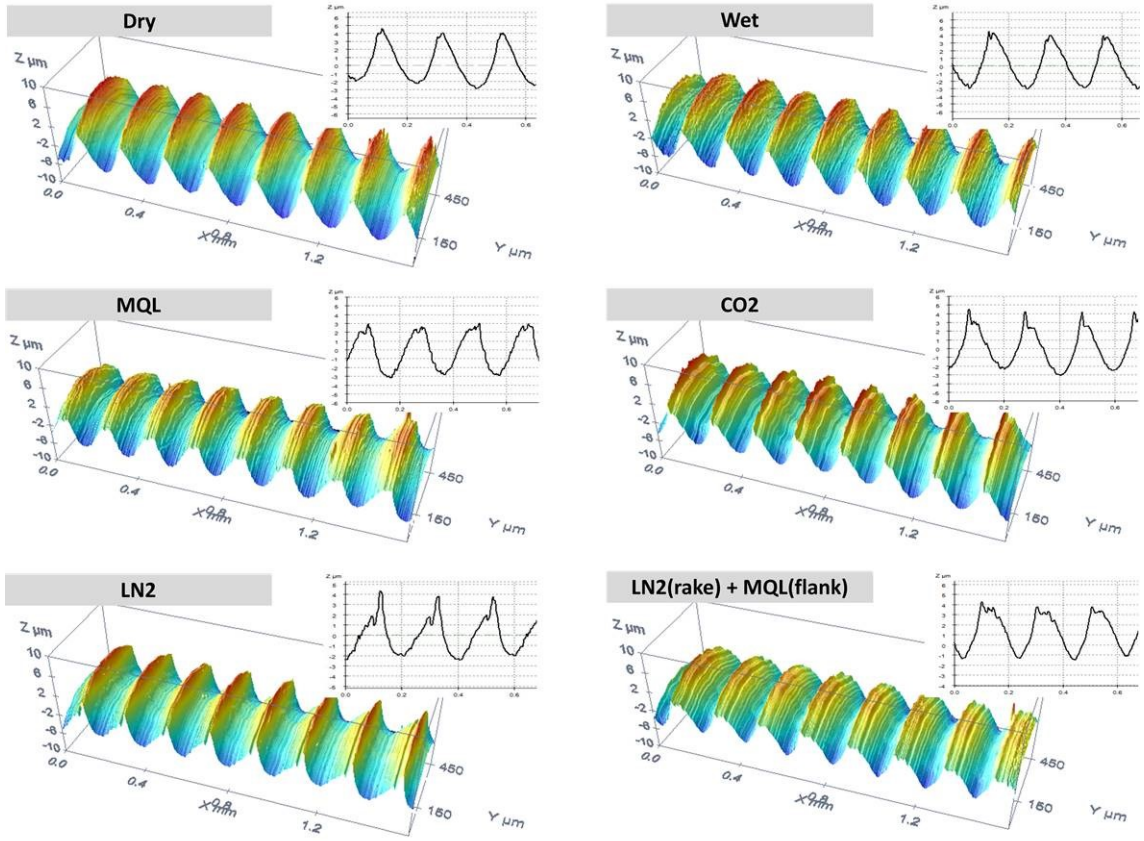

Figure 4.27. 3D and 2D surface topographies of samples machined under different lubricating/cooling strategies.

Figure 4.26 reports the thickness of the deformed layer for all the lubricating/cooling strategies. As expected, the dry cutting produced the highest microstructural deformation: the cooling absence determined the temperature increase responsible of the material thermal softening as well as the tool wear and friction increase that, in turn, increased the material work hardening. When applying the sole LN2, the drastic increase of the material hardening as a consequence of the low temperatures involved in the process induced a deformed layer comparable to that of the dry cutting condition (see Figure 4.28). On the other hand, the reduction of the friction coefficient when using conventional and MQL lubricating strategies helps in reducing also the extend of the deformed layer: a reduction of about 21.3% and 17.5% were found for the wet and MQL cases, respectively, compared to the dry one.

Surprisingly, among the non-hybrid strategies, the use of the sole CO2 determined the best result inducing a thickness of the deformed layer of about 7.6 µm: this may be due to

the efficient cooling provided by this technique, but without the increased hardening effect due to the low temperatures as it happened when using the LN2.
Lastly, comparable values of the deformed layer thickness were found for all the hybrid strategies, close to the one found in case of application of the sole CO2.

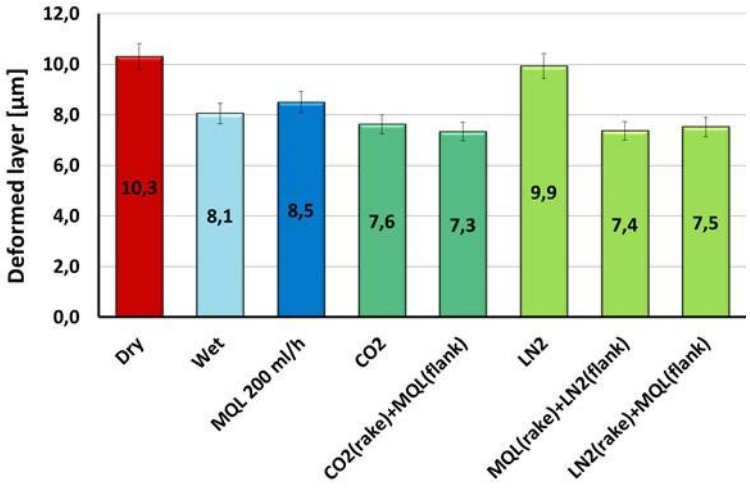

Figure 4.28. Thickness of the deformed layer as a function of the adopted lubricating/cooling strategies.

The lubricating effect of the cutting fluid helps in reducing the friction coefficient, and therefore reducing the deformed layer. On the other hand, the conventional wet strategy had also a discrete cooling capacity, as it determined a decrease of the deformed layer thickness.

4.5 Chapter concluding remarks

Based on the analyses of the tool wear and machined surface integrity when adopting different lubricating/cooling strategies in Ti6Al4V semi-finishing turning, the following considerations may be drawn:

- When applying cryogenic coolants (LN2 and CO2) the crater wear was drastically reduced, preserving the tool cutting edge geometry with a significant improvement of the machined surface roughness, especially in the case of LN2, even if a more jagged surface topography as a consequence of the material ductility drop was detected.
- Among the pure cooling strategies the lowest tool wear, in terms of both flank and crater wear, was detected for the sample machined using N2 cooled at -100°C: respect to the LN2 and CO2 condition the VBc reduction overtook the 43% and 31% respectively, while the crater depth was similar. However,

improvements with respect to the wet and LN2 cooling conditions were already evident when using N2 cooled at -50°C. In term of surface integrity instead the sample machined using N2 cooled at -100°C presented a reduced hardened layer of about 5.9 μm, 40% and 26.5% less than the ones found under LN2 and wet conditions respectively. The surface roughness and topography were comparable to those obtained using the conventional cutting fluid, as well as a surface almost free from those surface defects arising when using of dry (adhered and smeared material) and cryogenic (feed-marks irregularities and tearing) cooling conditions was noticed. All the machined samples presented a surface compressive stress state. However, the use of LN2 induced both the highest values of axial residual stresses and a general thickening of the compressive surface residual stress layer.

- Nano-properties were affected by the adopted cooling strategies compared to as-received condition. In particular, the dry condition produced an alteration of around 5% with respect to the reference condition. The nano-hardness of the machined surfaces was higher than the one of the as-received condition regardless the cooling strategy.
- The LN2 presented the highest cooling capacity (24.7 kW), one order of magnitude higher than the ones of the N2 cooled at different temperatures (2.4 kW and 0.2 kW at -150°C and 0°C, respectively); however, it was proved that a reduced cooling capacity, as in the case of N2 cooled at -100°C, was sufficient to optimize both the tool wear resistance and machined surface integrity, whereas its increase to a great extend reduced the process performances.
- The low cooling capacity of the MQL with and without the addition of PTFE particles was not able to eliminate the cratering phenomenon, whereas its dynamic viscosity, which was the highest among the tested strategies, assured a very low nose wear, limiting the abrasion of the cutting edge.
- The simultaneous cooling and lubricating capacities of the SL-assisted MQC strategies guaranteed the lowest tool wear in terms of both crater and nose wear with very slight differences as a function of the graphite content. The machined surface quality was less influenced by the tested cutting fluids. The machining-altered layer was the one showing the most significant differences: the use of the SL-assisted MQC strategies determined the best result reaching percentage

reductions equal to 44%, 36% and 29% compared to the dry, MQL and wet strategies, respectively.

- Among the tested lubricating techniques, the SL-assisted MQC one provided the best performances, and thanks to its low flow rate may be considered as the ideal substitute of the conventional wet strategy.
- The hybrid strategies combining LN2/MQL and CO2/MQL guarantee the advantages of both the techniques: in fact the cratering phenomenon was completely eliminated while the measured flank wear was comparable to that found when using the sole cutting fluids. Furthermore, the machined surface integrity significantly improved, highlighting lower values of the surface roughness and deformed layer thickness compared to the other tested strategies, with a reduction of about 29% and 15% compared to the dry cutting case, respectively. In the LN2/MQL combination, the position of the nozzles significantly affected the tool wear, the best solution being detected when directing the MQL to the tool flank face and the LN2 to the rake face

[1] S. Zhang, J. F. Li, J. X. Deng, and Y. S. Li, “Investigation on diffusion wear during high-speed machining Ti-6Al-4V alloy with straight tungsten carbide tools,” *Int J Adv Manuf Technol*, pp. 17–25, 2009.

[2] J. Salguero, M. Batista, M. Marcos, and A. Go, “Analysis of the evolution of the Built-Up Edge and Built-Up Layer formation mechanisms in the dry turning of aeronautical aluminium alloys,” vol. 302, pp. 1209–1218, 2013.

[3] O. Hatt, P. Crawforth, and M. Jackson, “On the mechanism of tool crater wear during titanium alloy machining,” *Wear*, vol. 374–375, pp. 15–20, 2017.

[4] J. Hua and R. Shivpuri, “A Cobalt Diffusion Based Model for Predicting Crater Wear of Carbide Tools in Machining Titanium Alloys,” *J. Eng. Mater. Technol.*, vol. 127, no. 1, p. 136, 2005.

[5] ISO3685.1993, “Tool life testing with single-point turning tools, 1993.”

[6] A. Ginting and M. Nouari, “Surface integrity of dry machined titanium alloys,” *Int. J. Mach. Tools Manuf.*, vol. 49, no. 3–4, pp. 325–332, 2009.

[7] C. H. Che-Haron and A. Jawaid, “The effect of machining on surface integrity of titanium,” *J. Mater. Process. Technol.*, no. 166, pp. 188–192, 2005.

[8] D. Green and R. Perry, *Perry’s chemical engineer’s handbook*. 2007.

[9] “NIST Chemistry WebBook https://www.nist.gov./chemistry/.”.

[10] A. F. Gerday, M. Ben Bettaieb, L. Duchêne, N. Clement, H. Diarra, and A. M. Habraken, “Material behavior of the hexagonal alpha phase of a titanium alloy identified from nanoindentation tests,” *Eur. J. Mech. / A Solids*, vol. 30, no. 3, pp. 248–255, 2011.

[11] M. Cornen, P. Castany, I. Péron, and T. Gloriant, “Materials Science & Engineering A Determination of hardness and elastic modulus inverse pole fi gures of a polycrystalline commercially pure titanium by coupling nanoindentation and EBSD techniques,” *Mater. Sci. Eng. A*, vol. 613, pp. 159–162, 2014.

[12] F. K. Mante, G. R. Baran, and B. Lucas, “Nanoindentation studies of titanium single crystals,” vol. 20, pp. 1051–1055, 1999.

[13] A. W. Warren and Y. B. Guo, “Machined surface properties determined by nanoindentation : Experimental and FEA studies on the effects of surface integrity and tip geometry,” vol. 201, pp. 423–433, 2006.

[14] G. Stachowiak and A. Batchelor, *Engineering Tribology*, 3rd ed. 2005.

[15] S. T. Methods, “Standard Test Methods for Rheological Properties of Non-Newtonian Materials by,” pp. 1–5, 2017.

Chapter 5.

Effect of different Ti6Al4V microstructures onto the tool wear mechanisms

5.1 Introduction

In the biomedical field the Additive Manufacturing (AM) technologies are increasingly being adopted for the production of near-net-shape products made in titanium alloys; however finishing machining operations can be necessary to obtain the required geometrical tolerances and surface characteristics. This section aims at investigating the effects of the workpiece microstructures on the tool wear behavior in semi-finishing turning of Ti6Al4V produced by Electron Beam Melting (EBM) and Direct Metal Laser Sintering (DMLS) AM technologies in comparison with the one of the wrought commercial alloy under dry cutting and cryogenic cooling strategies.

To this regard, the objective of the paper is twofold: (i) to correlate the thermal and mechanical properties of the Ti6Al4V in the different as-received conditions and the tool

wear mechanisms, showing that the characteristics of the as-received material strongly affect the wear phenomena regardless the adopted cooling strategy; (ii) to prove the effectiveness of the cryogenic cooling to reduce the tool wear compared to dry cutting regardless the Ti6Al4V as-received condition.

The Table 7.1 summarizes the experimental plan used in this work. The resulting tool wear was evaluated by means of Scanning Electron Microscopy (SEM) and 3D profiler analyses. The thermal and mechanical properties of the Ti6Al4V in the different initial states were identified in terms of hardness and thermal conductivity at varying temperature.

Table 5.1. Experimental plan for the turning tests.

Materials	**Cutting parameters**			**Tested technologies**
-	**Depth of cut (mm)**	**Feed rate (mm/rev)**	**Cutting speed (m/min)**	
Wrought – EBM – DMLS – heat treated DMLS	0.25	0.2	80	Dry – LN2

5.2 Experimental results

5.2.1 Thermal and mechanical characterization of the as-received alloys at varying temperature

The mechanical and thermal properties of the Ti6Al4V in the different as-received conditions were analysed at varying temperature in order to correlate them with the tool wear mechanisms arising during machining. Mechanical properties, such as the hardness, mainly influence the abrasive wear, while the thermal conductivity the diffusive and adhesive wear phenomena. These properties were measured in a range of temperature between room temperature and the maximum estimated one from thermal measurements during turning in dry conditions.

The hardness measurements were carried on an Instron^{TM} Wilson Wolpert series 2000 hardness tester equipped with a furnace for heating the material up to 750°C following the ISO 6508 standard [1].

The evaluation of the thermal characteristics was carried out by means of a hot disk apparatus based on the Transient Plane Source (TPS) method defined by Gustafsson [2] that enables to simultaneously measure the thermal conductivity λ [W/(m·K)] and the

volumetric heat capacity ρc [MJ/(m^3 K)]. This apparatus uses a plane sensor that consists of an electrically conducting pattern in the shape of a double spiral, etched out of a thin nickel foil. The spiral is sandwiched between two thin sheets of insulating material such as kapton or mica, the latter particularly suitable for operating at high temperature. The sensor, in addition to providing thermal power, works as a resistance thermometer and allows measuring the temperature increase of the specimen active surfaces, as a result of the applied thermal power. The method requires an appropriate testing time to make negligible the influence of the boundary conditions applied to a finite specimen: in this way, the heat transfer problem can be simulated as if the sensor was placed in an infinite medium.

An infra-red thermo-camera FLIR^{TM} Thermovision A40 was used for acquiring the thermal field on the tool rake face, showing an average temperature around 450°C after having reached the thermal steady state. The material emissivity was calibrated by heating up a heat-treated DMLS Ti6Al4V workpiece into a temperature-controlled muffle furnace, identifying an emissivity value of 0.5. The range of temperatures that was selected for the evaluation of the mechanical and thermal characteristics of the Ti6Al4V in the as-received conditions was between room temperature and 500°C; lower temperatures were not considered in this study being the thermally-activated wear mechanisms inhibited. Figure 5.1 shows the Ti6Al4V hardness values for the different as-received conditions as function of the temperature.

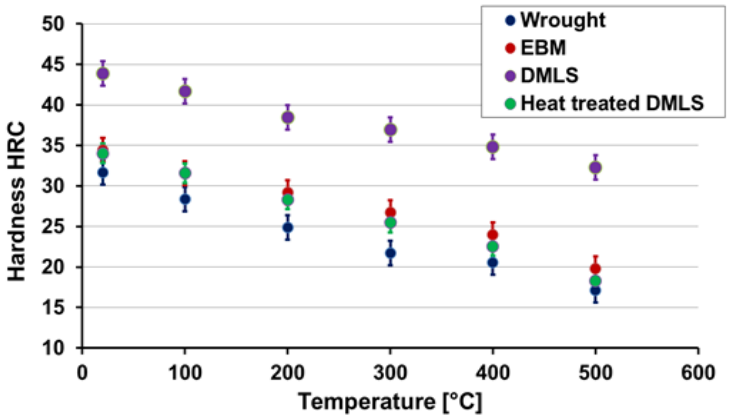

Figure 5.1. Influence of the temperature on the hardness of the Ti6Al4V in the different as-received conditions.

The results highlight that the temperature increase causes a thermal softening of the alloys: at the maximum tested temperature, the as-built DMLS alloy presents a hardness reduction of 23% compared to the room temperature value, while for the other as-

received conditions this reduction is up to 45%. The wrought, EBM and heat treated DMLS alloys show very similar hardness values regardless of the temperature, whereas the DMLS presents always higher values, being the percentage difference equal to 40% at 500°C.

Figure 5.2 shows the influence of the temperature on the thermal conductivity for the different as-received conditions of the Ti6Al4V. The EBM alloy shows the highest values of the thermal conductivity and the DMLS alloy the lowest one, regardless of the testing temperature. At the maximum investigated temperature, the EBM and DMLS alloys show the most significant difference (about 16%). On the other hand, the wrought and heat-treated DMLS alloys nearly present the same values with a reduction of 11.7% at 500°C compared to the EBM alloy.

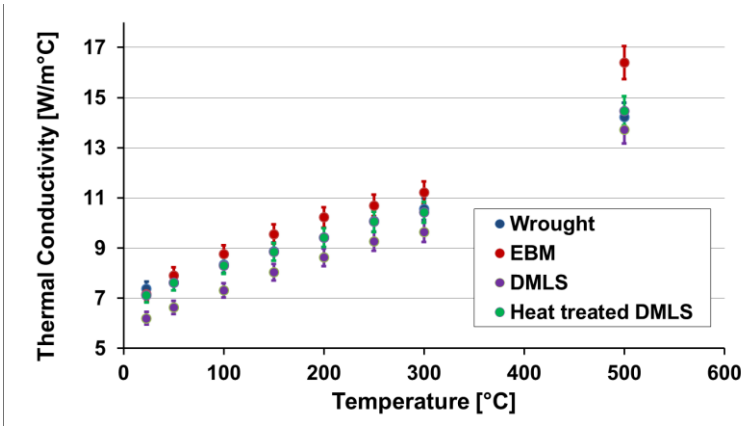

Figure 5.2. Influence of the temperature on the thermal conductivity of the Ti6Al4V in the different as-received conditions.

5.2.2 Tool wear

Regardless by tested the Ti6Al4V microstructures the presence of BUE and BUL onto the tool rake face highlights that the adhesion is once again the main wear mechanism (see Figure 5.3).

Another consequence of the adhesive wear is the chipping of the tool edge caused by the BUE instability during the cutting process, which periodically breaks taking off small lumps of the tool material. Figure 5.4 shows this phenomenon at different magnifications and cutting times for the tool that machined the heat-treated DMLS sample in dry conditions. In Figure 5.4A after 8 minutes of turning the presence of a welded chip onto the cutting edge was highlighted, which, afterwards, broke causing the tool chipping as shown in Figure 5.4B.

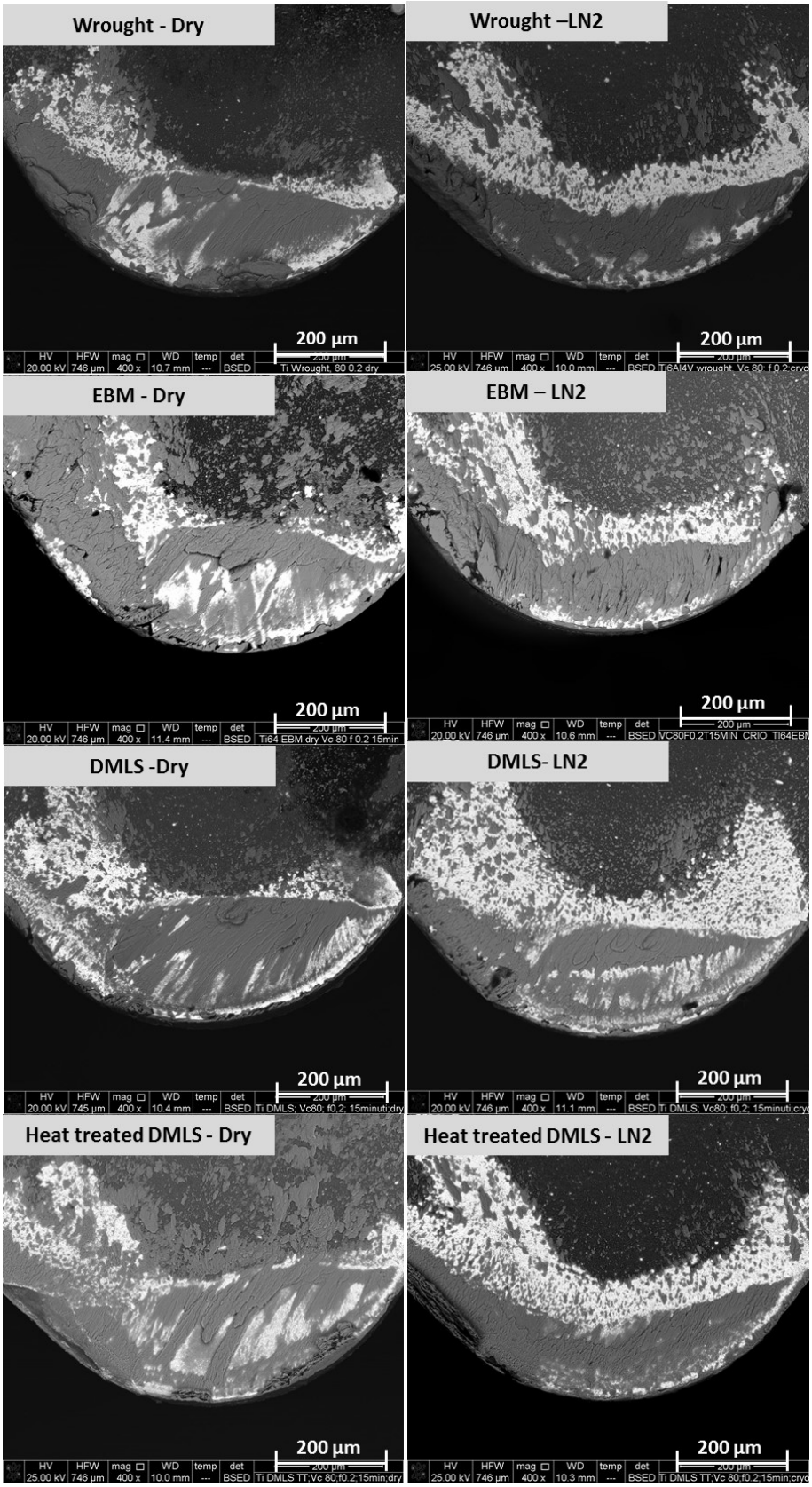

Figure 5.3. SEM images of the worn tool rake faces after 15 minutes of turning under dry cutting and cryogenic cooling.

The Figure 5.5 reports the tool rake 3D analysis, in details the blue profile represents the unworn insert, whereas the red, green, purple and orange lines the profiles of the worn tool rake faces after machining the EBM, DMLS, heat-treated DMLS and wrought Ti6Al4V, respectively. Regardless of the Ti6Al4V as-received conditions, the cratering phenomenon is always present in dry cutting: the crater depth values reported in Table 5.1 show that the maximum value was reached when turning the as-built DMLS sample and resulted to be 52.3 μm, while, when turning the EBM sample, the smallest value was found, being the percentage difference about the 55%.

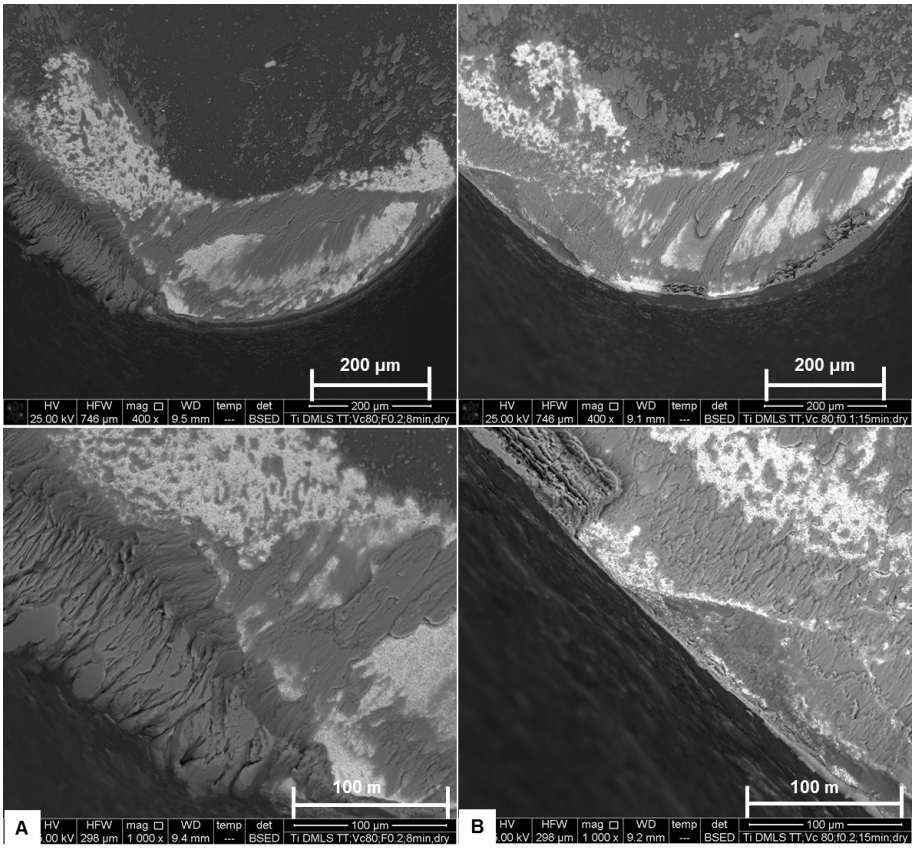

Figure 5.4. Chipping formation at different magnifications after: (A) 8 minutes, and (B) 15 minutes of turning the heat-treated DMLS Ti6Al4V under dry cutting.

Cryogenic cooling strongly reduces the occurrrence of the crater wear as shown in Fig. 5.5 B and Table 5.2. The best results when applying cryogenic cooling were obtained in turning the EBM sample since the crater wear was completely eliminated. The percentage reduction of the crater wear compared to dry cutting overtakes 58% for the DMLS sample and about 80% both for the heat-treated DMLS and wrought ones.

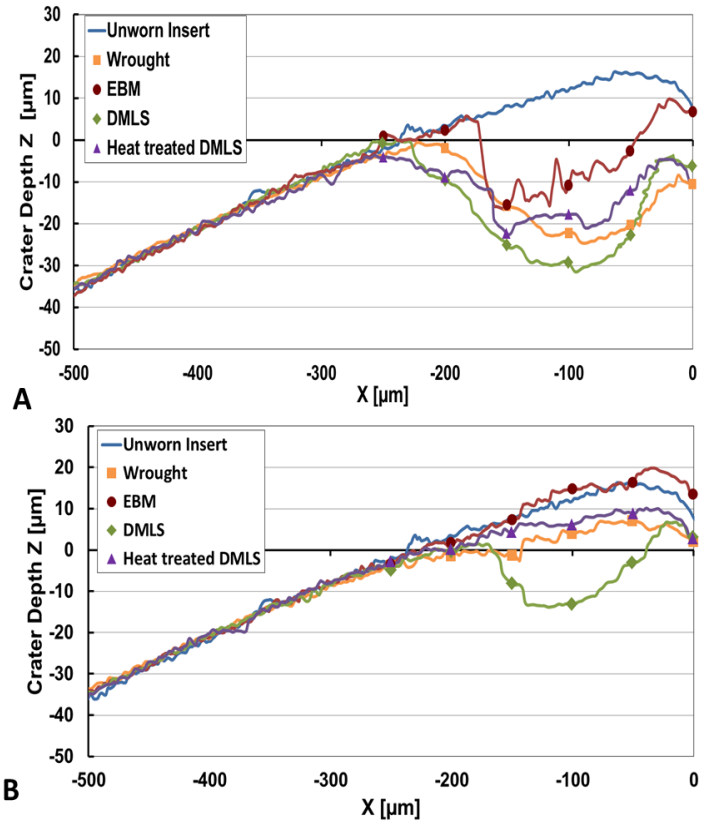

Figure 5.5. Tool rake face profiles after 15 minutes of turning under: (A) dry cutting, and (B) cryogenic cooling.

Table 5.2. Crater wear depth as a function of the Ti6Al4V as-received conditions and cutting strategies, with measurement uncertainty equal to 6%.

Ti6Al4V	Dry cutting Max crater depth Z (µm)	Cryogenic cooling Max crater depth Z (µm)
Wrought	-44.1	-7.4
EBM	-23.52	0
DMLS	-52.3	-21.6
Heat-treated DMLS	-42.2	-6.7

As for all the investigated cutting conditions, no V-shaped notch and catastrophic tool fracture were detected, the tool rejection criterion is determined only by the flank wear analysis in terms of the VBc parameter, which, as shown in Table 5.3, it was always respected, as the measured values never exceeded the fixed limit.

Table 5.3. Flank wear as a function of the Ti6Al4V as-received conditions and cutting strategies.

Ti6Al4V	Dry cutting Flank wear VBc (µm)	Cryogenic cooling Flank wear VBc (µm)
Wrought	76.1±3.2	65.2±4.7
EBM	75.9±4.7	60.2±3.6
DMLS	85.4±2.4	72.7±4.9
Heat-treated DMLS	74.6±4.9	69.9±2.9

It may be noted that the maximum flank wear in dry turning was detected for the DMLS sample (85.4 µm) while the others presented almost the same values (around 75 µm). The flank wear reduction thanks to cryogenic cooling compared to dry cutting for the wrought, EBM, DMLS and heat-treated DMLS alloys are 20.7%, 15.8 %, 14.1% and 6.3%, respectively, after 15 minutes of cutting, being the DMLS the alloy still provoking the highest flank wear. Moreover, only for the tool that machined the DMLS sample in dry conditions the presence of a crater on the flank face with characteristic abrasive marks was found as visible in Fig. 4.6A. However, the LN2 use completely eliminated it: only the coating loss without significant geometrical alterations of the cutting edge is, in fact, highlighted in Fig. 5.6B.

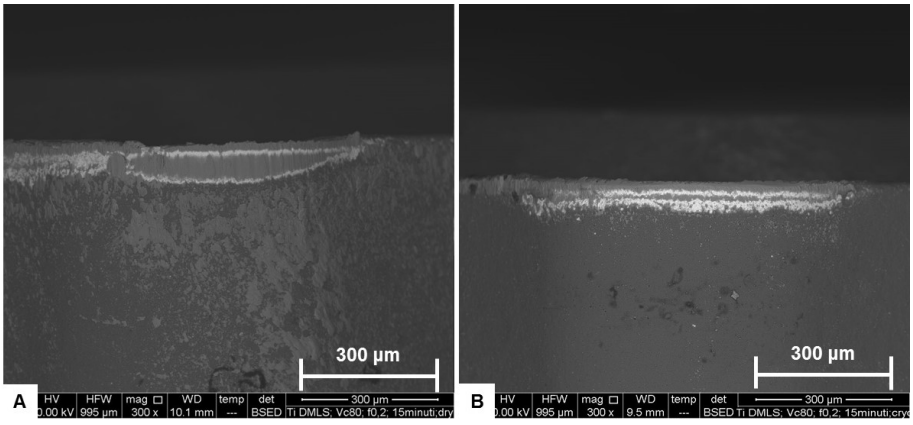

Figure 5.6. Tool flank after 15 minutes of turning the DMLS Ti6Al4V under: (A) dry cutting, and (B) cryogenic cooling.

Generally, it can be stated that, regardless the Ti6Al4V as-received conditions and cutting strategies, abrasion can be considered the most relevant flank wear mechanism though a protective layer of adhered material is always present onto the tool cutting edge.

5.3 Discussion

The tool wear analysis highlighted that the main wear mechanisms were adhesion, diffusion and abrasion, each of which differently influenced by the cutting strategies and the Ti6Al4V as-received conditions. Both hardness and thermal conductivity of the Ti6Al4V microstructural variants influence the occurrence of the different wear phenomena to a different extent. Hardness can be considered responsible of the tool abrasion resulting by the chip sliding while the thermal conductivity mainly influences the diffusive and adhesive wear mechanisms. In particular, a low thermal conductivity determines a higher surface temperature and, consequently, more diffusive exchange of the chemical elements between the tool and the adhered workpiece materials, being diffusion a thermally-activated process.

Cratering is the wear phenomenon mostly influenced by the material properties of the investigated Ti6Al4V in the different as-received conditions. The 3D profiler analysis showed that the deepest crater was found in the tool that worked the DMLS Ti6Al4V sample, which presents both the lowest thermal conductivity (and therefore the highest surface temperature) and the highest hardness at the maximum investigated temperature (see Figs. 2 and 3). On the other hand, the lowest crater was found for the tool that worked the EBM sample, which presents the highest thermal conductivity, and, therefore, dissipates better the generated heat compared to the other microstructural variants.

Under cryogenic cooling, the temperature in the cutting zone was reduced by the LN2 application, thus determining the inhibition of the diffusive process responsible of the embrittlement of the tool substrate: consequently, the crater wear is assumed to depend only on the alloy mechanical properties. As a proof of that, the cratering was found only on the rake face of the tool that machined the DMLS material, which is characterized by the highest hardness, whereas the tools that machined the other alloys presented either uniform abrasion of the notch or adhesive wear.

In the flank wear analysis the previously reported considerations can be considered still valid even if in this case the mechanical properties of the material to be machined play a predominant role with respect to the others investigated: regardless of the cutting strategy, the maximum values of flank wear were in fact measured when machining the DMLS sample that presents the highest hardness. In dry cutting condition, since the material undergoes a thermal softening, the flank abrasion should result lower than under cryogenic cooling, however this did not happen since the liquid nitrogen acting as a

lubricant reduces the required cutting forces and consequently also the abrasive mechanism.

5.4 Chapter concluding remarks

In this chapter, the effects of dry cutting and cryogenic cooling on the tool wear mechanisms were investigated when semi-finishing turning the Ti6Al4V titanium alloy provided in different as-received conditions, namely wrought and additive manufactured through EBM and DMLS Moreover, the correlation between the mechanical and thermal properties of the machined alloys and the main observed wear mechanisms was proved. Based on the obtained results, the following conclusions may be drawn:

- In dry turning the cratering phenomenon is always present, however the deepest crater is found in the tool that machined the DMLS alloy, due to both its highest hardness and lowest thermal conductivity. In case of the other alloys the detected differences can be exclusively attributed to their different values of thermal conductivity since their hardness is similar.
- The most significant effect of the application of cryogenic cooling is the reduction of the cutting temperature, which inhibits the diffusive wear responsible of the crater formation onto the tool rake face. In case of cryogenic cooling, the crater was found only in the tool that machined the DMLS material with, however, a percentage reduction of the maximum crater depth equal to 58 % compared to the dry cutting conditions.
- Both the abrasive wear on the cutting edge and flank wear were reduced applying the LN2, with, again, the most significant reduction in case of the tools that machined the as-built and heat-treated DMLS samples.
- According to the tool wear analysis and on the basis of the material mechanical and thermal characterization as function of the temperature, the EBM alloy presents the best machinability, the DMLS the worst one, whereas the wrought and heat-treated DMLS behaviours are comparable.

[1] “ISO 6508-1:2015. Metallic materials. Rockwell hardness test. Test method.”

[2] S. E. Gustafsson and S. E. Gustafsson, “Transient plane source techniques for thermal conductivity and thermal diffusivity measurements of solid materials Transient diffusivity plane source techniques for thermal conductivity measurements of solid materials and thermal,” vol. 797, no. 1991, pp. 797–804, 2008.

Chapter 6.

Wear mechanisms of uncoated and coated carbide tools when machining Ti6Al4V using LN2 and cooled N2

6.1 Introduction

One of the main challenges of the manufacturing industry is to optimize the cutting tool life in order to increase both the process productivity and the product surface quality in machining operations. Several innovative strategies were developed and tested as a function of both the workpiece material and peculiar machining operation, being the most interesting in case of difficult-to-cut alloys the use of low-temperature cutting fluids that would be able to inhibit the thermally-activated wear mechanisms responsible of the cutting edge geometrical alterations.

In this context, the aim of this work is to investigate the performance of cryogenic cooling technologies based on the use of Liquid Nitrogen (LN2) and cooled gaseous nitrogen (N2) at -100°C when using uncoated and coated cemented carbide inserts. Four

commercially available insert grades commonly used in machining heat-resistant alloys were tested using the cutting parameters recommended by the tool manufacturer. Being the insert geometry the same, the feed rate and depth of cut were chosen equal for each type of insert, namely 0.2 mm/rev and 0.25 mm. Whereas, as concerns the cutting speed, the maximum values recommended by the tool manufacturer were chosen as schematized in Figure 6.1. The dry cutting and wet strategies were used as reference. Since the wrought, EBM and heat treated DMLS Ti6Al4V alloys present similar tool wear behaviour as reported in the chapter 5, the turning tests were performed only onto the wrought alloy that nowadays represents the most used in many industrial fields.

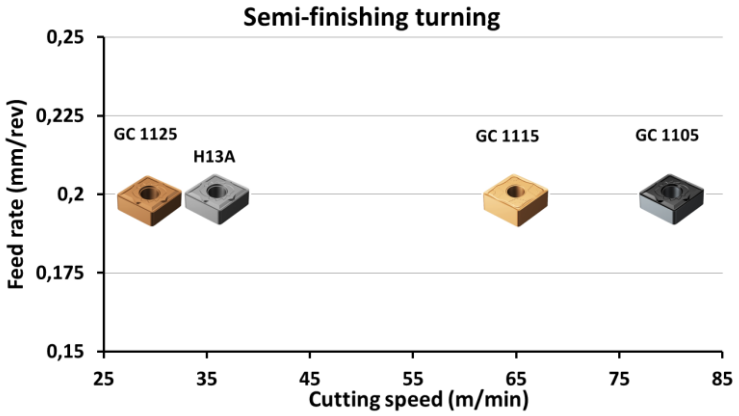

Figure 6.1. Cutting parameters used for the different inserts.

6.2 Experimental results: Tool wear

6.2.1 Crater wear

Also in this case the SEM analysis of the tool rake faces highlighted adhesion (BUE and BUL) and abrasion as the main wear mechanisms (see Figure 6.2), regardless of the cooling conditions, adopted inserts grade and cutting parameters (see Figure 6.3).

The mechanical abrasion of rake face is visible especially for the coated inserts in which the white areas represent the tool substrate made of WC while the dark grey is the coating, as confirmed from previous works described in §4.2.1.

The high chemical affinity between the titanium and the cobalt, which is present as binder in the tool matrix, together with the high cutting forces generated as a consequence of the cutting edge alteration, promotes further the adhesion process on the worn insert. The quantification of the adhered layer is commonly carried out through the measurements of the chip contact length (sticking zone) onto the tool rake face. A shorter

value of the tool-chip contact length will result in a greater coolant penetration, reduced friction and greater cooling efficiency, thus longer tool life. However, the crater wear present in several tools did not make possible this type of analysis, as the chip sliding direction was altered by the loss of the tool geometrical tolerances. The use of low-temperature coolants has no significant impact on the occurrence of the adhesive wear. The differences in terms of sticking zone thickness visible in Fig. 5 between insert GC 1125 and GC 1105 inserts are the consequence of the different adopted cutting speeds and insert coatings.

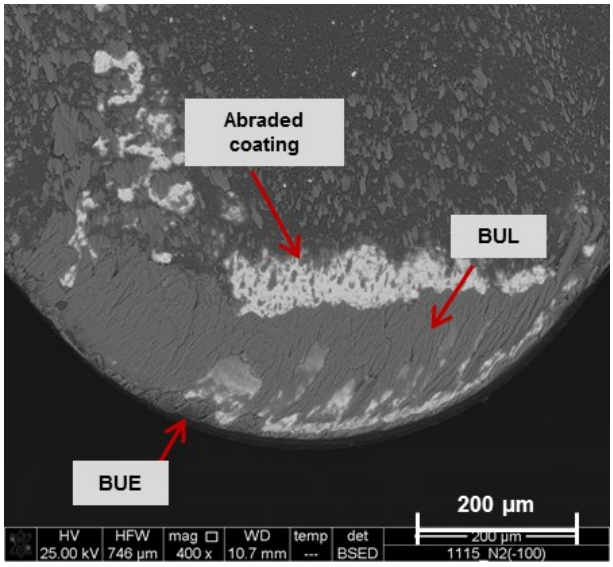

Figure 2.2 Main wear mechanisms detected after 15 minutes of turning on the tool rake face.

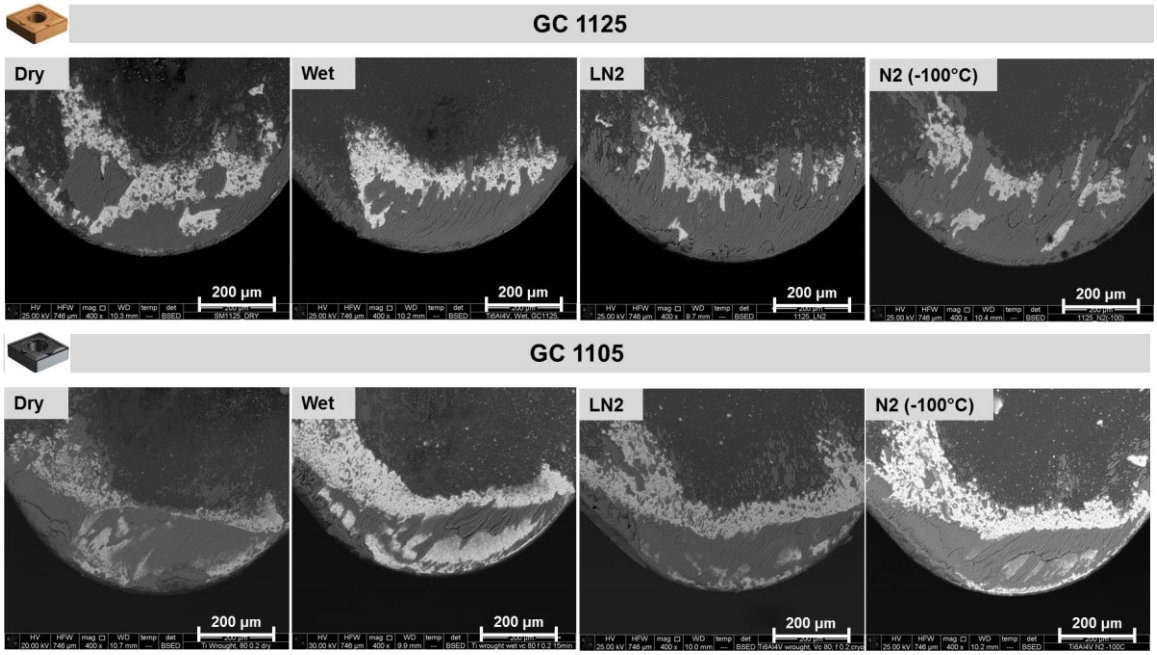

Figure 6.3. SEM images of the worn tool rake faces after 15 minutes of turning under dry, wet, LN2 and cooled gaseous N2 conditions.

As described previously the SEM analysis of the tool rake face allows to identify the main wear mechanisms but is not able to quantify the tool geometrical alterations induced by the turning operations. For this reason a profiler analysis (procedure detailed described in §3.4.1) was required.

Figure 6.4 reports the 2D profiles of the worn inserts that were used to machine under different cooling strategies (the purple, red, green and light blue lines represent the wet, dry cutting, LN2 and cooled gaseous N2 at -100°C conditions, respectively) compared to the unworn tool profile (blue line) for all the tested insert grades.

The analysis highlighted how the cooling strategies did not influence the crater wear of the uncoated insert (H13A) and the one coated with (Ti,Al)N–(Al,Cr)2O3 (GC 1125), while significant effects were measured for the other two tested inserts (GC 1115, GC 1105).

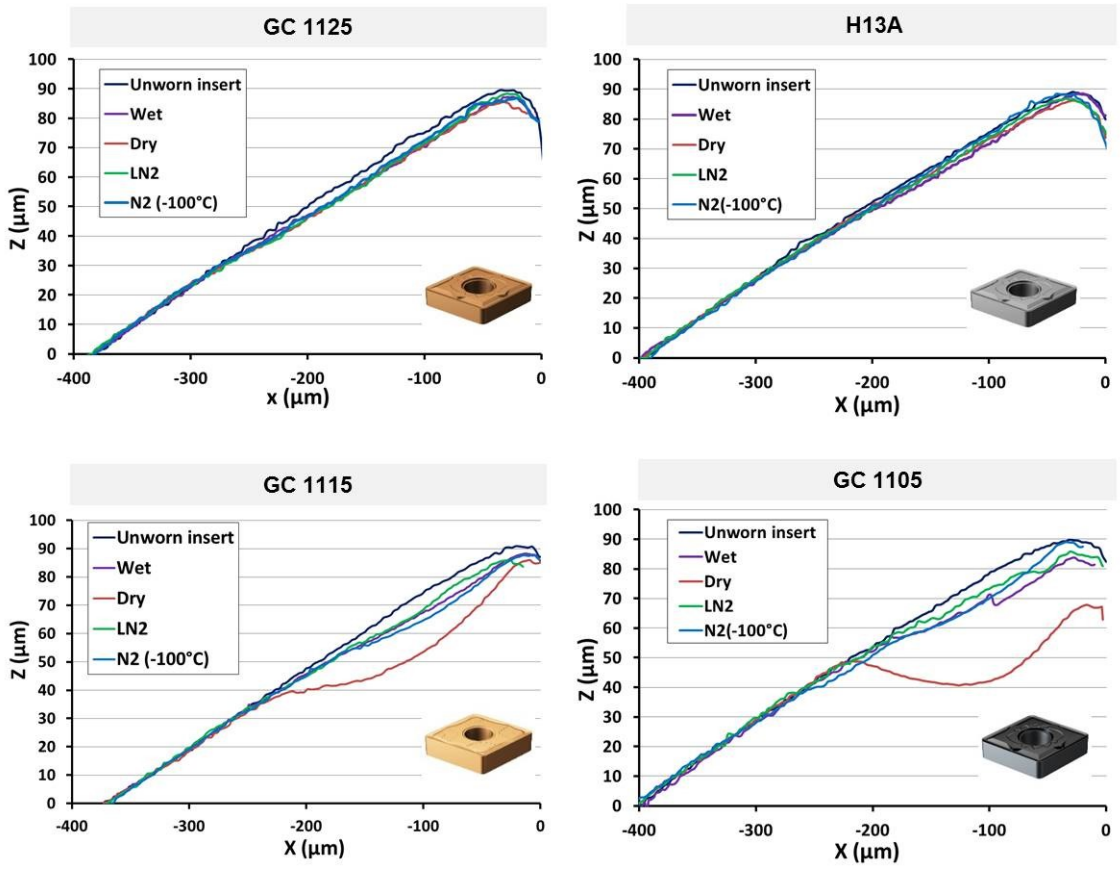

Figure 6.4. 2D profiles of the tool rake faces after 15 minutes of turning under dry, LN2 and cooled gaseous N2 conditions.

Table 6.3 reports the crater depth values: the maximum reduction of the wear crater was measured for the insert GC 1105 using cooled gaseous N2, being the percentage reduction with respect to the dry condition of about 81%, whereas the use of the LN2 led

to an improvement of about 77%. Despite the different coatings and adopted cutting speeds, the crater depth values for the inserts GC 1115 and GC 1105 under cryogenic cooling were very similar, namely about 7 μm.

The flood strategy led to results very close to those obtainable using the low-temperature cooling technologies, only the GC 1105 insert presented a significant difference, as with respect to the cooled N2 the crater depth passed from 6.17 μm to 8.31μm.

Table 6.2. Wear crater depth as a function of the adopted cooling strategies (measurement uncertainty equal to 6%).

	Max. crater depth (μm)			
Insert	**Dry**	**Wet**	**LN2**	**N2 (-100°C)**
GC 1125	-	-	-	-
H13A	-	-	-	-
GC 1115	17.96	6.09	5.68	7.31
GC 1105	32.72	8.31	7.55	6.17

Overall, the analysis of the tool rake face wear showed that for all the tested conditions the cryogenic cooling strategies permitted to effectively reduce the cratering phenomenon with the best results measured for the LN2 case. However, despite the LN2 presents the highest cooling capacity, the results in terms of crater depth highlighted that the difference between the LN2 and cooled N2 were minimal, making them comparable.

6.2.2 Flank wear

The adhered material present onto the cutting edge made it difficult to effectively measure the VBc: to overcome this difficulty, a chemical etching made of 95% hydrofluoric acid was used to eliminate the workpiece material without damaging the insert substrate and the coating. An example of the result of such etching is shown in Figure 6.5.

Figure 6.6 shows the effects of the different cooling strategies on the tool flank wear; the thickness average values of the abraded layer obtained from five measurements conducted on the SEM images are reported in Figure 6.7.

In case of the uncoated insert, the use of cryogenic coolants allowed inhibiting or, at least, reducing the adhesion mechanism favoured during the cutting process by the high chemical reactivity between the cobalt of the tool matrix and the workpiece material; on the other hand, an excessive cooling may cause a material hardening with consequent increase of the abrasion effect. In fact, the percentage reduction of the flank wear when

using the gaseous N2 cooled at -100°C compared to the dry and wet cutting conditions was about 55% and 41% respectively, but decreased to 10% when using the LN2. A similar behaviour was highlighted also for the insert coated with a single layer of (Ti,Al)N (GC 1105): with respect to the abovementioned case, the highest VBc measured in all conditions might be ascribed to the high cutting speed used in the turning trials as recommended by the tool's manufacturer, which would have accelerated both the abrasion and adhesion mechanisms. In this case, the LN2 use was more advantageous, with a VBc reduction of 28.5% compared to dry cutting, while the cooled N2 and conventional cutting fluid performed similarly.

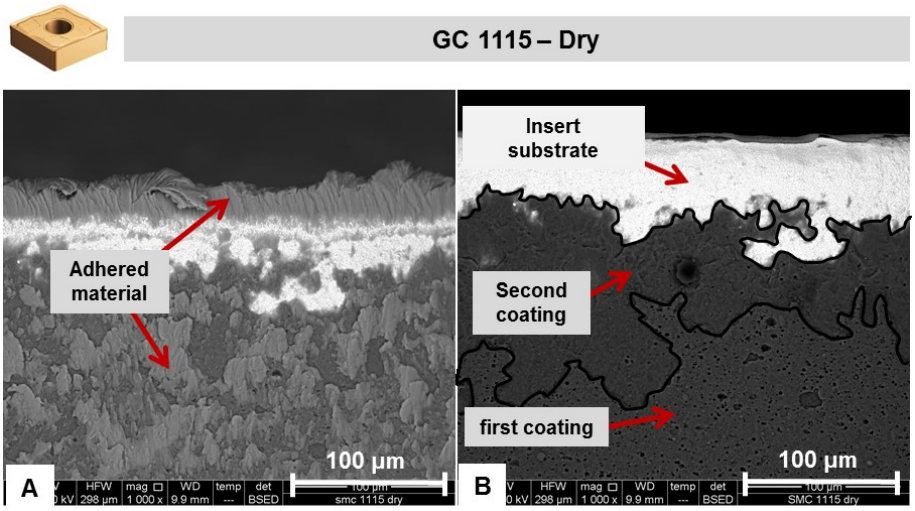

Figure 6.5. Tool flank face after 15 minutes of turning for the insert GD 1125 under LN2 cooling conditions: (A) before and (B) after the removal of the adhered material.

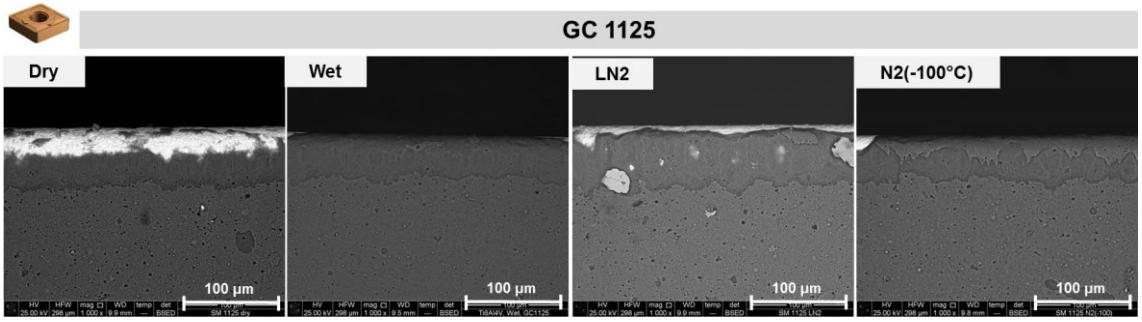

Figure 6.6. Tool flank wear after 15 minutes of turning under dry, LN2 and cooled gaseous N2 conditions.

Different considerations pertain to the inserts with a double coating (GC 1125 and GC 1115), in which the second deposited coating is composed by elements that do not exhibit chemical affinity with the workpiece material, thus minimizing the adhesion process. The overcooling induced by the LN2 may cause an excessive embrittlement of the material determining high abrasion with just a limitation of the adhesion. This behaviour pertains

especially to the insert with grade 1125, which was characterized by the highest abraded thickness when using the LN2.

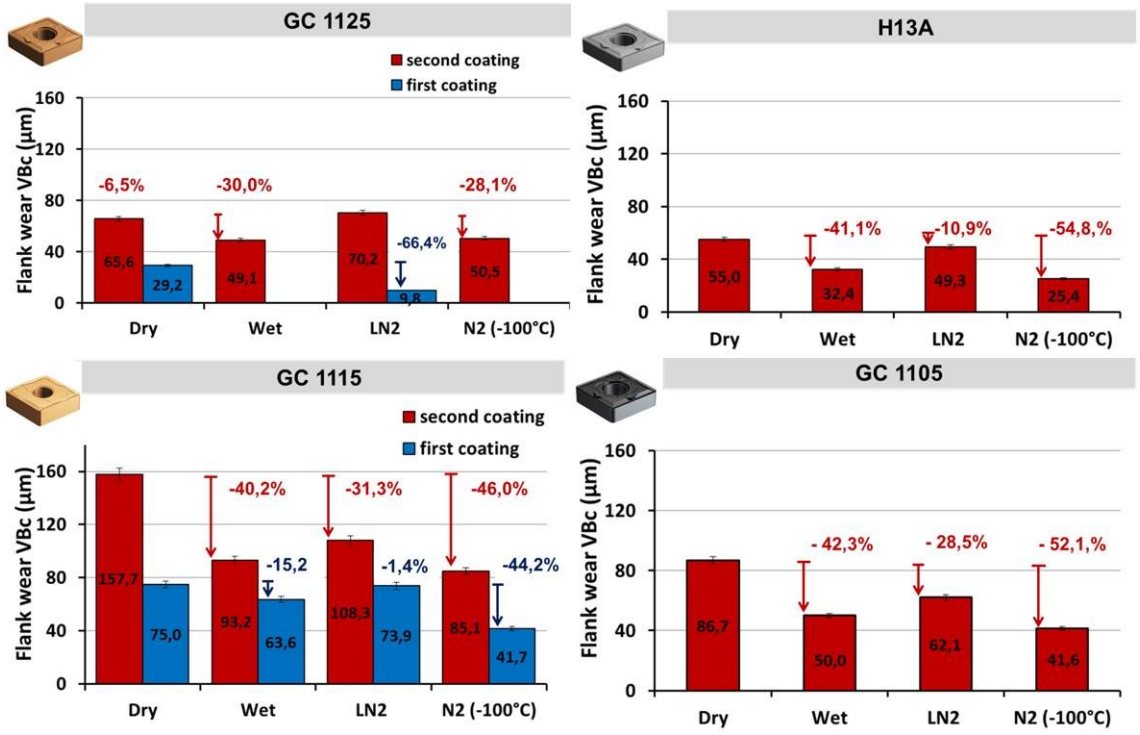

Figure 6.7. Tool flank wear VBc values.

The great potential of the cryogenic coolants was instead evident when the first deposited coating (as a consequence of the abrasion process) was exposed since it presented chemical affinity with the workpiece material; the use of the cooled gaseous N2 eliminated completely the abrasion, which was instead reduced of the 66% when using the LN2. For the insert GC 1125 the wet and cooled N2 strategies were comparable, as the same improvements with respect to the dry cutting were detected. Lastly, for the insert with grade 1115 the advantages of the tested cryogenic strategies with respect to the dry and wet cutting were highlighted in both cases, with more significant improvements than in the previous case.

The analysis of the flank wear of different commercial tool grades highlighted how the different cooling strategies produced different effects when using the cutting parameters recommended by the tool's manufacturer. The cooling technique based on the gaseous N2 cooled at -100°C gave always the best outcomes regardless the tested grade, whereas the LN2 produced interesting effects only when the highest cutting speeds (65 and 80 m/min) were adopted, with, instead, minimal differences compared to dry cutting at lower cutting speeds. The reason may be ascribed to the temperature field generated

during the cutting process, as the main effect of the cutting speed increase consists in higher heat production that can be better dissipated when adopting the LN2 characterized by a higher cooling capacity than the cooled N2.
On the other hand, even if the LN2 is able to assure a drastic cooling to completely eliminate the temperature effects, especially in those conditions in which the generated heat is low, it causes a material hardening effect that favours the flank face abrasion, thus limiting the overall advantages.

6.3 Chapter concluding remarks

The paper reported the results of an experimental wear analysis conducted on four different commercial inserts commonly used in Ti6Al4V semi-finishing turning using for each of them the maximum value of the cutting speed recommended by the tool's manufactures. The innovative cooling technique based on gaseous N2 cooled at -100°C was tested using dry cutting, conventional flood strategy and LN2 cooling as baseline. The main findings of this investigation can be summarised as follows:

- The use of different inserts significantly influenced the tool wear: the uncoated insert H13A and the coated one GC 1115 did not present the cratering phenomenon regardless the cooling strategy, whereas the measured deepest crater was found in the coated insert GC 1105 under dry cutting. After 15 minutes of turning the minimum flank alteration was highlighted for the uncoated insert, whereas the use of a double coating produced by means of PVD and CVD techniques (GC 1115 and GC 1125) determined the highest measured VBc.
- Regardless the tested inserts the use of the LN2 as coolant did not produce the best results, as the excessive workpiece cooling determined a material embrittlement/hardening with consequent increase of the abrasion effect, although the thermally-activated wear mechanisms were reduced limiting the crater wear formation. On the contrary, the gaseous N2 cooled at -100°C allowed reducing the heat generated during the cutting process, thus limiting the crater wear, but without modifying the initial material characteristics and thus limiting also the flank wear.
- The highest improvements in terms of flank wear were highlighted using the uncoated insert (H13A) when using the N2 cooled at -100°C.

On the basis of the experimental results the best performances were found for the N2 cooled at -100°C, making it an ideal substitute of the conventional wet strategy during semi-finishing turning operation of Ti6Al4V alloy.

Chapter 7.

Modelling the thermo-mechanical behaviour of a redesigned tool holder to reduce the component geometrical deviations in cryogenic machining

7.1 Approach

The renewed demand of increasing the machinability of the Ti6Al4V titanium alloy to produce biomedical and aerospace parts has recently led to the application of low-temperature coolants instead of conventional cutting fluids to increase both the tool life and the machined surface integrity as reported in the previous paragraphs. In particular, the liquid nitrogen directed to the tool rake face has shown a great capability of reducing the temperature at the chip-tool interface, as well as the chemical interaction between the tool coating and the titanium to be machined, therefore limiting the tool crater wear, and

improving, at the same time, the chip breakability [1] [2]. Moreover, Pusavec and al. [3] demonstrated that the cryogenic machining reduced the overall productions costs with respect to the conventional case up to 30% making it economically sustainable.

However, the above mentioned advantages are not sufficient to make this technology attractive for actual industrial applications, as the major drawback is represented by the extremely low temperatures (-196°C) of the cryogenic coolant that could damage the mechanical parts of the CNC machine and cause thermal distortions that cannot be offset with consequent loss of dimensional accuracy of the machined components.

To overcome the aforementioned drawback, in this section, the thermal field of the tool holder during cryogenic turning of the Ti6Al4V titanium alloy was measured; afterwards, in order to reduce the thermal distortion, safeguard the lathe revolver and stabilize its thermal field, the tool holder was re-designed using an embedded cartridge heater.

Moreover a thermo-mechanical model of the newly redesigned apparatus was developed and calibrated using the experimental outcomes from the cartridge heater-free cryogenic turning test, with particular attention to the identification of the heat exchange coefficients of the LN2 flowing inside the feeder channel of the tool holder. The model was then validated by applying it to the turning tests carried out using the cartridge heater with two heat power levels, comparing both the temperature evolution along the tool holder and the thermal distortions the tool holder underwent.

The achieved final target was then a reliable thermo-mechanical numerical model of the tool holder behavior during the cryogenic machining process that will be further applied to improve the tool holder redesign.

7.2 Experimental tests

The turning tests were realised by means of a Mori Seiki™ NL 1500 CNC lathe using a tungsten carbide insert coated by TiAlN supplied by Sandvik™ CNMG 120404-SM GC1105 already employed in the previous works presented in this thesis. The insert was modified in order to acquire its temperature close to the cutting zone during the machining process: a hole of 0.5 mm of diameter was realized by electro-discharge machining at 1 mm from the insert surface and 1 mm from the cutting edge of the insert as shown in Figure 7.1, and then a T-type thermocouple of 0.5 mm of diameter was inserted inside the hole and fixed with a thermal glue.

The tool holder on which the insert was clamped was a CLNR 2525 M12-CHP made of

Tungaloy^{TM}. This particular tool holder was chosen because it already presents channels for internal lubrication, which were used for providing the LN_2 directly to the cutting edge. The original telescopic nozzle at the top of the tool holder was modified in order to reduce its diameter from 2 mm to 0.8 mm, with the aim of reducing the flow rate of the cryogenic coolant and therefore its consumption costs.

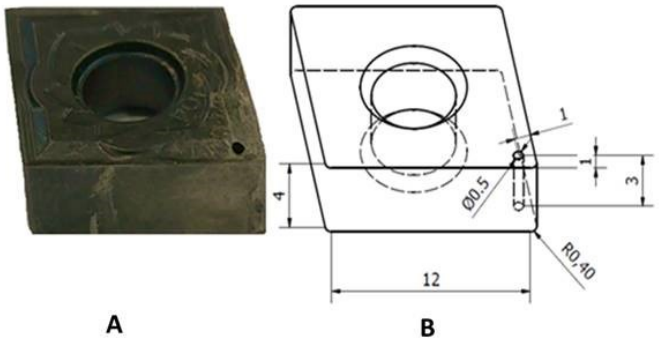

Figure 7.1. Photo of the actual tool modified by electro-discharge machining (A) and CAD drawing of the tool (B)

To evaluate the thermal field of the tool holder when using the cryogenic coolant, 3 K-type thermocouples were spot-welded on its surface, at 40, 50 and 60 mm from the top tip, respectively (see Figure 7.2). To process the thermocouple signals into temperature measurements, a LabVIEW^{TM} based program was developed that acquired the 4 thermocouple signals at the same time and displayed their evolution on a time-temperature graph.

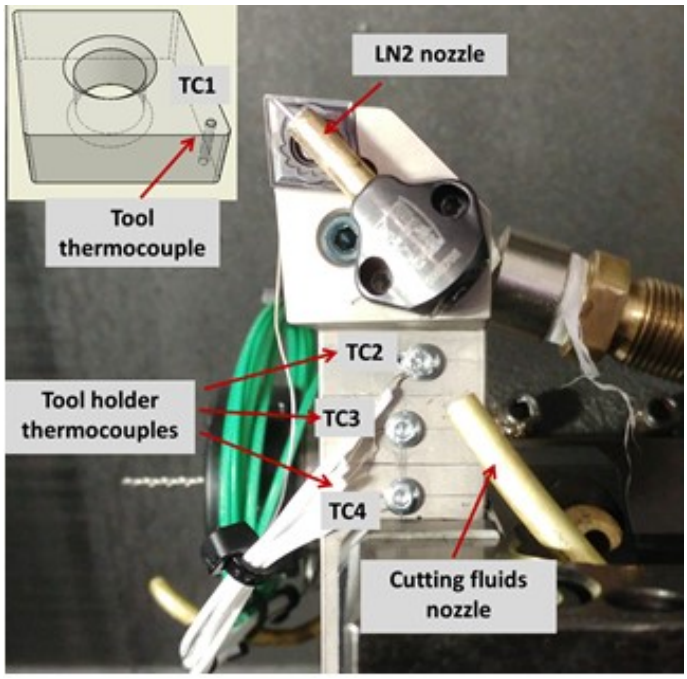

Figure 7.2. Experimental tool holder setup.

The turning tests were carried out under wet conditions and with the use of LN2 supplied at a pressure of 15 bar simultaneously to the tool flank and rake faces using the internal lubricating channels of the tool holder (detailed description of the cryogenic cooling line can be found in §3.3). A Ti6Al4V ELI bar was machined from a diameter of 40 mm to 38 mm, with a turning length of 40 mm using the cutting parameters recommended by the tool manufacturer, the machining time was slightly higher than 1 minute, anyway not sufficient to determine a significant tool wear. A fresh cutting edge was used for each trial thus avoiding the tool wear effects on the final dimensional accuracy of the machined sample. The experimental plan is shown in Table 7.1.

Table 7.1. Experimental plan for the turning tests.

Depth of cut (mm)	0.25
Cutting speed (m/min)	80
Initial diameter (mm)	40
Final diameter (mm)	38
Feed rate (mm/rev)	0.2
Cooling strategies	Wet, LN2

Hypothesizing that the geometrical deviations of the machined sample were mainly caused by the thermal contraction of the tool holder as a consequence of the low temperatures, in order to stabilize the thermal field and reduce the tool holder contraction, a heating cartridge was inserted inside the tool holder itself. The cartridge was kept in the right position using a spring and a tapping screw modified to allow the wires to pass through. Table 7.2 reports the main data of the thermal cartridge. The heating cartridge was controlled through an electrical panel, making possible to regulate the heat power, two value of electrical power were tested, respectively 75 and 150 W.

Table 7.2. Heating cartridge data [4]

Diameter (mm)	**Tolerance (mm)**	**Length (mm)**	**Max Power (W)**	**Potential (V)**	**Weight (g)**	**Power Density (W/cm^2)**
6.5	-0.05+0.03	50	150	220	10	20

After turning, the geometry of the machined cylindrical samples was measured using a Zeiss^{TM} Prisma 7 Vast coordinate measuring machine. A single stylus with a 3 mm diameter rubidium tip was used. The measurements were carried out in a temperature-controlled room at 20°C. The results of the measurements are reported in Table 4, each

one being the average of three measurements. The difference between the actual final diameter compared to that attained in wet conditions can be regarded as a quantitative index of the temperature-induced tooling distortions. The re-designed setup reduced the sample geometrical deviation with respect to the original tool holder: the best result was highlighted using the heat cartridge at 150 W leading to a reduction of the 38% of the geometrical deviation. Table 7.3 also reports the measured cylindricity of the machined samples: it is worth to notice that there is not particular difference between the different working strategies.

Table 7.3. Geometrical distortion of the machined samples

	Sample dia. (mm)	**Standard deviation (µm)**	**Difference (mm)**	**Cylindricity (µm)**	**Standard deviation (µm)**
Wet	38.13543	0.38	-	5.4	0.2
Original tool holder	38.34356	0.86	+0.208	7.1	0.6
Re-designed tool holder (75 W)	38.28970	0.47	+0.154	8.8	0.3
Re-designed tool holder (150 W)	38.26397	0.60	+0.129	8.7	0.3

The machined surface roughness was measured using the Sensofar PluNeos^{TM} optical profiler, being the measured area 1.5mm x 0.55 mm. The cut-off value was chosen equal to 0.8 mm according to ISO 4288:1996 [5]. The recorded roughness values are reported on Table 7.4. It is possible to observe that the roughness of the surface decreases when the LN_2 is used.

Table 7.4. Surface roughness of the machined samples

	Ra [µm]	**STD [µm]**	**Rq [µm]**	**STD [µm]**	**Rz [µm]**	**STD [µm]**
Wet	2.196	0.029	2.516	0.057	8.132	0.049
Original tool holder	2.070	0.033	2.395	0.031	8.449	0.140
Re-designed tool holder (75 W)	2.042	0.029	2.315	0.022	8.002	0.387
Re-designed tool holder (150 W)	2.070	0.0033	2.395	0.031	8.449	0.140

It is possible to observe that the roughness of the surface decrease when a cooling lubricant is used instead of the traditional oil-base lubricant, at the same cutting parameters, the use of the heating cartridge doesn't influence the superficial finishing of the component.

7.3 Numerical model of the tool holder

The numerical model of the tool holder was developed in order to simulate the temperature field during cryogenic machining and the consequent thermal shrinking of the tool holder itself.

The model was developed using the ANSYS^{TM} software with an implicit solution scheme applied to a coupled transient thermo-mechanical material model. The thermo-mechanical characteristics of the tool holder material were assumed from steel standard values and are summarized in Table 7.5

The 3D model of the entire lathe turret assembly was implemented, composed by:

- the tool insert;
- the tool holder (comprising the LN2 feeding system and the cartridge heater housing drilled in the holder body);
- the tool holder fastening system (comprising plates, wedges and bolts);
- the lathe turret;

Table 7.5. Thermo-mechanical characteristics of the tool holder material.

Material parameter	Value
Density (kg/m^3)	7850
Young modulus (MPa)	210000
Poisson ratio (-)	0.3
Thermal conductivity (W/Mk)	60
Specific heat (J/kgK)	435
Coefficient of thermal expansion (1/K)	1.1 10^{-5}

The lathe turret was discretized with a coarser mesh size of 1.5 mm, while the rest of the tooling with a finer one of 0.7 mm. Figure 7.3 highlights the main features of the model.

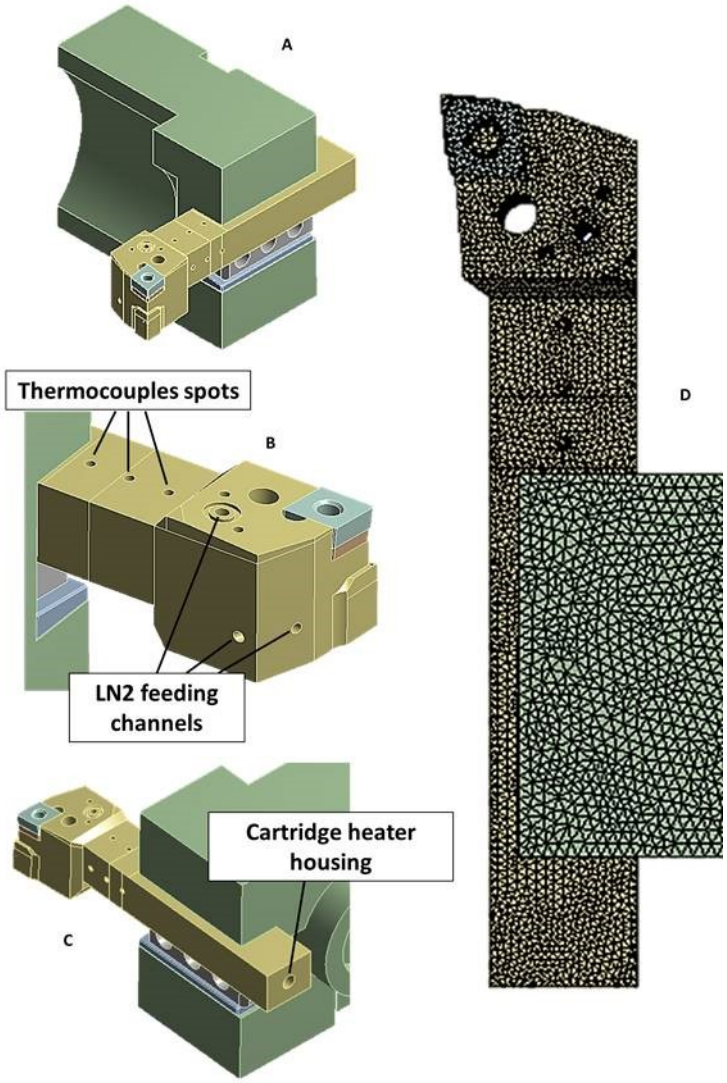

Figure 7.3. FEM model: A) general overview, B) detail of the tool holder, C) position of the cartridge heater housing, D) adopted meshes.

The main effort in the numerical model calibration consisted in setting the heat transfer boundary conditions, namely the Heat Transfer Coefficients (HTCs) at the various interfaces. Since the target was the accurate prediction of the temperature distribution along the tool holder, in order to predict its thermal distortions, the first assumption was to neglect the heat generated by the cutting process. This is reasonable since the heating generated by cutting is very localized at the tool tip where a strong cooling condition is imposed by the LN2 adduction, also confirmed by the experimental temperature evolution at the tool tip shown in purple in Figure 7.4 It is worth to note that the temperature evolution at the tool tip highlights two peaks corresponding to two cutting cycles, but no effect was propagated to the tool holder thermocouples. Therefore, the most critical heat transfer conditions to be calibrated were those between the LN2 and tooling both in the feeding channels and on the external surfaces. The evaluation of the

LN2 HTC has been rarely addressed in literature and usually just in the modelling of the LN2 external flow (i.e. between the cooling fluid and cutting tool). In [6] Hong and Ding evaluated different cooling systems both numerically and experimentally and an HTC values in the range of 20000-40000 W/m^2K was found. Also in the works of Kheirredine et al. [7] and Rotella and Umbrello [8] an HTC value of 20000 W/m^2K was used. In the work of Jin et al.[9], on the other hand, lower values were found, in the range of 0-3500 W/m^2K, as reported also by Pusavec et al.[10]. This is in agreement with the fact that in [9] the HTC was evaluated in still bath conditions and not in external turbulent ones, as in the other cited works.

In the present numerical model, the HTC was assumed to be 20000 W/m^2K on the external surface of the cutting tool, while for the internal feeding channels (which are supposedly the most important concerning the cooling of the tool holder), an optimal value was searched by inverse analysis in the range between 0 and 3500 W/m^2K.

To this regard it was observed that the HTC in the LN2 feeding channels cannot be constant during the whole turning test because the flow passes through transient states; in particular the following regimes can be observed:

- A N2 → LN2 transient regime in the first part of the test; in this stage the LN2 enters the feeding channel, which is still at room temperature, partially evaporating and reaching the nozzles in a mixed gaseous-liquid state.
- A LN2 steady state regime; in this stage there is a stable liquid flow through the device and the nozzles. It is reasonable to assume that the HTC is higher than in the previous stage, due to the higher thermal conductivity of the LN2 [9].
- A final stage in which the LN2 flow is interrupted; after the cutting operation is finished the flow is interrupted, the feeding channels remain still full of LN2, which is not moving anymore. In this case a smaller HTC can be expected, due to its reduced convective effect.

The occurrence of the aforementioned regimes is evident from the temperatures recorded by the four thermocouples for the cartridge heater-free test shown in Figure 7.4.

Even if the second LN2 regime is the most important for the temperature evolution, a reliable numerical model must be correctly calibrated for all the heat exchange conditions, to eventually take into account the repeated start-and-stops and tool changes of the cutting cycles.

The inverse analysis was carried out using a factorial plan of simulations testing different HTC sets searching the best fitting with the experimental temperature evolution. The optimal HTCs values found through inverse analysis are shown in Figure 7.4.

The optimal values of the HTCs are reported in Table 7.6, together with the other thermal parameters used in the model. In Figure 7.5 the comparison of the experimental and numerical temperature evolutions during the cryogenic turning test using the original tool holder is presented: a good agreement is shown with a maximum error of 9°C when the temperature steady state regime is reached.

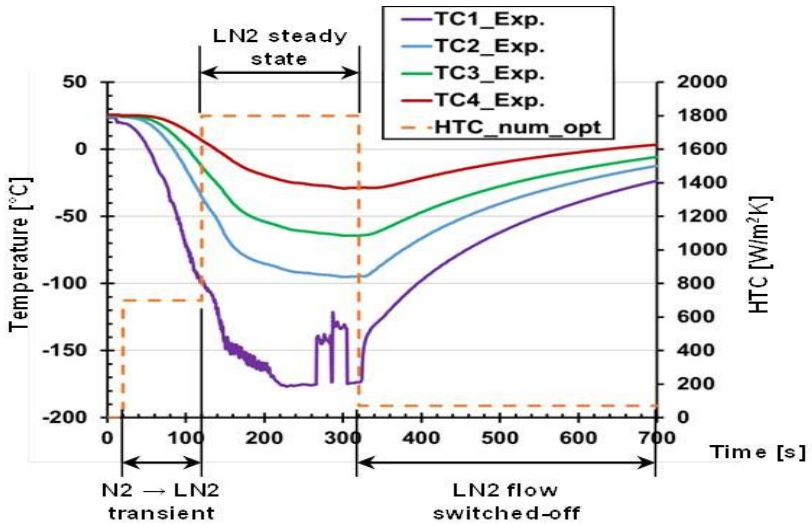

Figure 7.4. Temperature evolutions (continuous lines) recorded by the thermocouples in the cartridge heater-free test together with the optimal HTC values (dashed lines) corresponding to the three LN2 flow regimes found by inverse numerical analysis.

The coupled thermo-mechanical simulation allows also predicting the thermal shrinking of the tool assembly, as shown in Figure 7.6, in which the tool holder temperature distribution and horizontal displacement are illustrated.

Table 7.6. Thermal parameters implemented in the numerical model.

Parameter	Value
HTC feeding channel (W/m^{2}K) N2 → LN2 trans	700
HTC feeding channel (W/m^{2}K) LN2 steady state	1800
HTC feeding channel (W/m^{2}K) LN2 not moving	70
HTC cutting tool (W/m^{2}K)	20000
HTC with air (W/m^{2}K)	10
Room temperature (°C)	25
LN2 Temperature (°C)	-196

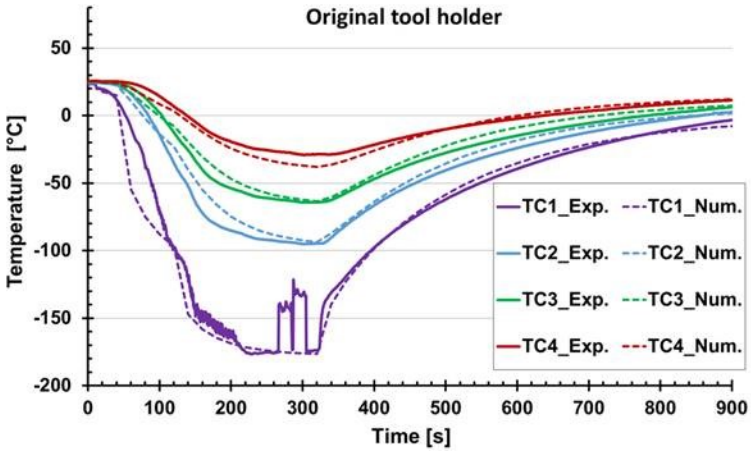

Figure 7.5. Comparison of experimental and numerical temperature evolutions for the cryogenic turning test with the original tool holder.

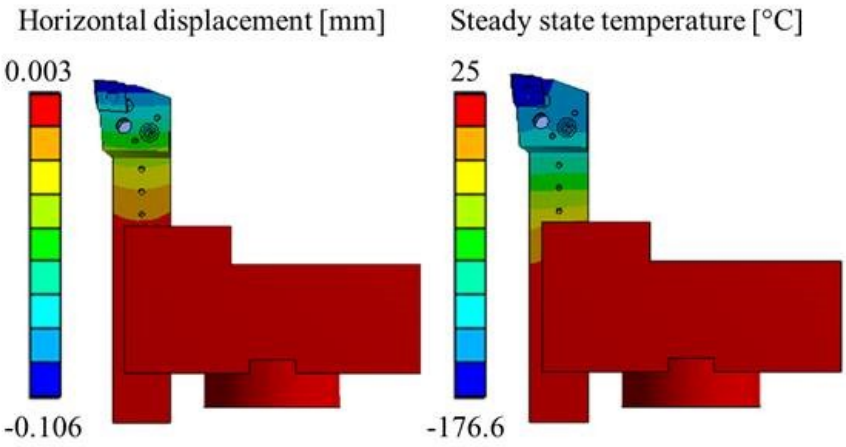

Figure 7.6. Numerical prediction of the horizontal displacement and temperature distribution in thermal steady state condition for the cryogenic turning test with the original tool holder.

7.4 Validation of the numerical model

The calibrated numerical model was then applied to the other two experimental cases, namely the ones with the cartridge heater working at 75 W and 150 W, respectively.

Except for the additional heat flow condition imposed, namely the heat flow provided by the cartridge heater at the contact surface in cartridge housing, the remaining thermal parameters were left unchanged, as from previous optimization. The resulting temperature evolutions comparison is shown in Figure 7.7. Excluding the cooling ramp slope, which has no significant effect on the steady state regime, the values are in good agreement with a maximum temperature error of 11°C for the farthest thermocouple in the 150 W heating case, see also Table 7.7. The validation was then further carried on assessing the geometrical distortion predicted by the numerical model and comparing it with the experimental outcomes. In order to do this, the maximum displacement of the

tool tip in steady state conditions resulting from the simulations was compared with the final part dimensions derived from experiments and already listed in Table 7.3.

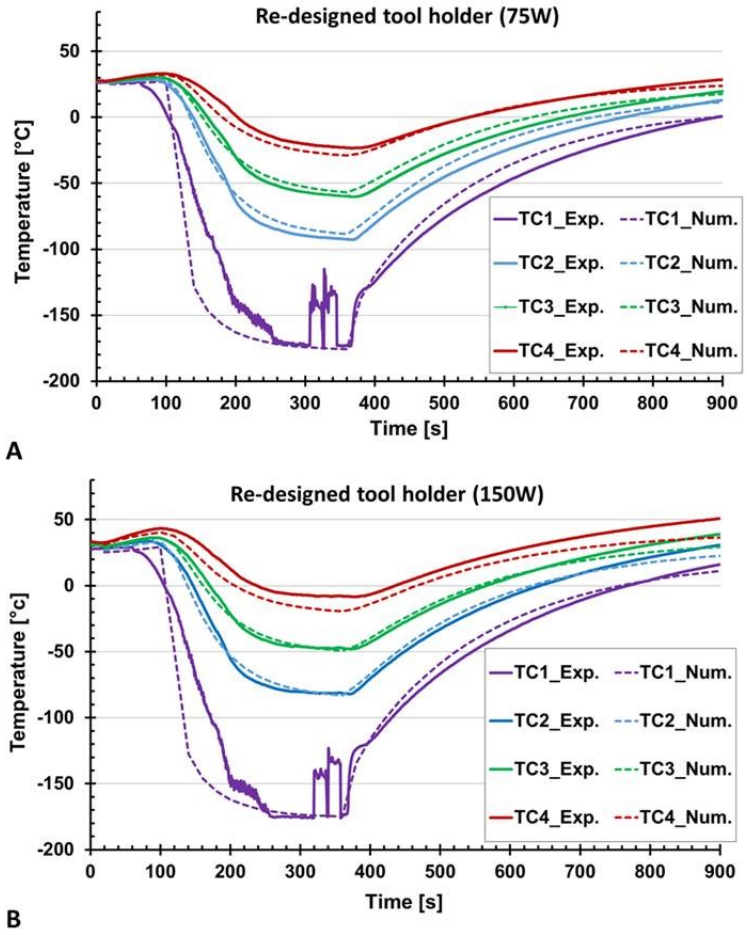

Figure 7.7. Numerical and experimental temperature evolutions for the: a) re-designed tool holder with cartridge heater at 75 W, and b) re-designed tool holder with cartridge heater at 150 W.

Table 7.7. Experimental and numerical temperature values (measurement uncertainty equal to 0.1°C)

	TC1 (°C)	**TC2 (°C)**	**TC3 (°C)**	**TC4 (°C)**
Original tool holder_exp.	-176.7	-95.2	-64.4	-29.2
Original tool holder_num.	-176.5	-93.6	-63.6	-38.1
Re-designed tool holder (75W)_exp.	-173.6	-92.7	-60.4	-23.6
Re-designed tool holder (75W)_num.	-175.8	-88.6	-56.7	-29.0
Re-designed tool holder (150W)_exp.	-176.1	-82.1	-48.1	-8.5
Re-designed tool holder (150W)_num.	-174.8	-83.0	-49.3	-19.4

Taking the wet cutting condition as reference, the difference in the machined samples diameter resulting from CMM measurements can be regarded as a reliable estimation of the total tooling shrinkage. To compare the experimental and numerical data the following relation was used on the basis that a tool tip certain displacement causes a double amount of diameter variation on the turned sample:

$$\Delta\phi_{num} = 2\Delta x_{num} \tag{7.1}$$

Where

$\Delta\phi_{num}$ is the numerical final samples diameter change

Δx_{num} is the numerical horizontal displacement of the tool tip.

The comparison between the experimental and numerical part diameter deviations are presented in Figure 7.8, showing a maximum error of 6% when using the 75 W cartridge heater.

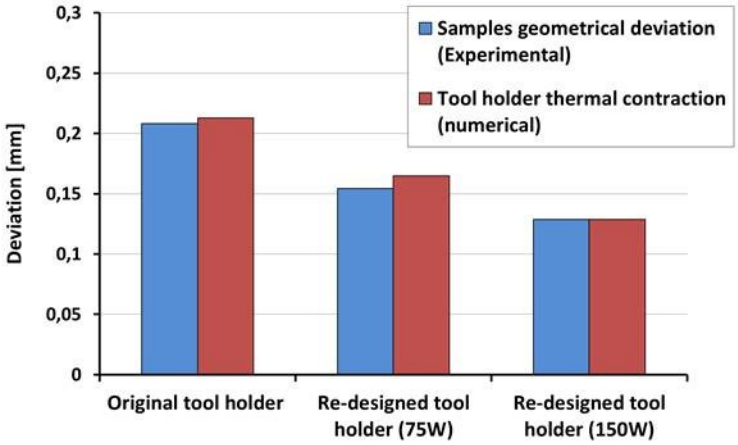

Figure 7.8. Comparison between the tool holder contractions determined through numerical simulation and the real dimensional deviations of the machined samples using the wet condition as baseline.

7.5 Chapter concluding remarks

The paper presents a feasibility study aimed at reducing the part geometrical deviations caused by the use of LN2 cooling during semi-finishing turning.

The adopted strategy consisted in the tool holder re-design embedding in the tool assembly a cartridge heater to provide a heat flow compensating the cooling action of the LN2. This device has also the beneficial effect of protecting the tool holder and the lathe turret structure from possible overcooling due to heavy-duty LN2 turning working cycles.

Based on the main findings, the following conclusions can be drawn:

- The sample cryogenically machined using the original tool holder presents a dimensional deviation of +0.208 mm with respect to the wet condition sample used as baseline; this deviation is not acceptable in many industrial applications.
- The use of cartridge heaters with electrical power of 150 W guaranteed a reduction of about 38% the geometrical deviations compared to the cryogenic turning test with the original tool holder; a further increase of the heating power should allow having a further compensation of the geometrical deviation.
- A thermo-mechanical model of the tool holder was developed in order to predict effectively the sample geometrical distortion related to the use of LN2.
- The numerical predictions are in good agreement with the experimental observations; the temperature percentage differences do not exceed 6% while the geometrical deviation shows a maximum error quantifiable around 7%.
- The proposed thermal-mechanical model represents a reliable prediction of the tool holder behavior and can be useful both for further improvements of the experimental apparatus in terms of cartridge heaters power and position and for more general cryogenic machining process design.

[1] M. J. Bermingham, J. Kirsch, S. Sun, S. Palanisamy, and M. S. Dargusch, “New observations on tool life, cutting forces and chip morphology in cryogenic machining Ti-6Al-4V,” *Int. J. Mach. Tools Manuf.*, vol. 51, no. 6, pp. 500–511, 2011.

[2] Y. Sun, B. Huang, D. A. Puleo, J. Schoop, and I. S. Jawahir, “Improved Surface Integrity from Cryogenic Machining of Ti-6Al-7Nb Alloy for Biomedical Applications,” *Procedia CIRP*, vol. 45, pp. 63–66, 2016.

[3] F. Pusavec, P. Krajnik, and J. Kopac, “Transitioning to sustainable production – Part I : application on machining technologies,” *J. Clean. Prod.*, vol. 18, no. 2, pp. 174–184, 2010.

[4] “Rotfil s.r.l., CartridgeHeaters_PDF-CAR-017-E, 2016.”.

[5] ISO 4288:1996 Geometrical Product Specifications (GPS) - Surface texture: Profile method -- Rules and procedures for the assessment of surface texture.

[6] S. Y. Hong and Y. Ding, “Cooling approaches and cutting temperatures in cryogenic machining of Ti-6Al-4V,” *Int. J. Mach. Tools Manuf.*, vol. 41, no. 10, pp. 1417–1437, 2001.

[7] A. H. Kheireddine, A. H. Ammouri, T. Lu, O. W. Dillon, R. F. Hamade, and I. S. Jawahir, “An experimental and numerical study of the effect of cryogenic cooling on the surface integrity of drilled holes in AZ31B Mg alloy,” *Int. J. Adv. Manuf. Technol.*, vol. 78, no. 1–4, pp. 269–279, 2015.

[8] G. Rotella and D. Umbrello, “Finite element modeling of microstructural changes in dry and cryogenic cutting of Ti6Al4V alloy,” *CIRP Ann. - Manuf. Technol.*, vol. 63, no. 1, pp. 69–72, 2014.

[9] T. Jin, J. Hong, H. Zheng, K. Tang, and Z. Gan, “Measurement of boiling heat transfer coefficient in liquid nitrogen bath by inverse heat conduction method,” *J. Zhejiang Univ. Sci. A*, vol. 10, no. 5, pp. 691–696, 2009.

[10] F. Pusavec *et al.*, “Analysis of the influence of nitrogen phase and surface heat transfer coefficient on cryogenic machining performance,” *J. Mater. Process. Technol.*, vol. 233, pp. 19–28, 2016.

Chapter 8.

Conclusions

In this chapter the findings and results of the current research are summarized with final remarks and conclusions. The concluding remarks are given in order to appearance in the chapters.

Semi-finishing turning experiments with the application of no-conventional coolants and lubricant as innovative method were conducted on the biomedical Ti6Al4V ELI titanium alloy produced by conventional and different Additive Manufacturing technologies. The aim of the research was investigating its machinability through both the experimental approaches under different process conditions, evaluating both the surface integrity and tool wear.

Moreover in this thesis a thermal-mechanical modeling of a new concept of tool holder properly designed to reduce the component geometrical deviations from its nominal

geometry to prevent mechanical damage of CNC components during cryogenic machining was proposed.

The major findings of this research are summarized below:

1. The tool wear analysis confirm the sticky tendency of Ti6Al4V alloy, the adhesive and diffusive mechanisms are the principal tool wear degradation modes. Regardless of the cooling/lubricating strategies severe adhesion of workpiece material on the tool cutting edge with the formation of Built-Up Edge and Built-Up Layer and in the worst case even the cratering phenomenon onto the tool rake was noticed.

2. SEM and EDS analysis revealed the strong dependency of the tool wear adhesion mechanism with the temperature arise in the cutting zone. The application of LN2 gave the lower tool wear (nose wear VBc and avoidance of cratering) respect to the wet and dry machining used as baseline, leading to an extension of the tool life and reduced waste of cutting insert. In term of surface integrity the cryogenic cooling led to cleaner machined surfaces. The adhered particles, smeared materials and grooves that are the typical defects obtainable in dry turning were drastically reduced. However due to the lower plasticity of the material induced by the lower cutting temperatures, the machined surfaces were wavier with the presence of jagged feed marks.

3. The study of a novel cooling technology based on the use of N2 cooled in the range 0°C and -150°C proved that the coolant temperature influences the alloy machinability and that a critical temperature existed below which no additional improvements were detected. The best solution was detected using N2 cooled at -150°C, which induced significant reduction of the rake and flank wear compared to LN2 and wet conditions, as well as the improvement of the surface integrity. The coolants cooling capacity was analytically modelled to explain the obtained experimental results. The results highlighted that the LN2 presents the highest cooling capacity, one order of magnitude higher than the ones of the N2 cooled at different temperatures; however, it was proved that a reduced cooling capacity, as in the case of N2 cooled at -100°C, was sufficient to optimize both the tool wear

resistance and machined surface integrity, whereas its increase to a great extend reduced the process performances.

4. Among the lubricating strategies the SL-assisted MQL and SL-assisted MQC ones represent interesting solutions able to reduce the cutting fluid consumption and to preserve the tool wear and the surface quality of the machined surfaces.
   The low cooling capacity of the MQL with and without the addition of PTFE particles was not able to eliminate the cratering phenomenon, whereas its dynamic viscosity, which was the highest among the tested strategies, assured a very low nose wear, limiting the abrasion of the cutting edge.
   The best machinability results were highlighted for the SL-assisted MQC strategy, in which both the cooling and lubricating capacity are guaranteed by the water-graphite solution used as cutting fluids: the water allowed dissipating the heat generated during the cutting process while the graphite particles reduced the friction.

5. Another method to improve the machinability of Ti6Al4V consists to adopting a hybrid technique. The simultaneous use of LN2 and MQL guarantee the advantages of both the techniques: in fact the cratering phenomenon is completely eliminated while the measured flank wear is comparable to that found when using the sole MQL technology. In the LN2/MQL combination, the position of the nozzles significantly affects the tool wear, the best solution being detected when directing the MQL to the tool flank face and the LN2 to the rake face.

6. In chapter 5 the correlation between the mechanical and thermal properties of the investigated alloys (EBM, DMLS, heat treated DMLS and Wrought) and the tool wear in dry and cryogenic semi finishing operation was proved. The martensitic microstructure detected in the DMLS sample since presents both the highest hardness values and the lowest thermal conductivity also at higher temperature determined the worst machinability results regardless by the adopted cooling strategies.

7. In according to the experimental evidence the EBM alloy presents the best machinability, the DMLS the worst one, whereas the wrought and heat-treated DMLS behaviours are comparable.

8. The results of an experimental wear analysis conducted on four different commercial inserts commonly used in Ti6Al4V machining highlighted that the innovative cooling technique based on N2 cooled at -100°C produces always the best results. The low temperature is able to inhibit the crater wear formation on to the tool rake face without improve the flank abrasion as instead it happened for the LN2 case. This evidence makes the cooled N2 strategies an ideal substitute of the conventional wet strategy during semi-finishing turning operation of Ti6Al4V alloy.

9. The tool holder was re-designed to overcome the freezing problems associated to the use of cryogenic coolant during the machining process. The adopted solutions allowed to reduce the geometric deviation of the machined samples and to preserve the mechanical components of the CNC machine from an excessive undercooling.

10. A thermo-mechanical model of the tool holder was developed in order to predict effectively the sample geometrical distortion related to the use of LN2. It was calibrated using the experimental outcomes from the cartridge heater-free cryogenic turning test, with particular attention to the identification of the heat exchange coefficients of the LN2 flowing inside the feeder channel of the tool holder. The model was then validated by applying it to the turning tests carried out using the cartridge heater with two heat power levels, comparing both the temperature evolution along the tool holder and the thermal distortions the tool holder underwent. The numerical predictions in good agreements with the experimental observation, both the temperature and geometrical deviations differences do not exceed the 6% and 7% respectively. The proposed thermal-mechanical model represents a reliable prediction of the tool holder behavior and can be useful both for further improvements of the experimental apparatus in

terms of cartridge heaters power and position and for more general cryogenic machining process design.